TECHNIQUES TO IMPROVE ULTRASOUND-SWITCHABLE FLUORESCENCE IMAGING

by

JAYANTH KANDUKURI

Presented to the Faculty of the Graduate School of

The University of Texas at Arlington in Partial Fulfilment

of the Requirements

for the Degree of

DOCTOR OF PHILOSOPHY

THE UNIVERSITY OF TEXAS AT ARLINGTON

August 2017

Acknowledgements

I would like to express my special thanks to Dr. Baohong Yuan, for his guidance, patience, understanding and encouragement throughout my graduate studies. He has been a great mentor and influence to me. I deeply appreciate the independent work platform he provides with tremendous support, resources and trust. His philosophy as a professor is, “always be motivated to implement new ideas and don’t get discouraged from failure”. His passion and dedication for science has always intrigued me. His honest and humble academic attitude has been a great model for me. His guidance has helped me to be a better researcher and person.

It is my privilege to have Dr. Hanli Liu, Dr. Kytai Nguyen, Dr. Yi Hong, Dr. Georgios Alexandrakis and Dr. Jun Liao on my dissertation committee or as a co-advisor. I am sincerely grateful for all the insightful criticisms and suggestions given for this dissertation. Individually, I would like to express my gratitude to Dr. Liu, for providing advice and support to successful complete my work; to Dr. Hong, Dr. Liao and Dr. Nguyen, for their collaboration and valuable suggestions on the biochemical experiment designs; and to Dr. Alexandrakis, from whom I have learned a lot about optics.

I am very grateful to Dr. Yanbo Pei, and Dr. Mingyuan Wei, who as good friends and colleagues, has given me enormous help on designing protocols, conducting experiments, and proofreading papers in the past four years. Working with all of them has been highly efficient and fruitful.

I would like to thank professors Dr. Kambiz Alavi and Dr. Mingwu Jin for all the collaboration and positive influences. Many thanks to my colleagues and friends, Dr. Yuan Liu, Dr. Bingbing Cheng, Dr. Hua Cao, Mr. Shuai Yu, Mr. Tingfeng Yao and Ms. Bahar Saremi, for their professional contributions, discussions, companions, and support during my stay in US for seven years.

I would also like to thank the Office of Graduate Studies Dissertation Fellowship, which supports me to focus effort on completing this dissertation.

I was fortunate to have many wonderful friends, Raja, Aruna, Rahul, Amruta, Vishal, Sarkar, Diya, Bipin, Ankita, and many more. They are like my extended families in US, who always encourage me and have faith in me.

I am very thankful to my wife, Neelima. Her confidence, support and unwavering love accompanied me through the hardest times. She always has positive attitude in life, and brings out the best in me.

I am, most importantly, very thankful for continuous support from my sister and brother-in-law whose encouragement and confidence towards me has motivated and propelled me to complete my research work. I'm especially blessed to know a little prince, my nephew Ajay, who brought happiness and joy in my life.

Last but not least, I can never be thankful enough to my beloved parents, Mrs. Bharathi Kandukuri and Dr. Madusudan Kandukuri whose love and support are the constant source of strength and inspiration for me.

August 11, 2017

Abstract

TECHNIQUES TO IMPROVE ULTRASOUND-SWITCHABLE FLUORESCENCE IMAGING

Jayanth Kandukuri, PhD

The University of Texas at Arlington, 2017

Supervising Professor: Dr. Baohong Yuan.

Novel approaches to the improvement of ultrasound-switchable fluorescence (USF) imaging—a relatively new imaging modality that combines ultrasound and optical imaging techniques—have been proposed for early cancer detection. In USF, a high-intensity focused ultrasound (HIFU) beam is used to induce temperature rise within its acoustic focal region due to which a thermo-sensitive USF contrast agent undergoes a switch in its state by increasing the output of fluorescence photons. By using an increase in fluorescence, one can isolate and quantify the fluorescence properties within the ultrasonic focal area. Therefore, USF is able to provide fluorescence contrast while maintaining ultrasound resolution in tissue. The major challenge of the conventional USF technique is its low axial resolution and its sensitivity (i.e. its signal-to-noise ratio (SNR)). This work focuses on investigating and developing a novel USF system design that can improve the resolution and SNR of USF imaging for biological applications.

This work can be divided into two major parts: characterizing the performance of a high-intensity focused ultrasound transducer; and improving the axial resolution and sensitivity of the USF technique. Preliminary investigation was conducted by using an IR camera setup to detect temperature variation and thereby study the performance of the

high-intensity focused ultrasound transducer to quantify different parameters of ultrasound-induced temperature focal size (UTFS). Investigations are conducted for the purpose of high-resolution imaging with an emphasis on HIFU-induced thermal focus size, short duration of HIFU-induced temperature increase (to avoid thermal diffusion or conduction), and control of HIFU-induced temperature increase within a few degrees Celsius. Next, the focus was shifted to improving the sensitivity of the ultrasound-switchable fluorescence-imaging technique. In this study, the USF signal is encoded with the modulation frequency of the ultrasound by modulating the induced temperature. Later, two approaches were adopted to modify the USF design to improve the resolution of the conventional USF imaging technique. The first approach aims to improve the axial resolution of conventional USF technique, which involves changing the USF system to adopt a dual-HIFU transducer arrangement (in which the transducers are 90 degree with respect to each other) for use as the heating source. The overlapped region of the two crossed foci (OR-TCF) of the dual-HIFU transducer module is expected to have small thermal size along both lateral and axial directions; thus, it could improve the axial resolution of the USF imaging technique. The second approach aims to demonstrate the improvement of resolution via a single-element HIFU transducer with a high frequency (15 MHz). The high frequency of the ultrasound transducer would have smaller acoustic lateral and axial size and should therefore have smaller thermal size. Thus, both approaches should be able to reduce the focal region of heating and thereby improve the resolution of the USF imaging.

Results show that the driving power and exposure time of the HIFU transducer significantly influence the ultrasound-induced temperature focal size (UTFS). Interestingly, a nonlinear acoustic effect was observed at certain variations of the ultrasound exposure power while satisfying the thermal confinement within UTFS. This has been shown to reduce UTFS beyond the acoustic diffraction limit, while the ultrasound-induced thermal

energy, which is confined within the focal volume, can induce a desired peak-temperature increase of a few degrees. On other hand, after encoding the HIFU exposure and therefore the detected USF signal with a modulation frequency, the SNR (sensitivity) and full width at half maximum (FWHM) along the lateral direction of the USF image was calculated to be ~114 and ~0.95 mm for a micro-tube with an inner diameter of 0.31 mm (ID), respectively. In comparison, they are ~95 and ~1.1 mm when using a non-modulated conventional USF imaging technique. In the case of improving the axial resolution of USF imaging for a similar target size, the dual-HIFU USF design was able to achieve ~1.07 and ~1.5 mm along lateral (*x)* and axial (*z)* directions, respectively. Adopting the second approach of using single 15 MHz HIFU transducer for USF imaging, the axial resolution was calculated to be 0.67±0.02 mm and 1.71±0.24 mm along lateral (*x)* and axial (*z)* directions, respectively. Thus, high-resolution ultrasound-switchable fluorescence with good sensitivity can be designed for biomedical applications.

TABLE OF CONTENTS

List of Illustrations

List of Tables

Chapter 1

Introduction

1.1 Motivation of Ultrasound-switchable Fluorescence Techniques.

For many years, investigators have sought non-invasive biomedical imaging techniques that can play a crucial role in cancer detection and staging [1]. In a few cases, medical imaging techniques have become a first step in preventing the spread of cancer through early detection; and in several cases, cure and/or elimination of the cancer altogether is possible. According to the National Cancer Institute's recent breast-cancer statistics, the average 5-year survival rate for people with breast cancer is 90% and diminishes to 26% if the cancer has spread to a distant part of the body [2]. For cancer detection and staging, significant advancements have been made in the prevailing imaging modalities—such as ultrasound (US) imaging, computer-tomography (CT) imaging, magnetic-resonance (MR) imaging, X-ray imaging and mammography—but these techniques generally suffer from low specificity (from mill mole/kilogram to μmole/kilogram) and are therefore mostly inadequate for detecting lesions <1 cm in size [3]. To extend the survival rate of many such patients, early-detection of cancer has become a paramount goal for medical investigators; thus, new imaging modalities are desired.

Over the past decade in clinical medicine, one relatively new imaging modality that has shown its prominence is fluorescence imaging. It has shown itself to be a potent tool especially for molecular imaging in disease and therapy [4-6]. Besides adopting non-ionizing radiation and being cost-efficient, it has flexibility in the broad selection of well-developed and inexpensive imaging probes (such as quantum dots, fluorescent proteins, etc.), and it is highly sensitive (fM-nM, 10^{-15} to 10^{-9} mole/kg) [5-7]. In particular, highly specific and sensitive information associated with the microenvironment—such as tissue

pH, temperature, gas/ion concentrations, etc.—can be efficiently obtained using fluorescence imaging. Such information can reveal the tissue functions of both healthy and diseased tissue, thereby aiding in the diagnosis of underlying abnormalities. For example, in the case of cancer imaging, it can be used to detect abnormalities such as angiogenesis, hypoxia, metastasis, etc. it is also used as a guide for drug delivery and targeted therapy [8-10]. A major drawback of fluorescence imaging is that it suffers from the strong absorption and scattering of focused light by body fluids and tissues, and is thereby compromised in either depth or resolution of imaging [7, 11].

On the other hand, ultrasound imaging is another imaging modality that is both cost-effective and uses non-ionizing radiation. Ultrasound's ability to characterize tissues has made it a most popular diagnostic tool for tumour detection (such as breast, liver and thyroid tumours, etc.). [1]. While adopting wide range of frequencies, ultrasound can achieve a broad range of resolutions and imaging depths. This signifies that it can accomplish good spatial resolution while maintaining higher penetration depths. This is because, diagnostic ultrasound, which is usually in the MHz range, has a scattering coefficient that is approximately three orders of magnitude less than that of light in biological tissue [7, 11]. But it is severely limited by low sensitivity to underlying micro-information, for functional and molecular imaging, due to lack of imaging contrast for specificity. Therefore, fluorescence and ultrasound technologies can complement each other's strengths while overcoming disadvantages in both resolution and contrast for revealing micro-information, thereby achieving high-resolution deep-tissue imaging [12-15].

To achieve this aim, several techniques that combine ultrasound and fluorescence technologies have been recently proposed and demonstrated, such as multispectral opto-acoustic tomography [16], ultrasound-modulated fluorescence [14, 17], and ultrasound-

induced temperature-controlled fluorescence [12, 13, 15, 18, 19]. For ultrasound-switchable fluorescence (USF) imaging, a short and focused ultrasound pulse (ranging from a few to hundreds of milliseconds) with high-intensity is used to induce up to a few degrees Celsius of heat (T) in its focal volume [12, 13, 15]. Here, polarity-sensitive fluorophores (high-quantum yields in a low-polarity environment) encapsulated into nanoparticles (made of thermo-sensitive polymers) are used as a USF contrast agent [20]. During USF imaging, when the ultrasound-induced temperature (T) of the USF contrast agent goes above the threshold temperature of the thermo-sensitive polymers or nanoparticles, these polymers or nanoparticles experience a reversible phase transition. This phase transition leads to the emission of a unique fluorescent signal (called a USF signal). After ultrasound exposure, the thermal energy is diffused quickly, and the temperature recovers to background temperature; thus, fluorophores are switched off. By specifically analysing the USF photons, one can isolate and quantify the fluorescence properties within the ultrasonic focal area. As a result, USF may provide anatomical, functional, and molecular information of tissue via appropriate fluorescent probes while maintaining ultrasonic resolution and imaging depth [12, 13, 15, 21], as is shown in Table 1-1. Moreover, by using different wavelength-specific USF probes, USF techniques can potentially be used to image multiple molecules simultaneously, thereby providing a multi-colour fluorescence-imaging technique.

Table 1-1 Motivation for Ultrasound-switchable Fluorescent Imaging [13, 14]

Modalities / Imaging parameters	USF	FDOT	Ultrasound
Contrast	Optical contrast (=FDOT)	Optical contrast (functional and	Acoustic contrast (structural or

		molecular information)	anatomical information)
Sensitivity	Very good (=FDOT)	Very good (fM-nM, 10^{-15}-10^{-9} mole/kilogram	Relative poor
Imaging depth	Good and scalable (=Ultrasound)	Good (~5 cm)	Scalable (~mm to ~3 cm)
Resolution	Good and Scalable (=Ultrasound)	Poor (~ 1 to 5 mm)	Scalable (~10^1 μm to ~10^2 μm)
Multi-molecular imaging	Possible (=FDOT)	Possible: with multiple dyes	Not possible

Currently, two major challenges facing USF are the axial resolution and sensitivity of the USF system. Our study accordingly focuses on investigating novel system designs for USF imaging toward improving its resolution and sensitivity. If successfully optimized, this technique can in the future be a powerful tool in the study of tumour development and metastasis, can provide guidance for drug delivery and targeted therapy, and can aid in the evaluation of tumour treatment efficiency.

1.2 Basic USF Imaging Principles

The basic mechanisms of USF imaging have now been discussed, as is shown in Figure 1-1. [12, 14, 15, 17, 20, 21]. The USF imaging technique is made up of two main components: (1) USF contrast agents, and (2) an acoustic-optical imaging system. In brief, the principle of USF imaging is to use a high-intensity focused ultrasound beam to non-invasively and locally control fluorophores emission from its confined volume (close to or even smaller than ultrasound focal volume) [12, 13, 15].

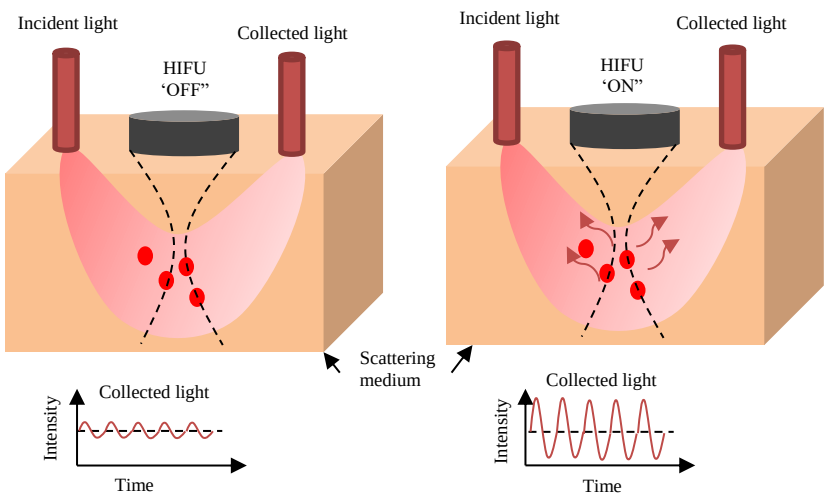

Figure 1-1 Schematic diagram of Ultrasound-switchable fluorescence principle

USF imaging depends upon two states/phases of the USF contrast agent - when USF contrast agent is switched 'OFF' and 'ON'. USF contrast agent, which is a thermo-sensitive, is switched 'ON' when temperature in its environment is increased beyond a threshold (lower-critical solution temperature (LCST)). Desired temperature is induced, by tissue absorption of acoustic energy, when the ultrasonic energy is applied using the high-intensity focused ultrasound (HIFU) transducer. Therefore, HIFU transducer can be considered as a heating source in USF imaging system. Also, desired temperature increase is tightly constrained in the focal volume of the HIFU transducer therefore the focal volume of HIFU transducer determines the resolution of the USF system.

While performing USF imaging, in absence of ultrasonic energy (HIFU – 'OFF'), fluorescence signal detected by USF imaging system is considered to be noise. This noise signal consists of (non-100% off) fluorescence signal of USF contrast agent ('OFF') and/or tissue auto-fluorescence. Using unique design of USF system, the noise is kept to

minimum as possible. On other hand, when the HIFU transducer applies tightly focused ultrasonic energy inside the sample, USF contrast agents in a small volume (usually within the ultrasound focal volume) are switched on and fluoresce. The relative change in the fluorescence intensity is considered as USF signal. By scanning the ultrasound focus, the distribution of the USF contrast agents can be imaged [13, 15, 17].

In-depth understanding of the USF imaging principle is obtained by understanding the USF contrast agent mechanism and the working of the high-intensity, focused ultrasound-transducer module. For the purpose of this study, only the fluorophore-encapsulated nanoparticles (FEN) [12, 13, 15, 20] based USF contrast agents is discussed. Here, fluorophores used are polarity-sensitive therefore they exhibit high-quantum yield in low polarity environment. These fluorophores are encapsulated into nanoparticles that are made of thermo-sensitive polymers, as shown in Figure 1-3 [13]. Therefore, this combination of polarity-sensitive dye encapsulated in thermo-sensitive nanoparticles (NPs) exhibit unique mechanism with respect to temperature change. This is determined by the threshold or the lower critical solution temperature (LCST) of the USF contrast agent. In one case, when the HIFU is off or US not applied, the temperature around NPs is below the threshold due to which a non-viscous, polar and water-rich microenvironment is provided to the fluorophore dye by the nanocapsule by exhibiting hydrophilicity. This state/phase is referred to as ‘OFF’ since it exhibits very low emission efficiency. In another case, when the HIFU is on or US is applied, a relatively long, high-intensity and focused ultrasound pulse (with duration of few to hundreds of milliseconds) induces heat within its focal volume inside the sample up to a few degrees Celsius [13, 15]. This temperature increase alters the NPs to exhibit hydrophobicity by shrinking and expelling water molecules. Due to which, a non-polar, polymer-rich, viscous

microenvironment is created by NPs for the encapsulated polarity-sensitive fluorophore. This state/phase is referred to as 'ON' since it exhibits strong emission efficiency. This temperature (T) at which the phase transition occurs is referred to as the lower critical solution temperature (LCST) of the USF contrast agent. Also, this phase transition is shown to be reversible with respect to temperature change. In summary, when the HIFU is applied, temperature (T) is greater than LCST (T>LCST) thereby switching the USF contrast agent 'ON'. On other hand, when the HIFU is not applied, temperature (T) falls below or is lower than LCST (T<LCST) thereby switching the USF contrast agent 'OFF'. This concept is schematically displayed in Figure 1-3 [13, 20]. Note, the fluorophores outside the focal zone of US, where T<LCST, will be unresponsive and will remain insensitive ('OFF') [13, 15, 21].

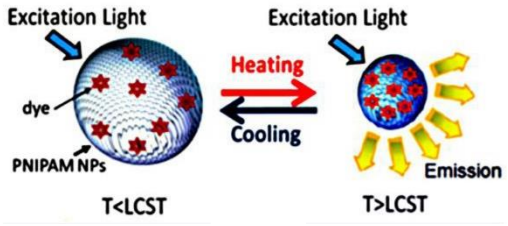

Figure 1-2 Schematic diagram showing the USF principle based a NP structure. Obtained from previous work of Bing et al [13]

1.3 Characterization of the USF contrast agent

USF contrast agents have been characterized using the following parameters [13, 20]: (1) peak excitation and emission wavelengths (λ_{ex} and λ_{em}); (2) ratio of the fluorescence intensity during on and off states (I_{On}/I_{Off}); (3) temperature threshold (LCST) required to switch on fluorophore (T_{th}); and (4) temperature transition bandwidth (T_{BW}). Performance of the USF contrast agent is determined by SNR of the USF signal acquired.

Best SNR is accomplished by either decreasing the background noise of the USF system or increasing the USF signal strength, or both. By adopting red or near-infrared (NIR) for both λ_{ex} and $\lambda_{em,}$ maximum penetration (by low tissue absorption) and low background fluorescence noise (auto-fluorescence) can be achieved. By adopting unique USF system design (combination of interference and absorptive optical filters) the non-100% off (background) fluorescence can be reduced. USF system's SNR can be increased by using ratios of I_{On}/I_{Off}. Also, by having large fluorescence emission intensity (I_{On}) when the USF contrast agent is in 'ON' state, the I_{On}/I_{Off} can be increased further thus increasing the SNR of the USF imaging. Another consideration during USF imaging is to avoid tissue damage due to thermal ablation. This determines that duration to induce desired temperature (about few degree Celsius) should be short. Therefore, the USF contrast agent should exhibit narrow temperature transition bandwidth (T_{BW}). Also, USF contrast agents with different threshold, T_{th}, temperatures (LCST) are required depending upon the application. For example, phantom studies requires LCST around 24 to 30 degrees Celsius while the *in vivo* studies require LCST above ~37 degree Celsius (physiological body temperature) [13]. Pragmatic consideration of a single USF contrast agent requires parameter optimization based on specific applications, since it is highly unlikely that any single USF contrast agent could exhibit the best values of all the above parameters simultaneously.

1.4 USF Contrast Agents:

For ultrasound-switchable fluorescence (USF) imaging, two types of USF contrast agents were used. These differed based on the NIR dye used and their respective excitation and emission wavelengths. They are categorized as follows:

a) ICG-based USF contrast agent: For the synthesis of ICG-based USF contrast agent, nanoparticles (NPs) about 70 and 150 nm in size are made of thermo-sensitive polymers of either poly (N-isopropylacrylamide) (PNIPAM) or its copolymer with acrylamide (AAm) or N-tert-butylacrylamide (TBAm), as shown in Figure 1-3 (a). By copolymerizing an appropriate amount of AAm or TBAm (and therefore the switching threshold) compared with the pure PNIPAM polymer, the LCST of the copolymer can be increased or decreased. ICG is a near-infrared (NIR) dye with a peak excitation at 780 nm and a peak emission at 830 nm [13, 21, 22]. Also, ICG is more sensitive to the change of the solvent's polarity than to its viscosity [21]. .

As shown in Figure 1-3 (b), four ICG-based USF contrast agents were synthesized with LCSTs at about 28, 31, 37 and 41 degree Celcius for our previous work. These are the following: ICG-encapsulated P(NIPAM-TBAm 185:15) NPs, ICG-encapsulated PNIPAM NPs, ICG-encapsulated P(NIPAM-AAm 90:10) NPs, and ICG-encapsulated P(NIPAM-AAm 86:14) NPs. Because of the extremely high temperature sensitivity of PNIPA, the I_{ON}/I_{OFF} can reach 2.9, 3.3, 9.1, and 9.1, respectively, corresponding to the four LCSTs, which are 1.6–5.1 times higher than those of other contrast agents [18, 19]. Due to the relatively large molecular weight (774.96 g mol^{-1}) of the ICG molecules compared with that of a water molecule (18 g mol^{-1}), they are unlikely to be released in short period usage [21, 23].

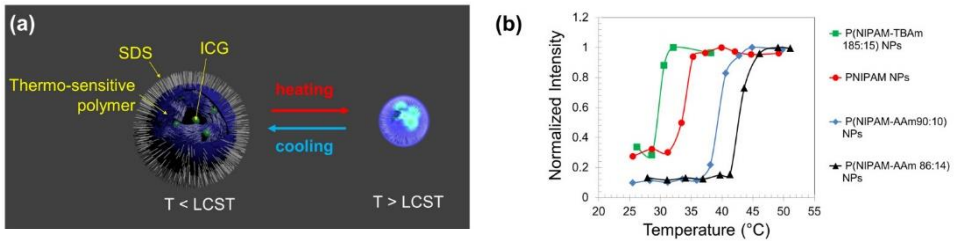

Figure 1-3 (a) Illustration of ICG-encapsulated thermo-sensitive nanoparticles (NPs) as a USF contrast agent. (b) Normalized fluorescence intensity vs. the sample temperature of the four ICG based USF contrast agents. Obtained from the previous work of Pei et al [21]

b) For ADP-based USF contrast agent: From our earlier work done by Cheng et al [12], the synthesis of ADP-based USF contrast agent is discussed as follows: ADP, abbreviation of aza-BODIPY, is a high polarity-sensitive NIR dye. It chemically reacted with two cyanocinnamic acids (CA), and it is therefore denoted as $ADP(CA)_2$. For this study, we used another dye, $ADP(OH)_2$, which has the same properties as the $ADP(CA)_2$. Both have peak excitation/emission wavelengths of 683/717. Note that the ADP core has an excitation/emission wavelength of 656/690 nm. It is therefore an excellent candidate for USF imaging.

From our previous work [12], the synthesis protocol and ADP-based USF contrast with different LCSTs is discussed as follows. To synthesize thermo-sensitive nano-capsules (in the range of 20–70 nm) for encapsulating the $ADP(CA)_2$, we selected pluronics polymers and their co-polymers with polyethylene glycol (PEG), as shown in Figure 1-4 (a). These polymers are Pluronic-F127, Pluronic-F98, Pluronic-F98~PEG20k, Pluronic-F98~PEG30k, and Pluronic-F98~PEG40k with respective LCSTs of 23, 30.5, 35.5, 45.6 and 45.2

degree Celsius, as shown in Figure 1-4 (b). All the intensity ratios (I_{ON}/I_{OFF}) are >200, while previously developed agents have I_{ON}/I_{OFF} <10 [13, 18, 19, 21].

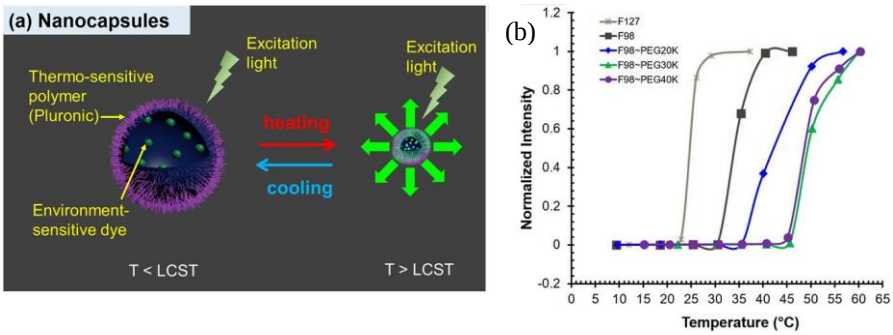

Figure 1-4 (a) Illustration of ADP-encapsulated, thermo-sensitive nanoparticles (NPs) as a USF contrast agent. (b) Normalized fluorescence intensity vs. the sample temperature of the ADP-based USF contrast agents. Obtained from previous work of Cheng et al [12].

1.5 High-intensity focused ultrasound

High-intensity focused ultrasound is emerging as one of a potential cancer-treatment modality in medicine. Its major recognition is for its non-invasive method and use of non-ionizing radiation [24]. The theoretical principal revolves around the idea that the larger, concave geometry of piezoelectric crystals could be driven with higher voltages, thereby generating greater-than-normal pressures waves that are concentrated at regions or areas much smaller than the focal area of conventional focused ultrasound transducers (in the order of or less than a few mm). The immense magnitude of pressure and the limitation of the area of exposure along with the absorption characteristics of the medium increases the chance of energy dissipation through the generation of correspondingly high temperature elevation. The HIFU-generated heat is highly dependent on the method of excitation of the HIFU transducer, which controls the increase of moderate (>2 ^{o}C) to high

temperatures (>50 ^{o}C) over a small region of interest (ROI), which depends intrinsically upon the frequency of the transducer over considerable less exposure time (<1S). This thermal absorption of HIFU energy leads to lesion formation, which becomes the basis for a phenomenon known as thermal ablation [25]. It is used in intensive clinical research and regulatory activity for the localized thermal ablation of a focused tissue volume with minimal to no damage to the surrounding tissues [26]. Therefore, it can be used for various treatments such as for tumours, debulking uterine fibroids, cardiac ablation during surgery, and stemming blood flow via acoustic cauterization [27]. The ODE (Office of Device Evaluation, a component of the FDA) has classified the HIFU device as either a Class III or ll, depending on its intended usage. The Class III classification is for high-risk devices or for devices that use new technologies that raise new safety or effectiveness questions. Premarket approval (PMA) is mandatory, and human clinical trials are normally conducted as part of the regulatory review [27].

1.5.1 Controlling induced temperature using HIFU transducer

The main purpose of using HIFU transducer is to generate a controlled temperature ^{o}C increase which can also be considered throughout the rest of the discussions as temperature rise. Keeping this as the primary constraint other characteristics that can be controlled are,

a. The burst width that governs the duration for which the HIFU transducer.
b. Power delivered at the focus which is directly dependent on voltage parameters of the source driving signal such a Voltage peak to peak (V_{pp}) thereby the Voltage root mean square (V_{rms}).

$$P_{avg} = (V_{rms})^2 \times Y$$

$$V_{rms} = V_{pp}/\sqrt{2}$$

c. Duration between burst, controls the interval for which the specimen, in our case a phantom or a tissue, needs to be exposed to US pressure waves.

, where Y is admittance.

The physical characteristics of the HIFU transducer also govern the major behaviour of the HIFU. The area of exposure (AOE), also known as focal volume, is governed by the concave shape of the HIFU transducer and the diameter of the circular shape of the transducer. However, the actual size of the convergence of the pressure waves from the surface of the HIFU's piezoelectric crystal depends primarily on the frequency at which the HIFU is driven.

1.5.2 Theory behind HIFU induced Heat Generation:

In theory, the temperature rise, *T*, at the focal volume of the focused ultrasound wave can be better understood by using the bio-heat transfer equation widely known as Penn's equation, which is stated below in its general form [28, 29]:

$$\rho C \frac{\partial T}{\partial t} = W_b C_b (T_b - T) + Q_m + Q - k\nabla^2 T,$$

where ρ is the density, c the speed of sound in the tissue (in our case TMM), W_b is the blood perfusion (kg /m^3. s), k the thermal conductivity coefficient, C_b is the specific heat of blood, T is tissue temperature, Q_m is the metabolic heat generation, t is time and Q is heat source [29].

The exposure time of the HIFU for our investigation is very short (about <0.1s); therefore, blood perfusion and metabolic heat can be ignored. The heat source can be considered to have two integral terms, as stated below [29]:

$$Q = \mu_a I + Q_{vis},$$

where μ_a is the intensity absorption coefficient, Q_{vis} is the rate of conversion of ultrasound energy to heat per unit volume via viscous interactions, and I is the *in situ* temporal average

intensity. It is inferred that the thermal and acoustic tissue properties for a given tissue or TMM are greatly influenced by both position and temperature. It can also be admitted that Penn's equation shows a linear dependency with respect to temperature rise (*T*). Here, the temperature rise (*T*) is contributed by T_{abs} and T_{vis}, which arise from acoustic energy absorption and viscous interaction, respectively. Hence by considering the thermal properties of medium to be homogenous, Penn's equation can be rewritten as [28],

$$\rho C\frac{\partial T}{\partial t} = [\mu_a I - k\nabla^2 T_{abs}] + [Q_{vis} - k\nabla^2 T_{vis}],$$

The right-hand side of above equation has the ultrasound-absorption component in the medium and the component of viscous interactions, respectively. An assumption put forth by Dr. Hynynen and Dr. Clarke is that the thermal diffusion of the absorptive heating contribution takes place on a much longer timescale than the viscous heating diffusion. In order to verify this assumption, Dr. Hugh et al. suggest that thermal conduction in typical HIFU fields becomes significant and is sometimes critically close to or less than 0.1 sec. Thus, the previous practice of ignoring the initial temperature rise to avoid the false temperature rise due to viscous heating is no longer feasible for short-duration HIFU exposures [28]. Thus, the above equation can be further simplified by considering the very short duration of HIFU exposure (ignoring the viscous heating influence) and a fixed source of acoustic energy as [29]:

$$\rho C\frac{\Delta T(z,r)}{\Delta t} = 2\mu_a I,$$

Thus, a linear relationship can be established between the distribution of temperature and sound intensity for the very short HIFU exposure time. Therefore, we can consider the temperature distribution at the focus to be interdependent of the sound field distribution [29].

1.5.3 Parameters that define ultrasound focus

The spatial resolution of an ultrasound transducer can be classified into axial resolution and lateral resolution. Axial resolution is the ability of the transducer or imaging system to recognize or distinguish two different regions or objects located at slightly different depths from the transducer along the axis of ultrasound beam propagation. Thus it is given by [30]:

$$\text{Axial resolution} = \frac{\lambda \,.(\#\text{ of cycles in one pulse})}{2},$$

Axial resolution can thus be improved by using UST operated at high frequencies. But the extent of penetration of the ultrasound beam decreases considerably.

The distance between the location for maximum echo in the focal zone and the piezoelectric element responsible for focusing the ultrasound beam would be considered as the focal length of the transducer. The piezoelectric crystal used for focusing applications is shaped like a concave disk. For an ultrasound beam with a circular cross section, focusing characteristics such as pulse-echo response width and relative sensitivity along the beam axis depend on the wavelength of the ultrasound and on the focal length 'f' and radius 'r' (D=2r) of the transducer's focusing element. These variables may be used to distinguish the degree of focusing of transducers by dividing the near field length (r^2/λ) by the focal length (f). The length of the focal zone of a particular ultrasound beam is the distance over which a reasonable focus and pulse-echo response are obtained and can be estimated by the following equation,

$$\text{Focal zone length} = 10\lambda\left(\frac{\text{f}}{\text{D}}\right)^2$$

On the other hand, lateral resolution is the ability of the transducer or imaging system to recognize or distinguish regions or objects that are closely situated along the

plane perpendicular to the direction of the propagation of the ultrasound beam. It is dependent on the beam width of the UST, which in turn depends upon the transducer's operating frequency, the focusing of the beam, and the gain applied to the captured echo signal. Lateral resolution is usually equal to beam width, as given by [30]:

$$\text{Lateral Resolution} = \frac{\lambda}{\text{NA}},$$

where *NA* represents the numerical aperture.

For a conventional circular probe, the beam width (BW) or beam diameter (BD) is defined by the points at which it has dropped by -6dB from its maximum on both sides of the beam. It is given by [30]:

$$BD = 1.02\ \frac{F\lambda}{D},$$

where *F* is the focal length and *D* is the element diameter of the probe. For a rectangular or flat probe such as a single element of an array, the beam width is given by [6]:

$$BD = 0.2568\frac{DF}{N},$$

where *N* is the near field of the probe and the ratio *F/N* equals one for a flat transducer.

1.6 Conventional USF imaging system

A brief overview of the setup of the USF imaging system [21] is shown in Figure 1-5. The system consists of three main subsystems: (1) an optical system for the delivery of the excitation light and the collection of the emission light, (2) an ultrasonic system HIFU transducer to induce temperature rise, and (3) an electronic control system to control source, scanning and data acquisition. The excitation light is generated either from a 671 nm or an 808 nm laser (continuous mode), depending upon the USF contrast agent used for the study. It is delivered to the bottom of the tissue sample (S) *via* filter (F_1) and the fibre bundle (EF). The second fibre bundle (CF) collects the fluorescence photons, which are

received by a set of emission filters and detected by a photomultiplier tube (PMT). A set of emission filters containing a combination of four carefully designed filters (F_2-F_5) allows the emission fluorescence photons to pass and efficiently rejects the excitation photons. The electronic signal after the PMT is further amplified and then acquired by an acquisition card (ACQ) for post-processing. The ultrasonic system consists of the HIFU transducer—which is driven by a function generator (FG) *via* an impedance matching network (NWM) to reduce power loss—and by a radio-frequency (RF) power amplifier, which is used to drive the HIFU at higher power. The MT controls the entire system, including the firing of the HIFU heating pulse and the data acquisition of the oscilloscope. Depending on the study, the ultrasonic exposure time is varied, as determined by the width of the gating pulse from the MT. During the ultrasonic exposure period, the tissue temperature at the HIFU focus rises. At end of the exposure, the temperature gradually reduces as a result of thermal diffusion. During heating (HIFU – 'ON') and non-heating phases (HIFU – 'OFF', couples of seconds), the fluorescence signal is acquired by the oscilloscope, which is triggered by a pulse from the MT. The HIFU transducer is scanned by a three-dimensional translation stage.

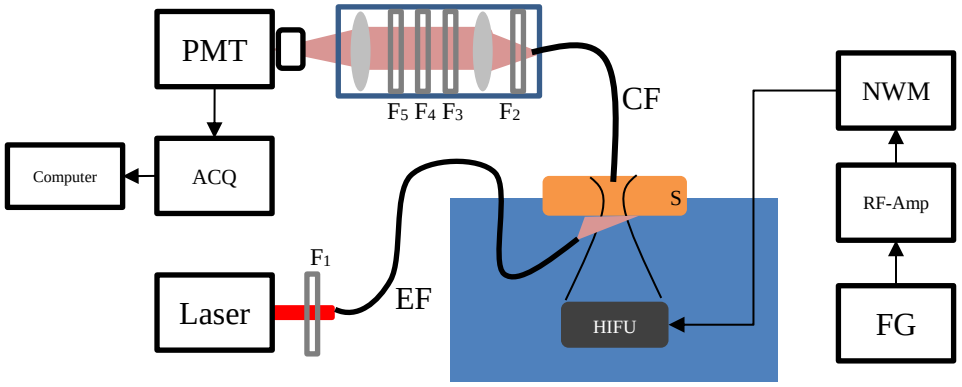

Figure 1-5 The schematic diagram of the USF imaging system, similar to the previous work done by Pei et al [21]

The photons received by PMT can be differentiated into four components: (1) leakage signal (leakage of laser-source excitation photons through the emission filters, (2) auto-fluorescence signal (tissue auto-fluorescence photons within the pass band of the emission filters), (3) background fluorescence signal (photons emitted from the non–100% off USF contrast agents), and (4) USF photons. Since the first three components are generated from the entire tissue sample and are not correlated with the ultrasound focus, they can be considered to be the major sources of noise. On other hand, the USF photons are a desired optical signal that is uniquely related to the ultrasound focus. Here, the smaller focal size of the HIFU transducer signifies high resolution, but the amount of USF contrast agent in the focal volume will be correspondingly less. This in turn suggests that the USF contrast agents that can switch on will also be less (low SNR). Hence, the SNR rapidly reduces as the resolution increases. Thus, the number of detectable USF photons (the desired signal) dramatically decreases as the resolution increases, while the number of noise photons remains stable because the noise is not correlated with the focal size and the resolution. Subsequently, it is imperative to minimize the optical photon related to the

first three components described above and to increase the USF signal level. In response, the basic USF system is designed such that the laser leakage has been significantly suppressed by using the specially designed combination of emission filters ($F_1$to F_5). By using NIR USF contrast agents, auto-fluorescence noise is avoided. Achieving a large value of I_{ON}/I_{OFF} limits the noise generated from the fluorescence of the contrast agents in the 'OFF' state and also improves the USF signal. Therefore, by directly observing the fluorescence intensity change at various scan locations, we can effectively differentiate the USF signal from the overall noise. The mechanical index (MI) was estimated to be ~2.5 and is slightly higher than the FDA-required MI < 1.9 for humans in diagnostic ultrasound. However, it is worth pointing out that MI = 2.5 is not required, and that a lower MI should also work for USF imaging. [21]

One of the limitations of previous USF imaging is the poor axial resolution due to the large thermal axial size, which is about ~4-7 times the lateral thermal size of its focal volume, especially in case of a low-frequency (2.5 MHz) HIFU transducer [31, 32]. Another part of the USF system that could be improved is its sensitivity. This could be done by encoding the USF signal with a frequency related to US switching. Therefore, in this study, an in-depth investigation is proposed and demonstrated to characterize the HIFU transducer with respect to its driving power and exposure duration, and novel modifications to the USF system are conducted to improve its resolution and sensitivity.

1.7 Objectives of this dissertation

The motivation of the dissertation is to investigate different parameters of the USF system so as to improve the sensitivity and resolution of the USF technique. The approach is to study the behaviour of the HIFU transducer and its driving parameters and the corresponding novel design of the USF system.

Chapter 2 investigated the behaviour of the HIFU transducer and its parameter to induce controlled temperature rise within a tissue sample. It considered whether the exposure duration and/or the driving power of the HIFU transducer significantly influence the temperature rise and focal volume of the HIFU transducer. We hypothesized that high-resolution USF imaging can be achieved by two mechanisms that may lead to breaking the acoustic diffraction.

Chapter 3 proposed a novel USF system design to improve the sensitivity of the system to the USF signal. The fundamental idea is to modulate the temperature within the tissue sample, thereby modulating the USF signal. Modulation of the temperature is achieved by modulating the US pressure wave by controlled switching of the HIFU transducer during USF imaging. This indirectly encodes the collected USF signal with the frequency of modulation of the HIFU transducer.

In Chapter 4, the emphasis of this study was to overcome the major limitation of the present USF system in terms of its axial resolution or resolution along the depth with respect to US wave propagation. Here, the indirect but effective method of using dual HIFU transducers placed perpendicular to each other is used in place of a single US transducer. This confocal transducer's overlapped region should have a relatively higher temperature than the individual transducer. This could contribute to a uniform thermal distribution in its lateral and axial direction, thereby improving the axial resolution of USF imaging without compromising the lateral resolution. This study also considers multi-colour USF imaging of multiple targets by using contrast agents with different excitation and emission wavelengths. This shows the ability of USF imaging to image multiple types of molecules, which is usually difficult for non-optical imaging techniques.

Chapter 5 proposed and discussed a relatively simple approach to improving the axial resolution of the USF imaging. For a HIFU transducer with high frequency (15 MHz),

the lateral and axial thermal sizes are significantly constricted compared to those of a low-frequency (2.5 MHz) transducer. We accordingly hypothesized that, by using a high-frequency HIFU transducer, the axial resolution of the USF system can be improved. Here we did a comprehensive study involving multi-colour, multiple target, USF imaging followed by *in vivo* application of the proposed USF system.

The last chapter summarizes all the results and concludes this dissertation.

Chapter 2

High-Intensity focused Ultrasound study

2.1 Introduction

Optical imaging techniques generally have spatial resolution limited to ~millimeters due to tissue light scattering for a centimeter-deep tissues [33]. By incorporating ultrasonic techniques into optical methods, such as photo acoustic tomography (PAT) [34]and ultrasound-modulated optical tomography (UOT) [35] , significant improvement in spatial resolution (hundreds of microns in centimeter-deep tissues) has been achieved . Recently, ultrasound-induced temperature-controlled fluorescence (UTF) imaging techniques have been developed [15, 18, 19]. A high-intensity-focused-ultrasound (HIFU) transducer was used to heat temperature-sensitive fluorescent probes only in the HIFU focal volume. This enabled a HIFU-enhanced or -generated fluorescence signal to be detected for optical imaging with acoustic spatial resolution in deep tissues. This is a significant step to achieve deep-tissue high-resolution fluorescence imaging.

The above mentioned ultrasound-combined optical imaging techniques have spatial resolution essentially limited by acoustic diffraction. One such imaging technique, Ultrasound switchable fluorescence (USF), has shown a potential to break the acoustic diffraction limit based on a temperature threshold of switching on or off [15]. While the temperature-threshold based method is promising, the improvement in spatial resolution is relatively limited if used alone. Therefore, techniques that can potentially improve the spatial resolution of the USF- or UTF-based imaging techniques is highly desired. Here, the spatial resolution of the USF- or UTF-based imaging technique is significantly dependent on the ultrasound-induced temperature focal size (UTFS). Hence it is imperative to investigate methods that can reduce UTFS below the acoustic diffraction limited size.

Also, high-intensity focused ultrasound (HIFU) transducer is an integral part of USF imaging for deep-tissue high-resolution imaging [15, 17]. Here, effect of different parameter such has the driving power and exposure time of HIFU transducer on induced temperature rise and its UTFS needs to be studied in detail.

Foremost challenging reasons for characterizing and minimizing UTFS are as follows: First, studies have never been conducted to investigate how UTFS is affected by different experimental conditions for imaging purposes when increasing tissue temperature only a few Celsius degrees in a very short period (such as tens or hundreds of milliseconds) [15, 19]. Most of the current HIFU-related studies are focused on tissue treatment. Such treatments uses thermal ablation, a process that requires increasing tissue temperature tens of Celsius degrees within a much longer period (such as from seconds to minutes) in order to destroy diseased cells [36]. In such cases, the UTFS is usually large (a few millimeters) due to thermal diffusion, which makes reducing UTFS unnecessary in HIFU treatment experiments. Another challenging aspect is quantifying UTFS in real deep tissues for imaging purposes. Here, HIFU-induced thermal focus needs to be small for the purpose of high resolution imaging (the smallest one in this study is ~0.246 mm generated by a 2.5 MHz ultrasound transducer). In addition, HIFU-induced temperature increase should be rapid to avoid thermal diffusion or conduction (the shortest HIFU exposure time in this study is 50 ms) while achieving only a few Celsius degrees increase. Due to which temperature-induced imaging contrast is low between the heated and surrounding tissues. Therefore, few techniques are available for this type of study.

In this proposed study, a temperature imaging system based on a fast infrared (IR) camera because of its high spatial and temporal resolutions is adopted. Since in real biological tissues significant tissue absorption of IR light occurs, an IR partially transparent

phantom to simulate tissues [15] is adopted for the proposed IR camera based system. Also, to have minimum acoustic attenuation and retain a large ultrasound penetration depth, we selected 2.5 MHz (low frequency) HIFU transducer for the following study. The outcome of investigations revealed that the UTFS can be significantly reduced below its acoustic diffraction limit by appropriately controlling the HIFU exposure power and exposure time via acoustic nonlinear effect and thermal confinement. Second part of study involved using the IR camera setup to study repeatability and consistency of induced temperature size at the focus of HIFU transducer when used on the chicken tissue. The results showed minimal variation of temperature size and average temperature rise within its focal region. This indicates that by using the HIFU transducer desired temperature can be induced within the tissue sample and can effectively improve the resolution of Ultrasound-Switchable Fluorescence Imaging technique.

2.2 Calibration of IR camera for temperature variation:

Similar setup shown in Figure 2-5 (a) is opted to calibrate the IR camera for temperature measurement. Instead of using HIFU transducer to induce heating, the whole water bath is heated by heater coil and the temperature on the surface of the tissue phantom (chicken tissue sample of thickness 8mm) is measured using three temperature measurement tools, 1) thermocouple connected to digital thermometer (HH508, Omega, Norwalk, CT, USA), 2) laser pointer thermometer and 3) IR Camera (FLIR6000, FLIR, Massachusetts, USA). Temperature of water bath is varied and corresponding temperature measurements were recorded from each of the temperature measuring devises mentioned earlier. Later they are plotted against IR counts measured from a point (~50microns) and an area (~4mm) on the surface of the tissue phantom. Note: IR camera captures 2D image of the surface of the tissue phantom on which it is focused. Slopes are calculated from

these plots by linear fitting, and measured to be around ~53 counts for 1 degree Celsius increase.

2.3 Materials and Methods – Characterization of HIFU transducer with respect to driving power and exposure time

2.3.1 System setup:

A schematic diagram of the experimental setup is shown Figure 2-1 (a). A 2.5 MHz sinusoidal waves, provided by the function generator FG-1 (AFG3252, Tektronix, Oregon), is amplified by a radio-frequency power amplifier (RF-PA, 325LA, E&I, New York). The output amplified signal drives the 2.5 MHz HIFU transducer (H108, Sonic Concepts Inc, Washington) via a matching network (MNW). The HIFU transducer was submerged into a water bath and focused inside an IR partially transparent silicone phantom (VST-50, Factor II, Arizona) as shown in Figure 2-1 (a). Second channel of the FG-1 function generator is used to trigger the second function generator (FG 2, Agilent 33220 A, California). The FG 2 provided pulses to trigger the IR camera (SC6100, FLIR, Massachusetts) to acquire the temperature images. Thus ensuring the HIFU exposure was always synchronized with the IR image acquisition. Figure 2-1 (b) schematically displays the time sequence of the entire system. While the HIFU began exposing (the upper panel), the temperature started increasing (the middle panel). At the same time, the IR camera was triggered to acquire 2D image of the temperature distribution (the lower panel). Each frame was acquired by integrating 0.25 ms and multiple frames were acquired during and after the HIFU exposure. The total number of the frames was well controlled so that there is one frame right after the end of the HIFU exposure (see the frame overlapped with the dotted vertical line). This frame always showed the maximum temperature increase compared with other frames.

The IR camera lens was focused on the HIFU's focus by adjusting the lens to achieve a sharp image.

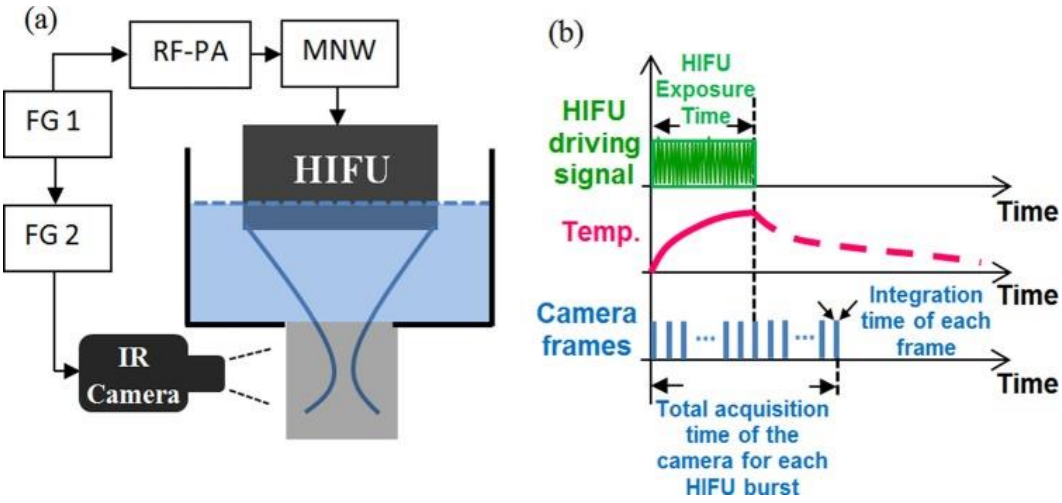

Figure 2-1 (a) A schematic diagram of the experiment system-1. FG: function generator; RF-PA: radio-frequency power amplifier; MNW: matching network; HIFU: high intensity focused ultrasound; IR: infrared. (b) A schematic diagram showing the time sequence of the entire system.

2.3.2 Signal processing:

To compare the measured UTFS (thermal focal size) with the acoustic focal size of the HIFU transducer in the silicone phantom, a similar method to the one described in Ref. [37] was adopted. Briefly, a hollow capillary tube (filled with air; CT-75-100-5, Paradigm Optics, Washington) was inserted into the silicone phantom and used as a small acoustic reflector. Its inner diameter was ~75 μm. A pulse transmitter-and-receiver (5073 PR, Olympus NDT, Massachusetts) generated a very narrow negative voltage pulse (peak voltage: ~−135 V; pulse rise time <2 ns and 4 μJ/pulse) to excite the HIFU transducer via the MNW. The HIFU transducer and the phantom were submerged into water. The HIFU transducer was well positioned so that the air-filled capillary tube was placed on the HIFU

focus. The reflected acoustic signal from the tube was collected and converted into electronic signal by the same HIFU transducer. The electronic signal was amplified by the pulse transmitter-and-receiver and digitized by an oscilloscope. The maximum peak-to-peak voltage of the reflected acoustic signal was recorded at each HIFU location. By scanning the HIFU transducer laterally and axially, the recorded signal can be plotted as a function of the HIFU location. The lateral and axial FWHMs were found as 0.55 and 2.8 mm, respectively, which was limited by acoustic diffraction [38]. Note that the measured FWHMs should represent the size of the acoustic intensity focus (rather than the size of the acoustic pressure focus). This is because the same transducer was used to transmit and receive the acoustic signal. Thus, the measured distribution represents the square of the one-way pressure distribution, which is equivalent to the intensity distribution [39]. This conclusion holds in conventional ultrasound imaging when a pulse-echo technique is used. Therefore, the measured lateral and axial FWHMs of the acoustic intensity focus also represent the lateral acoustic resolution and depth of field of the used transducer, respectively [39].

2.3.3 Results and discussion:

Figure 2-2 shows five typical and normalized IR images when the HIFU exposure power is 6.1, 9.5, 12.85, 15.65 and 16.64 W, respectively, and the HIFU exposure time is 0.1 s. Each IR image, in Figure 2-2, represents the frame acquired right after the end of the HIFU exposure when the temperature temporally reaches the peak value (see the bottom panel in Figure 2-1 (b)). Evidently, the results indicate that the UTFS significantly reduced when the HIFU exposure power increases. In addition, the axial location of the peak temperature slightly moves toward the HIFU transducer when the power increases, while the lateral location of the peak temperature remains fixed.

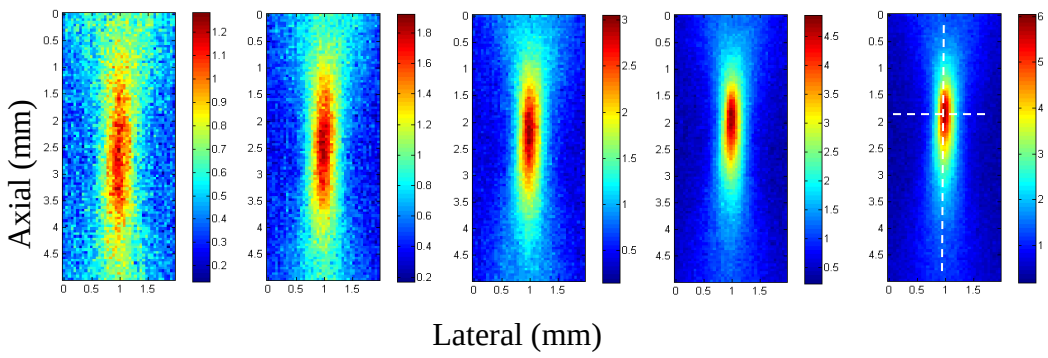

Figure 2-2 Normalized 2D temperature distribution acquired right after the 0.1 s HIFU exposure when the temperature temporally reaches the peak value with HIFU exposure power equal to (a) 6.1 (b) 9.5 (c) 12.85 (d) 15.65 and (e) 16.64 W. Both the two dotted lines in (c) pass through the maximum temperature and are used to plot the lateral and axial temperature profiles. A similar way was adopted for (a-d) to plot the profiles.

To quantitatively investigate UTFS, both the lateral and axial FWHMs of each image were calculated with reference to the peak temperature in each of the respective frame or IR image as shown in Figure 2-2. To calculate FWHMs a simple approach is adopted. The location of peak temperature in each of the frame is detected. Later, the lateral and axial line profiles that passed through these peak temperature locations were extracted (two dotted lines shown in Figure 2-2 (e)) and FWHM of the respective line profiles were calculated. Figure 2-3 (a) and (b) show the measured lateral and axial FWHMs, respectively, as a function of the HIFU exposure power. Evidently, when the power is relatively low (<~5 W for 0.2 s exposure time and <~8.8 W for 0.1 s exposure time), both the lateral and axial FWHMs are comparable to the measured diffraction-limited acoustic intensity focal size (indicated by the two dashed horizontal lines in Figure 2-3). In such cases, the lateral and axial FWHMs are less dependent on the power. On other hand,

when the power increases both the lateral and axial FWHMs of the temperature focus reduce significantly. This is mainly caused by the nonlinear acoustic effect. For example, the experimentally measured minimum lateral and axial FWHMs of the UTFS in Figure 2-3 (a) and (b) are 0.246 and 1.072 mm, respectively, for the HIFU exposure time of 0.1 s. In comparison, the diffraction-limited acoustic focal sizes are 0.55 (lateral) and 2.8 mm (axial), which are ~2.2 and ~2.6 times smaller to thermal FWHMs, respectively. On the other hand, with increase in HIFU exposure power, FWHMs also increases. This abrupt increase may be caused by HIFU-induced sample burning. Interestingly, Figure 2-3 implies that a smaller UTFS can be achieved with the exposure time of 0.2 s than the exposure time of 0.1 s at the same HIFU exposure power. Yet, this conclusion will not hold when the exposure time is long (such as seconds) since the thermal energy diffusion or conduction will be considerably predominant.

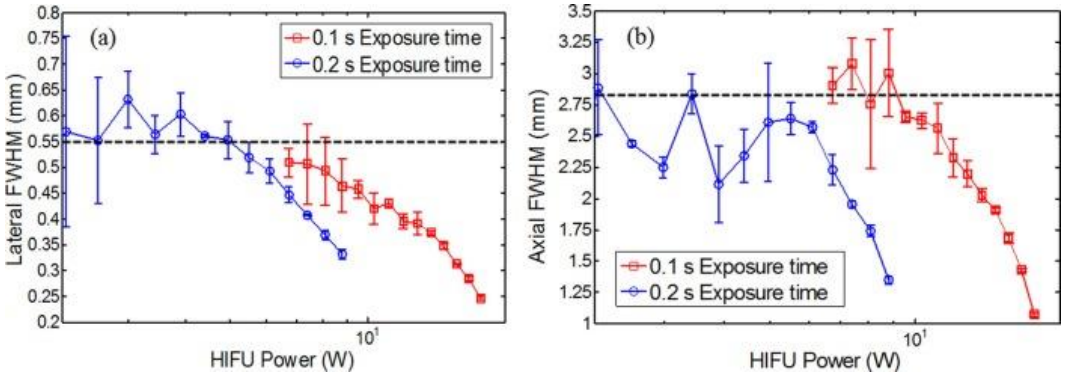

Figure 2-3 Measured (a) lateral and (b) axial FWHMs as a function of the HIFU exposure power.

To investigate the influence of exposure time of HIFU transducer on the HIFU-induced thermal sizes, the following figures (Figure 2-4 (a) and (b)) were generated. Here, the lateral and axial FWHMs of the UTFS are plotted as a function of the HIFU exposure

time, respectively. In case when the HIFU exposure power is low (0.38 W), depicted by lines with circles in Figure 2-4, both the lateral and axial FWHMs increase with the exposure time and they are much larger than the measured acoustic focal sizes (see the dashed horizontal lines in Figure 2-4). For example, for a very large exposure time of 20 s, the lateral and axial FWHMs can reach ~2.15 and ~6.0 mm, respectively. This noticeable increase in the UTFS is mainly caused by thermal diffusion. In comparison, when the HIFU exposure power is set to 13.75 W, depicted by the lines with squares in Figure 2-4, both the lateral and axial FWHMs (thermal sizes) are less the measured acoustic focal sizes. In addition, with increase in exposure time the thermal sizes decreased. This outcome suggests that the UTFS can be reduced below the diffraction-limited acoustic focal sizes. Therefore, by appropriately controlling the HIFU exposure power to stimulate the nonlinear acoustic effect and appropriately controlling the HIFU exposure time to confine the thermal energy in the focal volume, the UTFS can break the diffraction-limited acoustic focal sizes. For imaging purposes (instead of treatment purposes), the HIFU-induced peak temperature increase (ΔT_P) should be limited within a few Celsius degrees to avoid potential tissue thermal damage. ΔT_P was found to nonlinearly increase with the HIFU exposure power and exposure time when the nonlinear acoustic effect occurred.

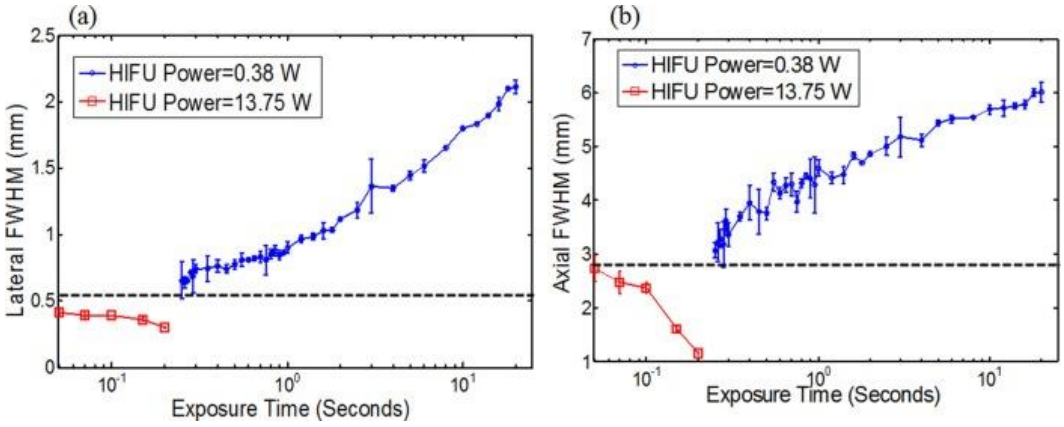

Figure 2-4 Measured (a) lateral and (b) axial FWHMs as a function of the HIFU exposure time.

Influence of nonlinear acoustic effect on the UTFS can be theoretically explained as follows: when nonlinear acoustic effect occurs, a part of acoustic energy at the fundamental frequency (f_0) can be transferred to higher harmonic frequency components (such as $2f_0$, $3f_0$, $4f_0$...) in the focal volume [36]. Higher frequencies of ultrasound have smaller focal volume. Therefore, higher order harmonic frequencies can be tightly focused compared with the fundamental frequency and hence is the major reason to reduce the UTFS. In addition, due to strong acoustic pressure, focal volume is formed by the fundamental frequency of HIFU transducer. This constraints the higher order harmonic frequencies to be generated only within this focal volume. Hence, the acoustic penetration depth is mainly determined by the fundamental frequency. Also, acoustic attenuation is considerably less for relatively low fundamental frequency (few MHz) of ultrasound energy thereby have large (a few centimeters) penetration depth. On other hand, when the heating time is longer than the characteristic time of thermal diffusion or conduction, smoothing of the spatial temperature distribution occurs [36]. Hence, to avoid thermal diffusion or conduction (known as thermal confinement) while confining the ultrasound-induced

temperature field within the heating source volume, the HIFU exposure time should be short [15]. Thus, acoustic nonlinear effect (controlled by HIFU exposure time) combined with thermal confinement (controlled by HIFU exposure time) can be adopted as a potential way to break acoustic diffraction limit for deep-tissue high-resolution imaging via USF- or UTF-based methods.

2.4 Materials and Methods – Consistency of induced temperature by HIFU transducer in chicken tissue.

2.4.1 System setup:

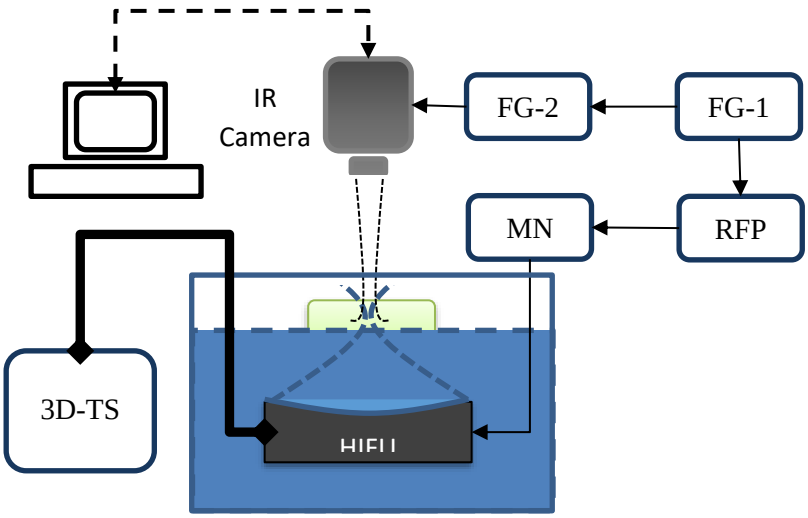

Figure 2-5 A schematic diagram of the experiment system-1-2

A schematic diagram of the experimental setup is shown Figure 2-5. The first function generator (FG 1, AFG3252, Tektronix, Oregon) provided a burst of sinusoidal waves at 2.5 MHz that was amplified by a radio-frequency power amplifier (RF-PA, 325LA, E&I, New York). The amplified signal was sent to the HIFU transducer (H108, Sonic

Concepts Inc, Washington) via a matching network (MNW). The HIFU transducer was submerged into a water bath and focused on the surface of the chicken tissue sample of thickness ~5-6 mm. Also, the HIFU transducer is mounted onto a 3-dimentional manual translation stage (3D-TS, PT-1, Thorlabs, NJ, USA) so that its focus can be moved to different locations on the surface of the tissue sample. It should be noted that, this study is performed to observe the consistency in thermal size only in lateral plane and induced temperature rise in its thermal region. While the FG 1 sent the driving signal to the HIFU transducer, it also triggered the second function generator (FG 2, Agilent 33220 A, California) so that the FG 2 provided pulses to trigger the IR camera (SC6100, FLIR, Massachusetts, USA) to acquire the temperature images. Thus, the HIFU exposure was always synchronized with the IR image acquisition. Figure 2-1 (b) schematically displays the time sequence of the entire system. While the HIFU began exposing (the upper panel), the temperature started increasing (the middle panel). At the same time, the IR camera was triggered to image the temperature distribution (the lower panel). Each frame was acquired by integrating 0.25 ms and multiple frames were acquired during and after the HIFU exposure. The total number of the frames was well controlled so that there is one frame right after the end of the HIFU exposure (see the frame overlapped with the dotted vertical line). This frame always showed the maximum temperature increase compared with other frames. The IR camera lens was focused on the surface of the tissue sample where the HIFU transduce is focused by adjusting the lens to achieve a sharp image. Note: the side of the tissue that is exposed to the IR camera is arranged such that it is just outside the water since IR camera is insensitive to temperature variations in water.

2.4.2 Signal processing:

High intensity focused ultrasound transducer focus was moved to multiple locations keeping the depth or axial focus of HIFU transducer always at constant depth and on the surface of the tissue sample. End-of-exposure frame is processed at each location with ~1.5 mm of distance between locations in ‘x’ or ‘y’ directions (lateral plane). Approximately 5x7 mm area is scanned on the tissue sample. Later each of the frames were normalized for each of the locations within the region of interest while recording temperature All the frames are combined into one image to observe the consistency of thermal size at different locations. For second set of data processing, three frames were selected, starting with End-of-exposure frame (EOE) and next two frames after the EOE frame with respect to time as shown in Figure 2-7. The thermal size and average temperature were calculated for each of this frames for each of the locations. This is performed to observe consistency the relatively variation of thermal size and temperature over time at different location in tissue sample.

2.4.3 Results and discussion:

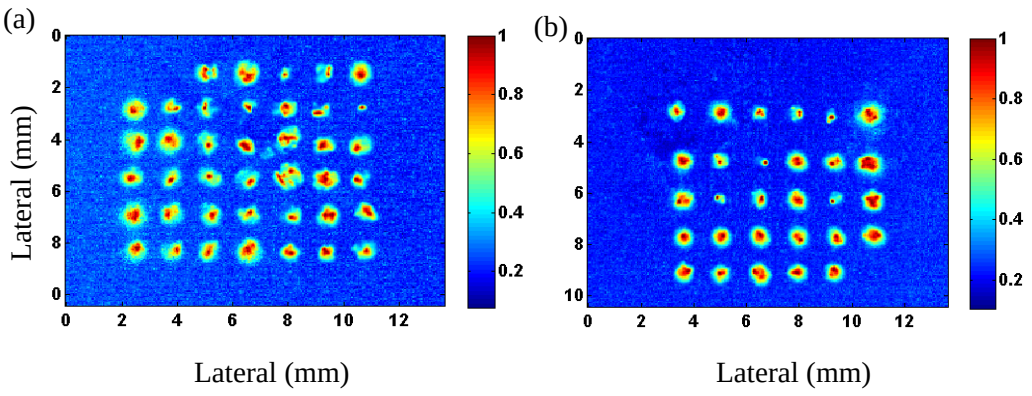

Figure 2-6 Normalized IR camera frame at end-of-exposusure(EOE) with (a) 30 ms and (b) 10 ms exposure time.

Figure 2-6 shows the normalized IR camera frame processed so that the normalized IR frames at end-of-exposure (EOE) from all the scanned locations are displaced in single image for exposure times of 30 ms and 10 ms Lower exposure time (at 10 ms and 30 ms) for HIFU transducer sonication was chosen to be studied to understand the induced thermal characteristics, like UTFS (spatial), thermal dissipation rate (temporal) and relative temperature change (SNR), and its consistency at different locations on the tissue phantom. It was observed that the thermal size (~0.55 mm) and average temperature rise (~4 degree Celsius) remained highly consistent and repeatable over an area of 5x7 mm which is typical scan area used by the USF system.

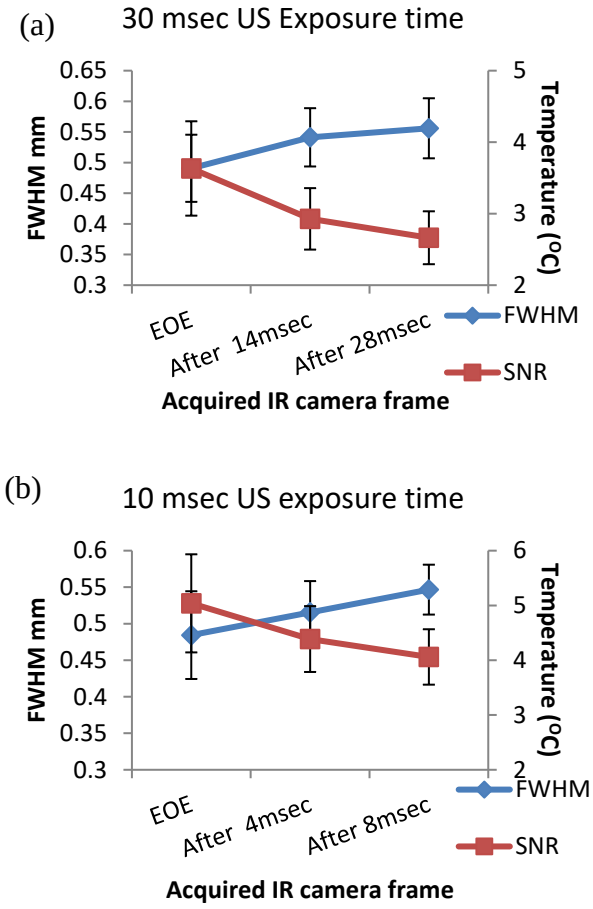

Figure 2-7 US induced thermal characteristics from multiple locations on chicken tissue surface

Figure 2-7 illustrates an comprehensive understanding of behavior of US induced temperature characteristics for 25 locations on the surface of the tissue phantom (chicken tissue). Figure 2-7 (a) and (b), corresponding to 30msec and 10 msec of HIFU exposure time respectively, shows UTFS (FWHM mm) and the relative temperature (IR counts / 53(calibrated value)) at end-of-exposure (EOE) and at two instances in time after EOE. It can be observed that the UTFS gradually increases and relative temperature gradually decreases over very small period of time (~tens of milliseconds) after the EOE. This is

understandable since the temperature diffusion is a complex phenomena and thus in nature a non-linear fast process that uniformly moves away from the point of exposure. This should hold for higher US exposure time since thermal diffusion for a given material is invariant. The repeatebility of constant temperature increase, around 4 degree Celsius, and UTFS consistency across 25 locations, on the surface of the tissue phantom, is also confirmed. This concludes that by using HIFU transducer with set driving parameters, a desired small temperature rise (here, ~4 degree Celsius) can be induced non-invasively within small volume (~0.55 mm in case of 2.5MHz, H108, Sonic concepts) with high consistency.

2.5 Summary and conclusion:

In summary, we experimentally demonstrated that ultrasound-induced temperature focal size can be significantly influence by the driving power and exposure time of HIFU transducer and is shown to reduce beyond the acoustic diffraction limit if nonlinear acoustic effect occurs and the ultrasound-induced thermal energy is confined within the focal volume. For USF- or UTF-based imaging techniques, the ultrasound-induced peak temperature increases only a few degrees. The nonlinear acoustic effect can occur by appropriately controlling the ultrasound exposure power, and the thermal confinement can be satisfied by appropriately controlling the ultrasound exposure time. Also, it was shown that thermal focal size and temperature rise remained consistent for small area of 5 x 7 mm for fixed parameters of HIFU transducer such as the exposure time, driving voltage and depth of focus of the transducer. Therefore, the proposed method in this study may be an alternative way to break the acoustic limit and can be potentially used for deep-tissue high-resolution imaging via USF or UTF techniques. High-resolution USF

imaging beyond the acoustic diffraction limit in deep tissues will be the focus of future studies.

Chapter 3

Improve sensitivity of Ultrasound-switchable Fluorescent Imaging using modulation of temperature

3.1 Introduction

Achieving both high signal-to-noise ratio (SNR) (and sensitivity) and high spatial resolution in deep tissue are highly desired in biomedical imaging [3, 11, 34, 40]. However, conventional imaging modality has a tradeoff between SNR (and sensitivity) and resolution. We recently developed a new imaging method for deep-tissue high-resolution imaging, which has been termed as ultrasound-switchable fluorescence (USF) [3, 11, 18, 19, 34, 40]. It has been demonstrated that USF can simultaneously achieve high SNR (or sensitivity) and high spatial resolution in tissue with a depth of centimeters [12, 13, 15, 21, 22, 31, 41]. In this study, we report a new method to further improve the SNR (or sensitivity) of the USF imaging without sacrificing the spatial resolution by modulating the ultrasound exposure. The modulation parameters and data processing methods are also investigated and compared.

The principle of USF imaging has been described in our recent publications [12, 13, 15, 21, 22, 31, 41]. For integrity, it is briefly introduced here. Two major components are included in USF imaging: (1) USF contrast agents and (2) an imaging system. When environment-sensitive fluorophores are conjugated on a thermo-sensitive polymer or encapsulated into a thermo-sensitive nanoparticle, the fluorescence intensity exhibits a switch-like function of the temperature. Below a temperature threshold (T_{th1}), the fluorophores either do not fluoresce or very weakly (i.e. at off state). When the temperature is above another threshold (T_{th2}), the fluorophores are completely switched on and emit strongly (i.e. at on state). Generally, the temperature difference between T_{th2} and T_{th1} is small (such as a few Celsius degrees). By using a high focused ultrasound transducer to

illuminate tissue, the temperature in the focal volume can be quickly increased a few Celsius degrees compared with the temperature outside the focal volume due to the tissue absorption of the ultrasound energy. Accordingly, the USF contrast agents within the focal volume can be switched on and generate fluorescence photons, which is called USF photons. Meanwhile, the contrast agents outside the focal volume remain off because the temperature is lower than the threshold (T_{th1}). By scanning the ultrasound focus point-by-point in the tissue, a high-resolution USF image can be generated. It has been well known that diffused (i.e. highly scattered) near infrared light can penetrate tissue several centimeters [33]. Therefore, USF imaging can achieve the similar depth [12, 13, 15, 21, 22, 31, 41].

We hypothesize that the SNR (or sensitivity) of the USF imaging can be improved by modulating ultrasound exposure via gating the high intensity focused ultrasound (HIFU) transducer. The gating signal applied on the transducer switches on and off the ultrasound exposure at a certain frequency, which further leads to the modulation of the temperature and the USF signal within the focal volume of the transducer. By detecting the modulated USF signal at this specific modulation frequency, the SNR (or sensitivity) can be increased.

3.2 USF imaging system

3.2.1 Hardware of the system

The diagram of the USF imaging system is shown in Figure 3-1 (a). The major components have been introduced in our previous publication [12, 21]. For integrity, we will very briefly introduce the entire system and emphasize the difference between current system and the previous USF system. Similar to the previous ones [12, 21], current USF sub-system includes the following modules: (1) an ultrasound heating and its driving

module, (2) an excitation light source, (3) a sample module, (4) an optical detection module and (5) a scanning module.

3.2.1.1 The ultrasound heating and its driving module.

A single element and water immersible HIFU transducer (H-108) was purchased from Sonic Concepts Ltd (Bothell, WA, USA) as shown in Figure 3-1 (a). It has a geometric focal length of ~50 mm and a central frequency of 2.5 MHz. Based on the manufacturer provided data, the lateral and axial pressure focal size are 0.51 and 3.28 mm, respectively. The HIFU transducer is driven by a function generator (FG-2, Agilent 33500B, Chicago, IL, USA) and a radio-frequency power amplifier (RFPA; 325LA, Electronics & Innovation, NY, USA). The exposure power of the HIFU transducer can be controlled by varying the peak-to-peak voltage (Vpp) of the 2.5-MHz sinusoidal wave from the FG-2. The exposure duration of the HIFU transducer is controlled by the width of the gating pulse train from another function generator (FG-1, AFG 3252, Tektronix, TX, USA). The FG-1 has two channels. The first channel of the FG-1 generates a gating pulse train that switches the FG-2 on and off. The number of pulses, the pulse width and the frequency ($f_{M\text{-}HIFU}$) can be programmed into the FG-1 and varied to generate different modulation patterns. The FG-1 is triggered by a pulse-delay generator (DG645, Stanford Research, Sunnyvale, CA, USA) which acts as a master trigger (MT) for the entire system as shown in Fig 1. MT is also responsible for triggering the data acquisition module to record data and will be discussed shortly. The second channel of the FG-1 is programmed to generate a continuous pulse train with the same frequency as the first channel ($f_{M\text{-}HIFU}$). This continuous pulse train is used as the reference for a lock-in amplifier (LIA-2; SR830, Stanford Research, Sunnyvale, CA, USA) to detect the HIFU-modulated USF signal. Note that the locked frequency by LIA-2 is $f_{M\text{-}HIFU}$ and is called HIFU-modulation frequency

(because it is the modulation frequency of the HIFU exposure), which is different from the optical modulation frequency discussed in next paragraph.

3.2.1.2 The excitation light source.

Similar to the previous systems [12, 21], a 671-nm laser (MLL-FN-671-500mW, Optoengine LLC, Midvale, UT, USA) was used as the excitation light and delivered to the bottom of the sample via a fiber bundle (OB-1). A bandpass filter of 671/11nm (FF01-673/11-25, Semrock, Rochester, NY, USA) was placed in front of the laser head to remove any unknown laser lines from the laser. The laser intensity was modulated into a sinusoidal wave at 1 kHz via the third function generator (FG-3, 33220A, Agilent, Chicago, IL, USA). The synchronized output (a 1-kHz square wave) from another channel of the FG-3 was used as a reference signal for another lock-in amplifier (LIA-1; SR830, Stanford Research, Sunnyvale, CA, USA) for detecting the 1-kHz fluorescence signal. Note that the locked frequency by LIA-1 is 1-kHz and is called optical modulation frequency ($f_{M\text{-}OPT}$) (because it is the modulation frequency of the optical exposure), which should not be confound with the previously discussed HIFU-modulation frequency ($f_{M\text{-}HIFU}$).

3.2.1.3 The sample configuration.

A silicone tube (ST; 60-011-01, Hellix Medical, Carpinteria, CA, USA) was filled with the solution of a USF contrast agent and embedded into a piece of porcine muscle tissue (Figure 3-1 (a) and (c)). Part I in Figure 3-1 (c) shows the *x-y* plane orientation which is the region scanned by HIFU transducer using the 3D-TS system (the USF images obtained in Figure 3-5 and Figure 3-7 corresponds to this scanning area). Part II in Fig.1(c), the *x-z* plane orientation corresponds to how the same sample with the embedded tube is arranged with respect to high intensity focused ultrasound (HIFU) transducer and the illumination of laser via optical bundle, OB-1, while performing the USF scanning. The

thickness of the muscle tissue was ~12 mm. The tube with an inner diameter (I.D) of 0.31 mm and an outer diameter (O.D) of 0.64 mm was located around the middle along the depth direction. The USF contrast agent is pluronic F98 nano-capsules in which fluorophores of aza-BODIPY conjugated with two hydroxyls at the bottom [denoted as $ADP(OH)_2$] were encapsulated .

3.2.1.4 The optical detection module.

Similar to the previous systems [12, 21], the emission photons were collected via another fiber bundle (OB-2) positioned on the top of the tissue sample. The collected photons were delivered to a collimation and filtering system for collimating the scattered photons and blocking the excitation light. This system consisted of the following components: (1) two NIR plano-convex lenses for collimation (L1 and L2, AC254-030-B, Thorlabs, Newton, NJ, USA), (2) two interference and two absorption filters for blocking exciting light (LP1 and LP2: 715-nm long pass interference filters, FF01-715/LP-25, Semrock, Rochester, NY, USA; RG1 and RG2: 695 nm long-wave pass cut-on filters, FSR-RG695, Newport, Irvine, CA, USA), and (3) two irises (IR1 and IR2, SM1D12SZ, Thorlabs, Newton, NJ, USA) for protecting the photo-detector by closing the optical path when needed and also controlling the aperture size for further blocking the background photons. The photons were eventually converted into electronic signal by a cooled photomultiplier tube (PMT, H7422-20, Hamamatsu, Bridgewater, NJ, USA) and further amplified by a low-noise pre-amplifier (PreAmp; SR570, Stanford Research, Sunnyvale, CA, USA). The electronic signal was input into the first lock-in amplifier (LIA-1; SR830, Stanford Research, Sunnyvale, CA, USA) for detecting the amplitude variation of the 1-kHz signal using the synchronized reference signal from the FG-3 (RS-1, at the same frequency of $f_{M\text{-}OPT}$ = 1-kHz).

In general, the 1-kHz optical signal consisted of both USF signal and background noise. As discussed previously [12, 21], the background noise mainly originated from: (1) laser leakage, (2) auto-fluorescence from the sample, and/or (3) fluorescence from those non-100%-off USF contrast agents. Fortunately, all these three components of the noise were independent of ultrasound. In contrast, the USF signal was uniquely controlled by the ultrasound (i.e. HIFU-induced temperature). Accordingly, the dynamic variation of the amplitude of the 1-kHz signal should follow the similar pattern as the variation of the HIFU-induced temperature. When the HIFU exposure was modulated with a central frequency of $f_{M\text{-}HIFU}$, the variation of the USF signal should have the same frequency. To sensitively detect this USF signal with the frequency of $f_{M\text{-}HIFU,}$ the output of the first lock-in amplifier LIA-1 was given as input to the second lock-in amplifier (LIA-2, SR830, Stanford Research, Sunnyvale, CA, USA). Reference for the LIA-2 (denoted as RS-2) was given from channel 2 of the FG-1 with the frequency of $f_{M\text{-}HIFU}$. Note that in this study the value of $f_{M\text{-}HIFU}$ was investigated based on signal-to-noise ratio. The time constant of LIA was set to less than 300 ms and the sensitivity varied between 50 to 500 mV nA depending upon the modulation pattern and signal strength. A national instrument data acquisition card (NI-DAQ; PCIE-6363, National Instruments, Dallas, TX, USA) was used to acquire the signals from both LIA-1 and LIA-2. The relationship among the modulation of the HIFU exposure, the HIFU-induced temperature modulation, the modulated excitation light, the modulated USF signal, the lock-in references and the outputs of the LIA-1 and LIA2 are schematically displayed in Figure 3-1 (b).

3.2.1.5 The scanning module.

The scanning module was the same as previous systems [12, 21]. Briefly, three motorized linear translational stages (3D-TS) were orthogonally stacked together to have

a 3D scanning capability (although in this study we only used 2D scanning) and controlled by the 3-axis programmable stepping motor controller (TS-CU). The controller was connected to a computer. A MATLAB GUI was programed to control the controller and further scan the HIFU transducer for acquiring USF images (in this study only 2D image was scanned).

(a)

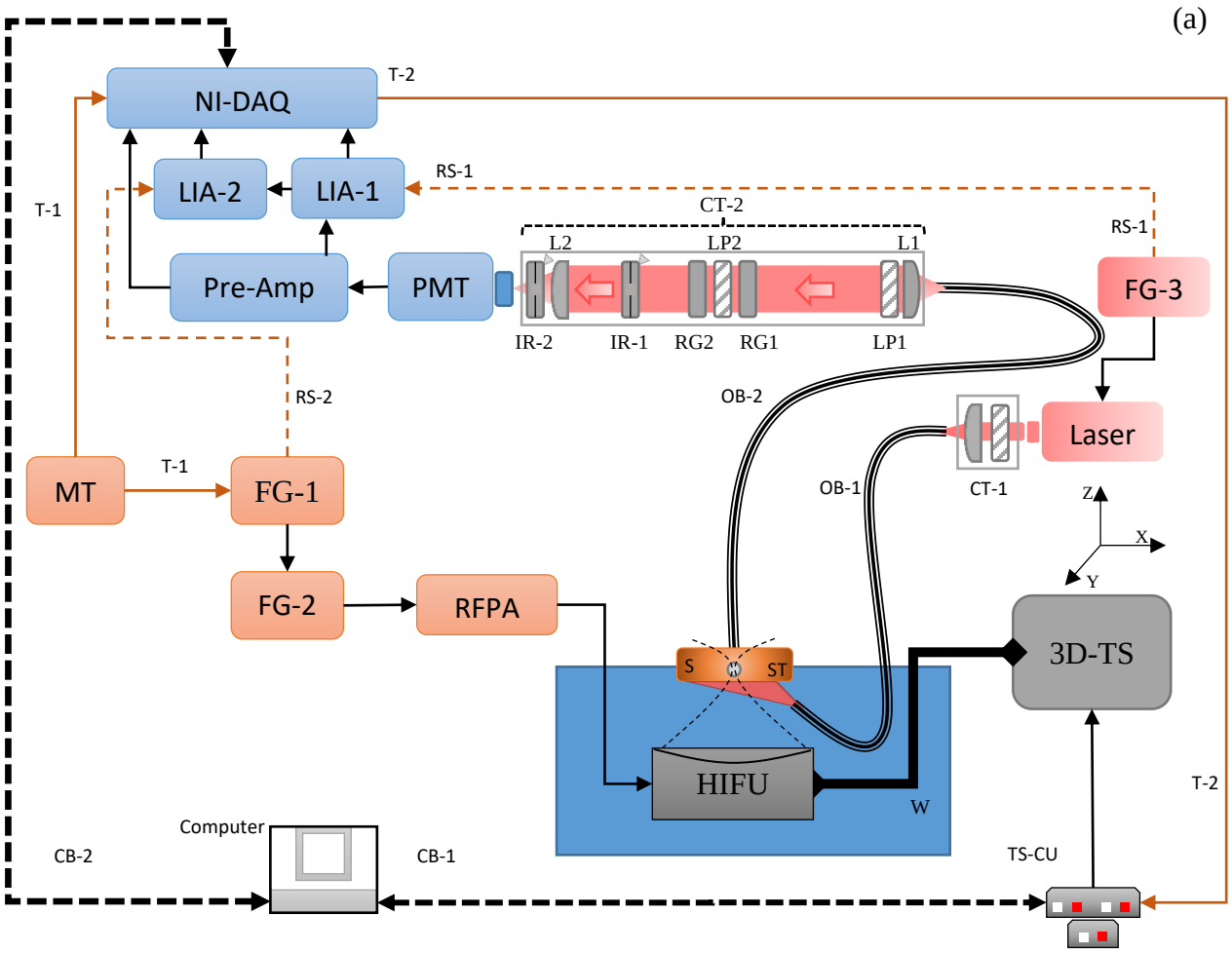

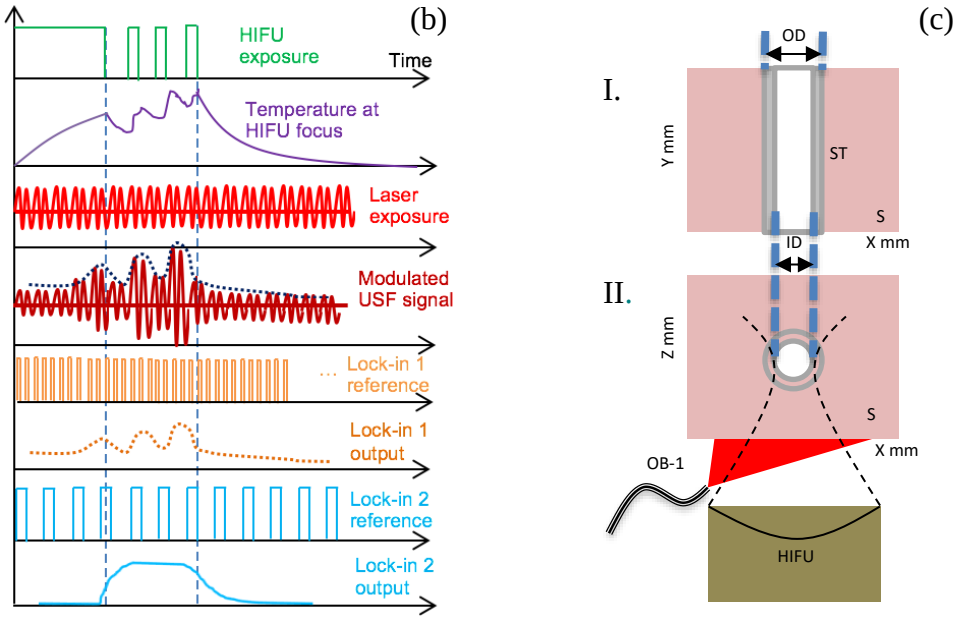

Figure 3-1 USF imaging using modulation of HIFU method (a) the experiment block diagram. (b) A schematic diagram of the time sequence of different signals. (c) Sample configuration including x-y (horizontal) and x-z (vertical) regions of USF Imaging. MT: A pulse delay generator serves as a master trigger (T-1) with 0.1-Hz frequency; FG-1: A function generator for gating the second function generator FG-2 to drive the HIFU transducer module (2.5MHz- HIFU), and generating a reference signal (RS-2) to LIA-2; FG-2: A function generator for driving the HIFU transducer by generating a 2.5 MHz sinusoidal signal and amplified by a radio frequency power amplifier (RFPA); FG-3: A function generator to modulate the excitation laser at a 1-KHz frequency and generate a reference signal (RS-1) for the lock-in amplifier; W: a water tank to immerse the HIFU transducer and partially immerse the sample (S); ST: A silicone tube with an inner diameter (ID) of 0.31mm and an outer diameter (OD) of 0.64mm; 3D-TS: the three dimensional translational stages; TS-CU: 3D translational stage motorized control units; CT-1: a collimation tube to focus the excitation laser into an optical bundle (OB-1); CT-2: an optimized collimation tube to guide the collected fluorescence from the optical bundle (OB-

2) to the photo detector (PMT) and best eliminate the excitation light and pass the emission light; PMT: A photo-multiplier tube to detect the optical fluorescence signal; Preamp: A preamplifier to amplify and filter the signal from the PMT; Laser: a 671- nm laser to irradiate the sample (S); LIA-1: A lock-in amplifier to detect the 1- KHz optical signal; LIA-2: A second lock-in amplifier to detect the signal with the HIFU-modulation frequency; Ni-DAQ: A national instrument data acquisition card; CB-1: serial communication bus to control TS-MCU; CB-2: communication bus to transfer data; RS-1: a 1-KHz reference signal for LIA-1; RS-1: a reference signal with the modulation frequency for LIA-2; T-1: a trigger signal for the NIDAQ card; T-2: a single cycle digital pulse signal to trigger the movement of the 3D-T.

3.2.2 System operational flow diagram:

The system operational flow diagram is shown in Figure 3-2. A master trigger (MT) started the entire system by triggering both the FG1 and the NI-DAQ. The typical duration of the optical signal acquisition was 4 to 8 seconds. Once all the data were acquired and stored, the MATLAB GUI will generate a voltage pulse via the output port of the NI-DAQ and trigger the Velmex 3D-translational stages to move to the next location. Care must be taken to ensure that the summation of the DAQ acquisition duration (4 to 8 seconds) and the movement duration of translational stages (less than 2 seconds) do not exceed the duration between the two adjacent master triggers. Hence, for this study, the master trigger was set to 0.1 – 0.05 Hz frequency (i.e. 10 to 20 seconds duration). The duration between the two master triggers determined the duration between the two scanning locations and thereby the overall duration of the system scan.

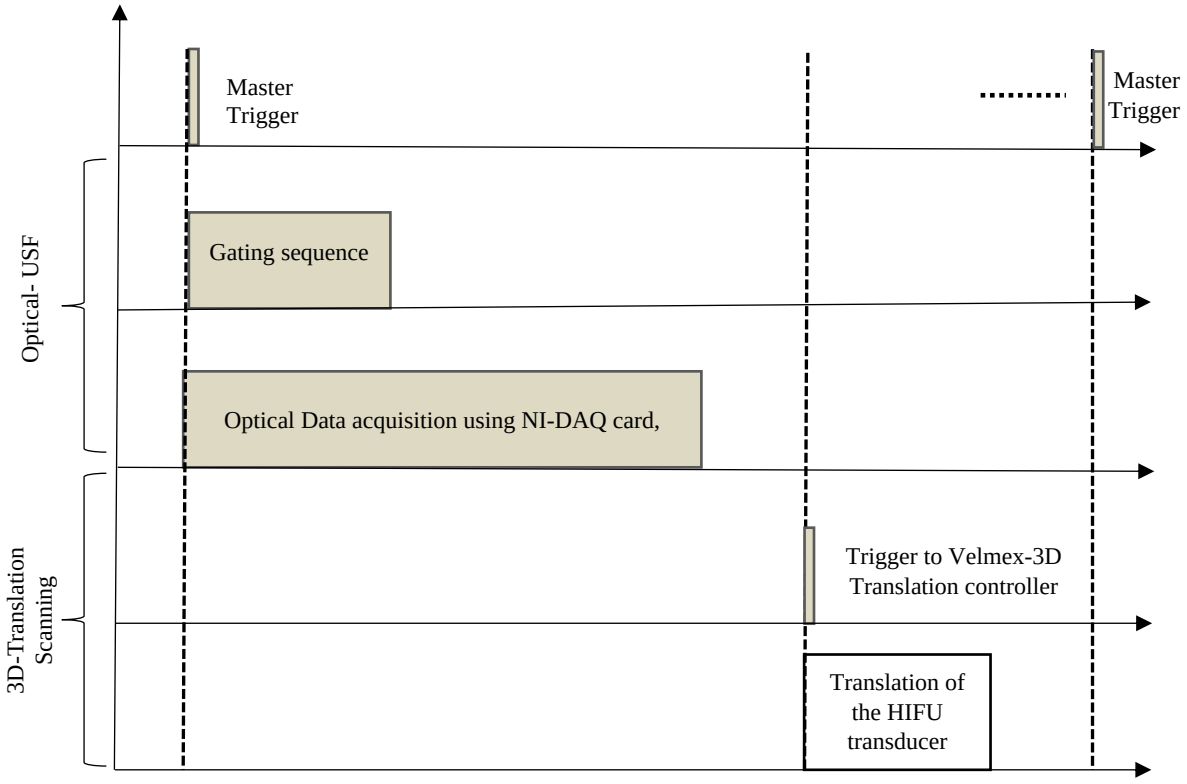

Figure 3-2 A time sequence diagram of the operation of the USF imaging system

3.2.3 HIFU modulation:

The HIFU modulation is schematically displayed in the second row in Figure 3-3. The shadowed areas represent that the HIFU is turned on and its duration is indicated as t_{on}. Otherwise, it means HIFU is off. The period of each cycle (T) is also indicated and equal to the inverse of the modulation frequency ($1/f_{M\text{-}HIFU}$). The duty cycle is defined as the percentage of the HIFU is turned on in one cycle, which is t_{on}/T multiplied with 100%. The total HIFU exposure time (T_{on}) is equal to the product between t_{on} and the number of the cycles.

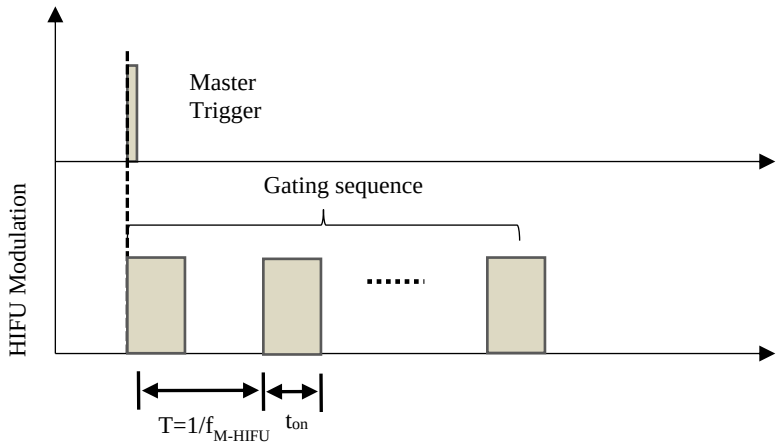

Figure 3-3 A time sequence diagram to show the HIFU modulation and related parameters.

3.3 Representations of USF signal strength:

In our previous studies, a single HIFU exposure pulse (with a typical pulse width of 300 ms) was adopted [12, 21]. The processing of previous USF data was as follows. The NI-DAQ card acquired the dynamic change of the amplitude of the 1-kHz signal before, during and after the HIFU heating. The difference between the maximum amplitude and the background amplitude (acquired before HIFU exposure) was used as the USF signal strength at each location. After scanning the HIFU transducer or sample, an image was acquired based on the calculated USF strength.

In this study, because the HIFU exposure was different from that in our previous work [12, 21], the data acquisition and processing were different too. The time constant of the LIA-1 was kept at 10 ms when the HIFU modulation frequency ($f_{M\text{-}HIFU}$) was 1 and 2 Hz. The sensitivity of the LIA-1 was kept at 200-500 mV nA. The sensitivity of the pre-amplifier is set to 50 nA/V for low-noise mode.

At each location of the HIFU transducer, three sets of data were simultaneously acquired. They were the data acquired from: 1) the pre-amplifier (Pre-Amp), which included the signals with both modulation frequencies ($f_{M\text{-}OPT}$ and $f_{M\text{-}HIFU}$); 2) the LIA-1, which was sensitive to the signal with the frequency of $f_{M\text{-}OPT}$ (i.e. 1-kHz) and detected its amplitude variation (at the frequency of $f_{M\text{-}HIFU}$); 3) the LIA-2, which was sensitive to the signal with the frequency of $f_{M\text{-}HIFU}$ and detected its strength. The relationships among these three sets of data are shown in Figure 3-4 and more details will be discussed in the section 3.5.

To quantify the USF strength at each location, Table 3-1 shows four methods (a-d) to process the acquired data. For data acquired from the pre-amplifier, the amplitude of the Fourier transform of the acquired signal at the frequency of $f_{M\text{-}HIFU}$ was adopted to represent the USF strength, which was the method (a) in Table 3-1. [Note that the raw signal acquired from the pre-amplifier is an amplitude-modulated (at the frequency of $f_{M\text{-}HIFU}$) sinusoidal wave (at a frequency of $f_{M\text{-}OPT}$)]. For data acquired from the LIA-1, the amplitude of its Fourier transform at the frequency of $f_{M\text{-}HIFU}$ was adopted to represent the USF strength, which was the method (b) in Table 3-1. (Note that the data acquired from the LIA-1 is a signal with a frequency of $f_{M\text{-}HIFU}$, which represents the amplitude profile of the signal from the pre-amplifier). For data acquired from the LIA-2, the maximum and the mean of the acquired signal (within a time window of the total duration of the HIFU exposure) were used to represent the USF strength, which were the method (c) and (d) in Table 3-1, respectively.

Table 3-1 Summary of the four methods to calculate USF signal strength. The letter (a)-(d) corresponds to the figure sequence in Figure 3-5.

Location where the signal was acquired	**Method of processing the data for representing the USF signal**

Pre-amplifier (a signal with frequency of $f_{M\text{-}OPT}$ but the amplitude was modulated at a frequency of $f_{M\text{-}HIFU)}$	(a) The amplitude of the Fourier transform of the acquired signal at the frequency of $f_{M\text{-}HIFU}$	
LIA-1 (a signal with a frequency of $f_{M\text{-}HIFU}$, which represents the amplitude profile of the signal from the pre-amplifier)	(b) The amplitude of the Fourier transform of the acquired signal at the frequency of $f_{M\text{-}HIFU}$	
LIA-2 (a quasi-DC signal, which represents the amplitude profile of the signal from the LIA-1)	(c) The maximum of the acquired signal within the time window	(d) The mean of the acquired signal within the time window.

3.4 USF contrast agents

The USF contrast agent used in this study was $ADP(OH)_2$-encapsulated Pluronic-F98 based thermos-sensitive nano-capsules. The details can be found in our previous publications [31]. The initial concentration of Pluronic-F98 in deionized water is 50 mg/ml. The peak excitation and emission wavelengths were around 680 and 715 nm, respectively. The temperature threshold (T_{th1}) is about 28 ^oC, which is slightly lower than our previous results [12] and may be because of different fluorophores, some measurement errors and/or bench variation.

3.5 Results and Discussions

3.5.1 Demonstration of USF modulation:

To demonstrate how USF signal is modulated by the variation of HIFU exposure, we show a set of USF signals in Figure 3-4, which were acquired respectively from the three different locations as described above. Specifically, the HIFU was turned on and off at a frequency of 1 Hz ($f_{M\text{-}HIFU}$) with a duty cycle of 10% and a total duration of 3 seconds.

This means within one second the HIFU was turned on 0.1 s and off 0.9 s and this on-and-off cycle was repeated three times. To be able to clearly visualize the modulation of USF signal, a relatively high signal-to-noise ratio (SNR) was adopted.

Figure 3-4 (a), (b) and (c) respectively show the acquired USF signals from the pre-amplifier, LIA-1 and LIA-2. The signal acquired from the pre-amplifier is an amplitude-modulated 1-kHz signal (i.e. $f_{M\text{-}OPT}$ =1 kHz and $f_{M\text{-}HIFU}$=1 Hz). The amplitude modulation can be seen from the three large and negative peaks (Figure 3-4 (a)). Note that the negative sign is caused by the PMT because usually a PMT generates a negative signal when optical intensity is increased. As discussed above, the LIA-1 functions as a demodulator to extract the variation of the amplitude of the 1-kHZ signal. Figure 3-4 (b) clearly shows the 1 Hz USF signal with 3 cycles, which represents the profile of the Figure 3-4 (a) after inverting the signal. Similarly, the LIA-2 functions as the 2nd demodulator to extract the profile of the 1 Hz modulation signal. Figure 3-4 (c) displays a quasi-DC (quasi direct current) signal, which represents the amplitude profile of the signal from the LIA-1 and proportional to the strength of the 1-Hz modulated USF signal.

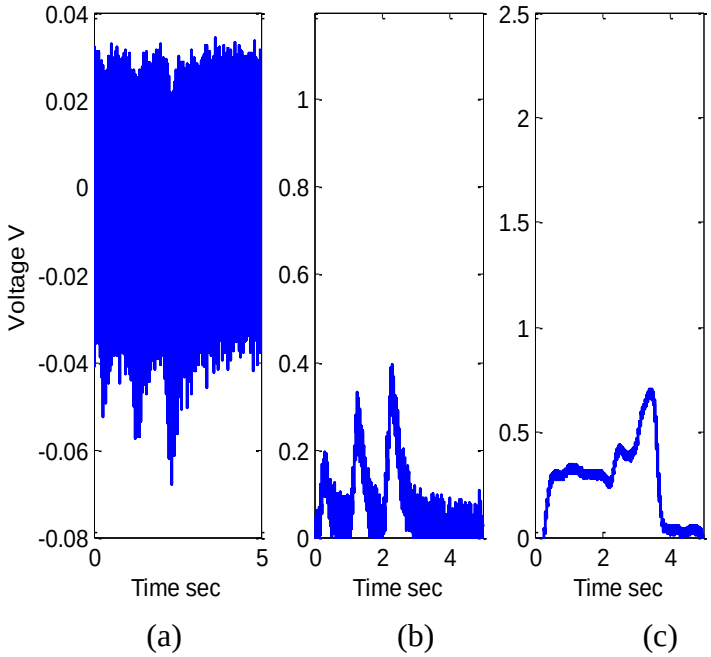

Figure 3-4 An example to show the modulation of USF signal at 1 Hz with 3 cycles and a 10% duty cycle) acquired from different locations: (a) acquired from the pre-amplifier, (b) acquired from the LIA-1, and (c) acquired from the LIA-2.

3.5.2 USF images using HIFU modulation method:

Figure 3-5 shows the normalized 2D USF images of a silicone tube (I.D=0.31 and O.D=0.64 mm) embedded in a piece of porcine muscle tissue with a thickness of ~12 mm. The 2-D USF images are obtained along the x-y plane across the silicone tube, as shown by the red dashed line in Figure 3-1 (c). Figure 3-5 (a)-(d) respectively display the USF images processed using the four methods discussed in Table 3-1 and Table 3-2. The details about the sample has been described in the section of the sample configuration. The HIFU modulation frequency is 2 Hz with a 10% duty cycle and a total of three cycles (controlled by FG-1). Thus, the total HIFU exposure time is 150 ms (i.e. the sum of three 50-ms on cycles). The driving signal of the HIFU is a 2.5-MHz sinusoidal waveform that is

generated by FG-2, gated by FG-1 and amplified by RFPA. The peak-to-peak voltage of the driving signal from the FG-2 is ~0.1 volt and after being amplified 50 dB by the RFPA the signal is ~32 volts at HIFU transducer.

In general, all the four methods clearly showed the tube via the modulation of USF. The full-width-at-half-maximum (FWHM) and SNR of each USF image were quantified and summarized in Table 3-2. The FWHMs of the USF images fall into the range from 0.95 to 1 mm, which is slightly larger than the tube O.D. and in agreement with our previous study [12]. This is because both studies used the same HIFU transducer that is the major factor determining the USF resolution. The SNRs of these USF images in Figure 3-5 are in the range from 62 to 114. The method (b) achieved the highest SNR of 114. Currently, it is unclear why the SNRs achieved by the methods of (c) and (d) are lower than the methods of (a) and (b). Further studies should be conducted to address this question in future.

Unlike FWHM, these SNRs are higher than what we achieved in our previous study where no HIFU modulation was adopted and other experimental conditions were similar [12]. Specifically, in our previous study [12], when the HIFU exposure was a single 300-ms burst (no modulation), the SNR was achieved ~40 in the similar sample using a time constant of 30 ms for LIA-1 (only one LIA was adopted in reference [12]). After using a correlation method in our previous studies [12], the SNR was improved from ~40 to ~95 that falls into the range of the current SNR values. This result indicates that the method developed in current study (i.e. the modulation of USF) is comparable to the correlation method developed in our previous study [12]. Mathematically, this is understandable because both modulation and correlation follow the similar rule to recognize signals, which is to encode USF signal with a unique temporal pattern and uses a reference to extract the signal. The method of modulation encodes USF signal with a specific frequency ($f_{M\text{-}HIFU}$)

while the correlation method takes advantage of the natural dynamic change of the USF signal to differentiate USF signal from the background noise. Note that the correlation method in our previous study [12] can be considered as a software-based off-line processing method, while the current method encodes the USF signal at a specific modulation frequency and can be considered a hardware-based online processing method. Another major difference is that the method of modulation has a specific modulation frequency so that the detection bandwidth may be narrower than that of the correlation method. Thus, the SNR (or sensitivity) of the modulation method should be relatively higher. If the SNR or sensitivity is similar, the applied HIFU power and/or exposure time should be lower or shorter. This is true if we compare the HIFU exposure parameters in our current and previous studies [12]. In current study, the HIFU was turned on totally 150 ms during a period of 1.5 second. In our previous study [12], the HIFU was turned on a total of 300 ms while the HIFU exposure power is similar. Thus, the HIFU-induced temperature in the focal volume should be lower in current study. Finally, we conclude that, compared with the non-modulation method but processed with the correlation algorithm [12], current modulation method can achieve the similar SNR but shorten the HIFU exposure time by half. Furthermore, compared with the non-modulation method without using the correlation algorithm, current method not only achieves higher SNR but also uses shorter exposure time. Therefore, although the modulated HIFU exposure may lead to lower temperature rise compared with that of continuous wave HIFU exposure, the SNR may not be sacrificed because of the higher sensitivity.

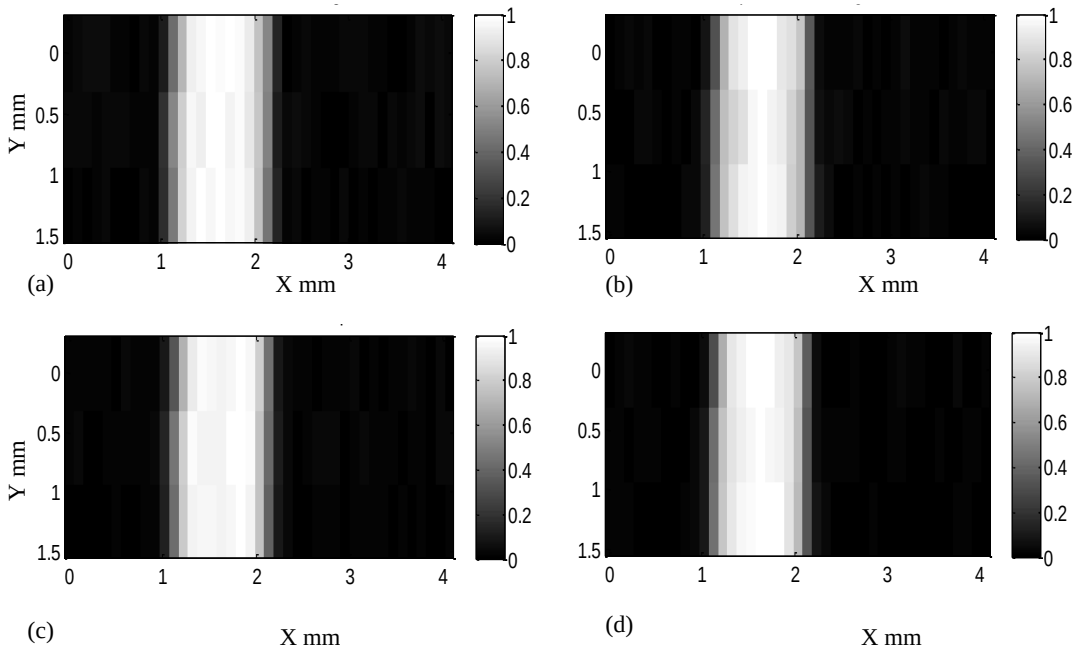

Figure 3-5 Normalized 2D USF images of the small tube embedded in the tissue sample. The images were processed using the four different methods of (a)-(d) in Table 1 and 2. The HIFU modulation pattern is 2 Hz with a 10% duty cycle and a total of 3 cycles.

Table 3-2 Calculated FWHMs and SNRs of USF images using different analysis methods.

	(a) FFT OF USF signal	*(b)* FFT of LIA-1	*(c)* Max of LIA-2	*(d)* Mean of LIA-2	Non-modulation USF
FWHM (mm)	0.95	0.95	1	0.96	~1.1
SNR	86	114	75	62	~40/~95

3.5.3 *Effect of the modulation frequency ($f_{M\text{-}HIFU}$) and duty cycle on USF images:*

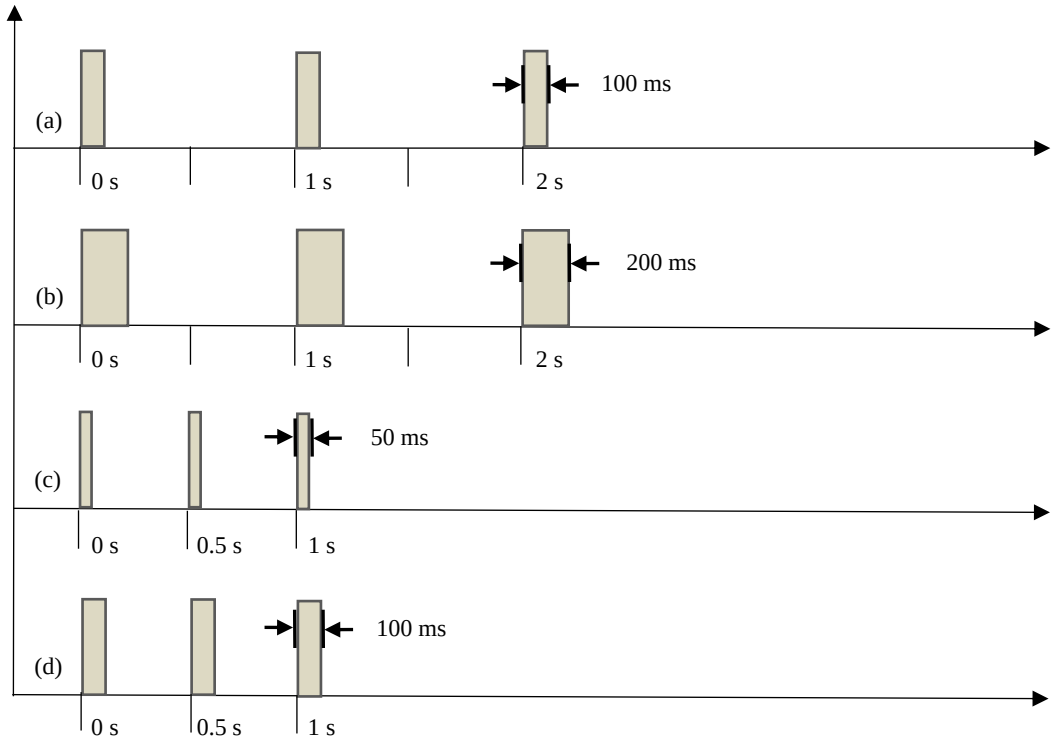

Figure 3-6 The time sequence diagram of four different HIFU modulation patterns: (a) 1 Hz with a 10% duty cycle, (b) 1 Hz with a 20% duty cycle, (c) 2 Hz with a 10% duty cycle, and (d) 2 Hz with a 20% duty cycle. All modulation patterns have 3 cycles.

Figure 3-6 shows the time sequence diagram of four different HIFU modulation patterns. Figure 3-6 (a) and (b) have a modulation frequency of 1 Hz with a duty cycle of 10% and 20%, respectively. Figure 3-6 (c) and (d) have a modulation frequency of 2 Hz with a duty cycle of 10% and 20%, respectively. There are three cycles for each HIFU exposure modulation. Figure 3-7 illustrates the normalized 2D USF image acquired from the four HIFU exposure patterns. Note that these images were processed using the method

of FFT of the LIA-1 output (method (b) in Table 3-1) since this method has relatively higher SNR in comparison to other methods.

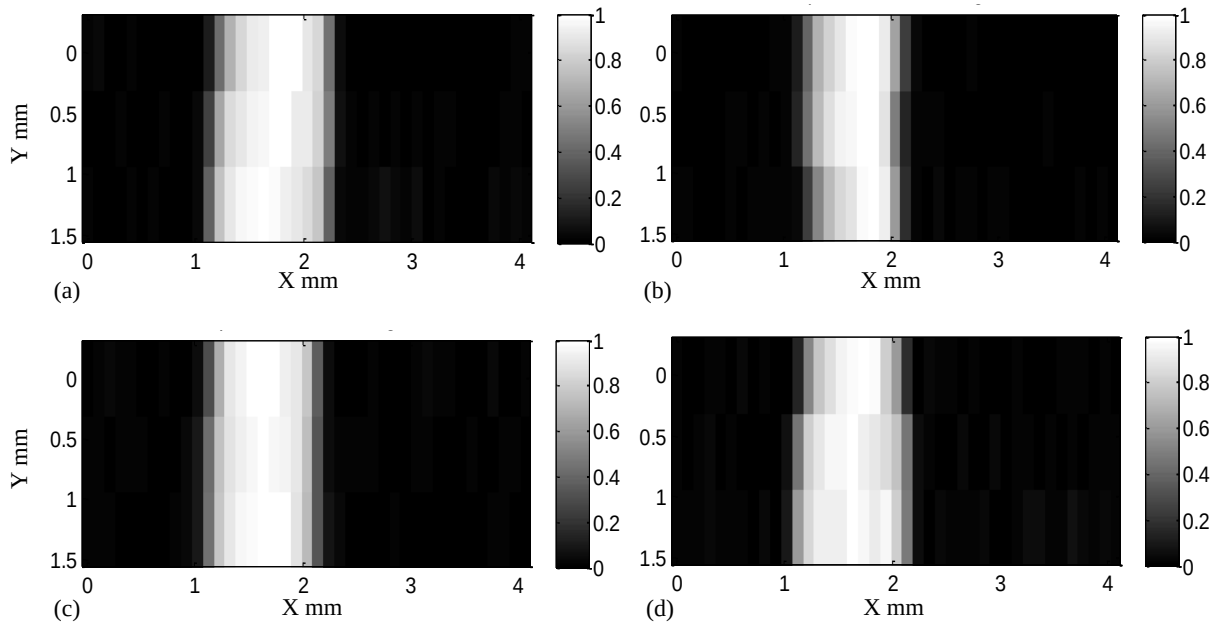

Figure 3-7 Normalized 2D USF images of the small tube embedded in the tissue sample with four different HIFU modulation patterns: (a) 1 Hz with a 10% duty cycle, (b) 1 Hz with a 20% duty cycle, (c) 2 Hz with a 10% duty cycle, and (d) 2 Hz with a 20% duty cycle. All modulation patterns have 3 cycles. The images were processed by using the method of the FFT of the LIA-1 signal.

Table 3-3 Calculated SNRs of USF images using the different analysis methods at different HIFU modulation exposures.

	(a) FFT of USF signal	(b) FFT LIA-1	(c) Max LIA-2	(d) Mean LIA-2
(a) 1Hz-10%-3cycles	76	144	67	50
(b) 1Hz-20%-3cycles	152	175	87	65

(c) 2Hz-10%-3cycles	86	114	75	62
(d) 2Hz-20%-3cycles	77	90	61	43

The SNRs are summarized in Table 3-3 for the four different HIFU modulation exposures. For $f_{M\text{-}HIFU}$=1 Hz, when increasing the duty cycle from 10% to 20% (i.e. from (a) to (b) in Table 3-3), all the SNRs acquired from the four processing methods increase obviously and consistently. This result can be explained using the concept of temperature modulation depth, which is usually defined as the ratio between the difference and the sum of the maximum and minimum temperature values. The above result indicates that the modulation depth of the HIFU-induced temperature increases with the increase of the duty cycle for these two cases. This is understandable because the higher duty cycle means longer HIFU exposure time for each cycle and therefore higher temperature rise and stronger USF signals. On the other hand, the time period when HIFU remains off is longer enough for these two cases to allow the temperature decreasing to generate the modulation pattern. This is because the modulation frequency is 1 Hz and the time period when HIFU remains off in each cycle is 0.9 and 0.8 s for the 10% and 20% duty cycle, respectively. Both values are usually longer than the thermal diffusion time constant in the adopted tissue phantom. Thus, the difference between the maximum and minimum temperature is large, which lead to large modulation depth and therefore high SNR.

However, when the HIFU modulation frequency increases to 2 Hz, rising the duty cycle from 10% to 20% (i.e. from (c) to (d) in Table 3-3) leads to slight and consistent decrease of SNRs. This results indicates that the modulation depth is reduced when increasing the duty cycle for 2-Hz exposure. This may be because the time period when HIFU remains off is not long enough to allow the temperature decreasing. For the

modulation frequency is 2 Hz, the time period when HIFU remains off in each cycle is 0.45 and 0.4 s for the 10% and 20% duty cycle, respectively. These two values may be close to the thermal diffusion time constant in the adopted tissue phantom. Thus, reducing the time period of off-cycle will limit the cooling time and therefore the temperature may not be able to reduce down enough. Accordingly, both the modulation depth and SNR reduce.

Comparing all the four modulation patterns, the SNRs achieve the highest level for all the four processing methods when $f_{M\text{-}HIFU}$=1 Hz with the 20% duty cycle (i.e. (b) in Table 3-3). In contrast, the SNRs fall down the lowest level when $f_{M\text{-}HIFU}$=2 Hz with the 20% duty cycle (i.e. (d) in Table 3-3). Lastly, the SNRs of the rest two cases (i.e. (a) and (c) in Table 3-3) are in between and also their SNRs are comparable. Therefore, the modulation pattern (a), $f_{M\text{-}HIFU}$=1 Hz with the 20% duty cycle, is the best of choice for this study. In addition, comparing all the four processing methods, the FFT of the signal from the LIA-1 always provides the highest SNRs, followed by the methods of the FFT of the filtered USF signal. The SNRs of the rest two methods where two LIAs were used are relatively lower for all the four HIFU exposure patterns. The reasons are unclear and should be investigated in future.

3.6 Conclusion

In conclusion, an innovative USF imaging method is developed in this study by modulating HIFU exposure at a specific frequency ($f_{M\text{-}HIFU}$=1-2 Hz) with a small duty cycle (10-20%). Thus, the temperature at the HIFU focal volume is modulated, which leads to the modulation of USF signal at the same modulation frequency. By specifically detecting this USF signal, the SNR of USF image (or equivalently the detection sensitivity) should be significantly improved. The modulation of USF signal has been clearly demonstrated.

Compared with our previous methods (without modulation and without processed by the correlation method), the SNR is significantly improved. A total of four HIFU modulation methods and four signal processing methods have been investigated. The highest SNR level is achieved by modulating the HIFU at $f_{M\text{-}HIFU}$=1 Hz with the 20% duty cycle and processed by using FFT of the signal from the first lock-in amplifier (LIA-1).

Chapter 4

Improve axial resolution of Ultrasound-switchable fluorescent Imaging using dual-HIFU transducer setup

4.1 Introduction

Simultaneous imaging of multiple targets (SIMT) with high spatial resolution is highly desirable and important in many biological and medical studies in which two or more bio-targets (such as biomarkers, molecules, proteins, cells, blood vessels, nerves/neurons, or signaling pathways) are involved and/or their interactions are interested, such as cancer metastasis, cancer angiogenesis, and neurovascular coupling. For example, when and how cancer cells metastasize into a blood vessel in an in-situ tumor is a crucial question for understanding and preventing cancer metastasis. Simultaneous imaging of both cancer cells and blood vessels provides a way to investigate their interactions. Another example is that multiple signaling pathways have been found to possibly regulate angiogenesis in most solid tumors. Therefore, compared with single target therapy, combination therapy, which means simultaneous use of multiple targeting drugs, has great potential to increase the treatment efficiency by simultaneously blocking multiple signaling pathways [42, 43]. Accordingly, SIMT can visualize multiple signaling pathways and their interactions [5, 44], which can significantly benefit to the investigation of drug resistance mechanisms and the monitoring or evaluation of targeted therapies [42, 45-50]. Unfortunately, to date, few techniques are available for SIMT [50-52]. Fluorescence techniques are highly sensitive and have potential to conduct SIMT based on spectroscopic methods. However, they suffer from poor spatial resolution (a few millimeters) when imaging relatively deep tissue (centimeters) due to strong light scattering of tissue [7, 33, 53-56]. Ultrasound, photoacoustic, and fluorescence technologies have been implemented into one system for multi-modality imaging [57, 58]. In this type of study, ultrasound waves do not physically

interact with fluorescence photons and therefore the spatial resolution of the fluorescence image does not improve. Recently, we developed a new technique, “ultrasound-switchable fluorescence” (USF) based on our recent finding that a focused ultrasound wave can potentially switch fluorescence emission on and off [17]. In USF, the excitation light is delivered into deep tissue via light scattering. When ultrasound is off, the USF agents are off although the excitation light is on. Ideally, no fluorescence is emitted. When ultrasound is on, only the USF agents in the ultrasound focal volume can be switched on to emit fluorescence. The emission photons can propagate out of the tissues via light scattering. Thus, USF can provides fluorescence images of deep tissue with ultrasonic resolution [17, 37, 59-61]. Compared with pure fluorescence techniques, USF overcomes the limitation of the spatial resolution caused by tissue light scattering. Compared with pure ultrasound techniques (US), USF can conduct SIMT based on fluorescence spectroscopy. This study aims to address the following challenge in USF imaging by developing a dual-modality ultrasound-switchable fluorescence and ultrasound system for both optical and acoustic imaging. Currently, USF can provide in-plane fluorescence images on the x-y horizontal plane with excellent resolution. This is because its axial resolution along z direction, which is the ultrasound wave propagation direction, is ~4–7 times lower than its in-plane lateral resolution (i.e., along x or y direction). Thus, it degrades the image quality along z direction, which is also true for optical microscopy. On the other hand, ultrasound B-mode image shows tissue information on a vertical plane (i.e., x-z or y-z plane, so-called tissue cross section plane). In this study, to improve USF axial resolution and be able to co-register USF with ultrasound B-mode imaging, we developed a new dual-modality imaging system via a customized ultrasound transducer that includes two confocal 90^{O}-cross transducers. This new system can simultaneously image tissue cross-section (i.e., x-z plane) using USF and ultrasound B-mode technologies. We demonstrated that USF simultaneously imaged

the distribution of two fluorophores with different excitation and emission spectra for the purpose of SIMT via the optical spectroscopic technology in a tissue phantom. On the other hand, a co-registered B-mode ultrasound image shows the acoustic structure of the tissue phantom. In summary, we improved USF axial resolution, achieved multi-color USF imaging on the cross section plane of the tissue sample for future SIMT, and lastly co-registered USF and B-mode ultrasound imaging for simultaneous dual-modality imaging.

4.2 Dual-Modality Imaging System

4.2.1 Basic Principles of USF and US Imaging

The principle of USF imaging based on fluorophore-encapsulated thermo-sensitive nanoparticles has been described in our recent publications [12, 13, 15, 21, 43]. Briefly, there are two key components in USF imaging: excellent USF contrast agents and a sensitive USF imaging system. Recently, we developed a serial of thermo-sensitive fluorescent nanoparticles [12, 13, 21]. When encapsulating environment-sensitive fluorophores into a thermo-sensitive nanoparticle, the fluorescence emission shows a switch-like function of the temperature. When the temperature is lower than a threshold (T_{th1}), the fluorophores either do not fluoresce or fluoresce very weakly (so-called OFF). When the temperature is higher than another threshold (T_{th2}), the fluorophores fluoresce strongly (so-called ON). If the temperature difference between the two thresholds (T_{th2}-T_{th1}) is narrow (such as a few degrees Celsius), these nanoparticles are called fluorescence switchable contrast agents. When a relatively strong and long strong and long ultrasound pulse (200 ms long in this study) is focused into tissue, the temperature in the focal zone can be increased a few degrees Celsius due to the absorption of the acoustic energy. Thus, the contrast agents in the focal zone can be switched on to emit fluorescence, while

contrast agents outside the focus remain off. A high-resolution USF image can be generated when scanning the ultrasound focus point-by-point. Note that the delivery of the excitation light and the collection of emission light are based on highly scattered near-infrared photons, USF can image tissues several centimeters deep [12, 13, 15, 21].

In this study, the conventional ultrasound B-mode imaging principle is adopted. Briefly, a relatively short ultrasound pulse (microseconds long in this study) was sent into tissue samples and the echoes reflected from different depths due to the acoustic impedance mismatch were detected. At each location, an averaged A-line was acquired. The envelope profile of this A-line was calculated, which represented tissue's acoustic information along the depth direction (i.e., *z* direction in this study). By scanning the transducer laterally (i.e., *x* or *y* direction in this study), a serial of A-lines was acquired. Thus, by displaying the envelope profiles of all the A-lines in one figure, a B-mode ultrasound image was generated. Accordingly, a line scanning was conducted for B-mode ultrasound imaging, which is different from USF's point scanning strategy.

4.2.2 Hardware of the System

The block diagram of the dual-modality imaging system is shown in Figure 4-1 (a). It includes three sub-systems: (1) USF for fluorescence imaging; (2) US for B-mode acoustic imaging; and (3) synchronization of USF and US sub-systems.

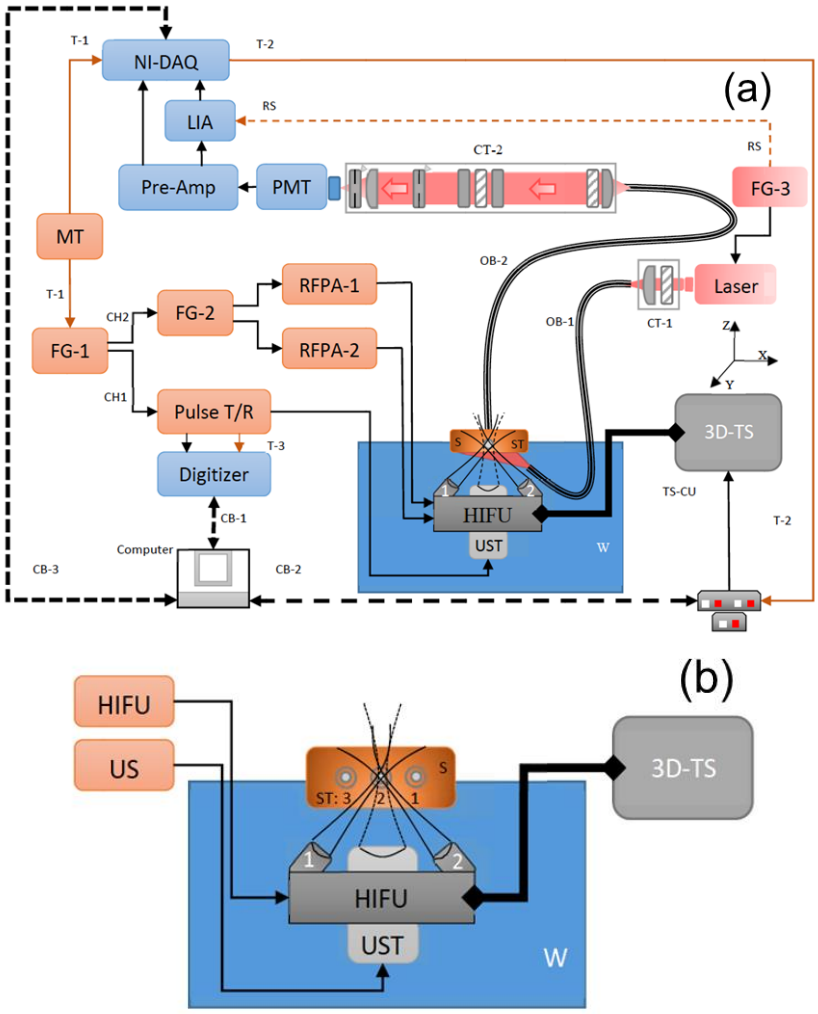
(a)
T-1
NI-DAQ
T-2
LIA
RS
Pre-Amp
PMT
CT-2
RS
FG-3
MT
OB-2
Laser
T-1
CH2
FG-2
RFPA-1
OB-1
CT-1
FG-1
RFPA-2
Z
X
Y
CH1
Pulse T/R
3D-TS
T-3
S
ST
Digitizer
1
2
TS-CU
HIFU
CB-1
T-2
Computer
UST
W
CB-3
CB-2
(b)
HIFU
US
3D-TS
S
ST: 3
2
1
1
2
HIFU
UST
W

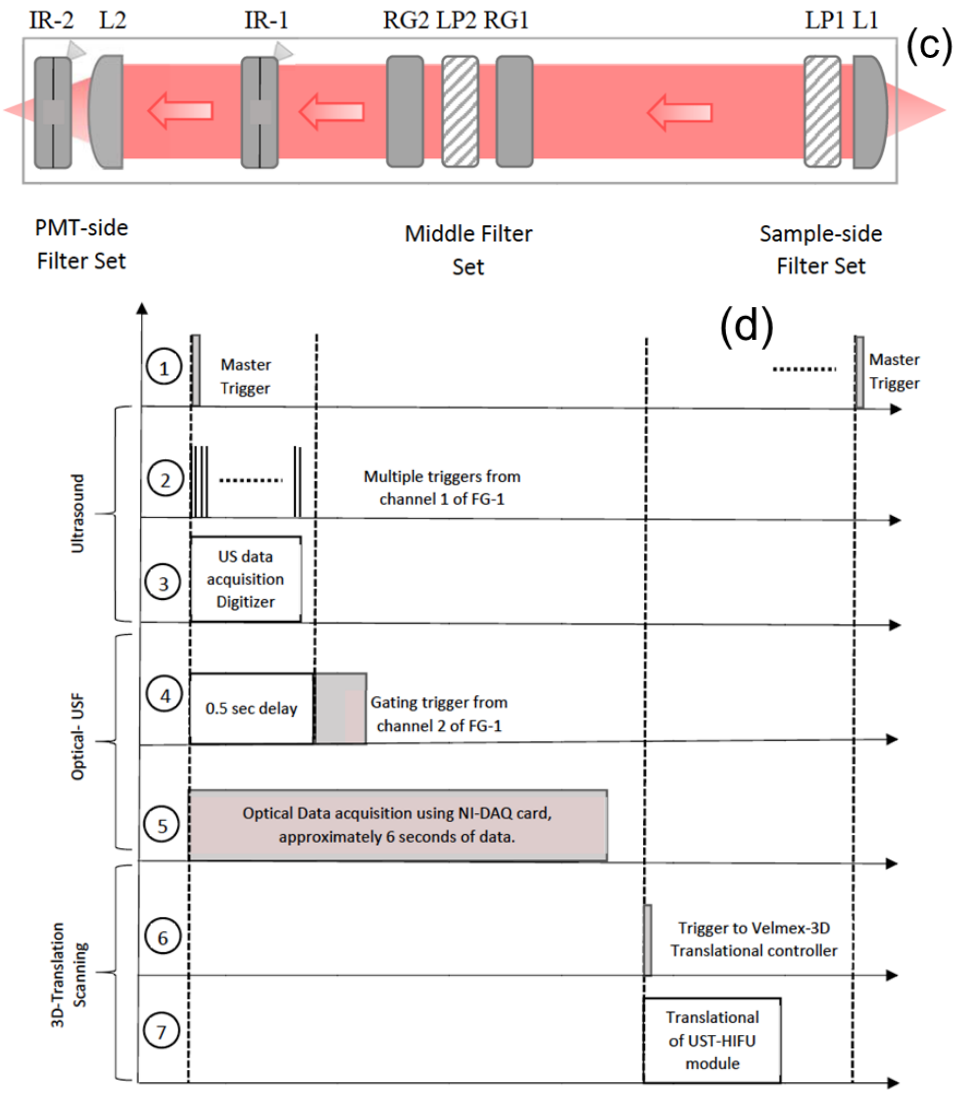

Figure 4-1 (a) Schematic diagram of the dual-modality (Ultrasound B-mode and Ultrasound-Switchable fluorescence) imaging system; (b) Schematic diagram depicting the dual-modality setup with dual-confocal focused HIFU with their respective projected ultrasound focuses into sample setup; (**c**) Schematic diagram of optical module of acquisition setup; (**d**) Time sequence event diagram of dual-modality imaging system. MT: Master trigger (T-1) with 0.1-Hz frequency, to trigger FG-1 and NI-DAQ modules; FG-1:

Function generator, Channel-2 for gating (single cycle, pulse signal with 0.5msec delay) and Channel-1 for triggering (1-KHz, 300 cycles, pulse signal) Ultrasound transducer (UST) module; FG-2: Function generator for driving each of the dual-HIFU(HIFU-1 and HIFU-2) by means of power amplifier (RFA-1 and RFA-2) respectively using 9MHz sinusoidal signal; Pulse T/R: pulse transmitter and receiver to drive the UST; FG-3: Function generator to modulate, at 1-KHz frequency, the excitation laser source (Laser); W: water tank to immerse the dual-HIFU-UST module and partially immerse the sample (S); ST: Silicone tube of inner diameter (ID) : 0.31mm and outer diameter (OD) : 0.64mm; 3D-TS: three dimensional translational stages; TS-MCU: 3D translational stage motorized control unit; CT-1: collimation tube to focus the excitations laser source into optical bundle (OB-1); CT-2: Optimized collimation tube to guide the collected fluorescence signal from optical bundle (OB-2) from within sample (S); PMT: photo-multiplier tube to detect the optical fluorescence signal; Pre-amp: preamplifier to filter detected optical signal from PMT; LIA: Lock-in amplifier to detect 1-KHz frequency signal from detected optical signal; NI-DAQ: National instrument data acquisition module to record optical signal; Digitizer: National instrument data acquisition module to record ultrasound signal; CB-1: communication bus to transfer ultrasound signal data; CB-2: serial communication bus to control TS-MCU; CB-3: communication bus to transfer optical signal data; RS: pulse signal with 1-KHz frequency from FG-3 which serves as reference signal to LIA; T-2: single cycle digital pulse signal from NI-DAQ output port to trigger the movement of 3D-TS; T-3: a trigger signal to start acquisition by Digitizer.

4.2.3 USF Sub-System

The USF sub-system includes the following modules: (1) an ultrasound heating and its driving module; (2) an excitation light source; (3) a sample module; (4) an optical detection module; and (5) a scanning module.

4.2.3.1 The ultrasound heating and its driving module.

An ultrasound-heating system (SU-109) was customized and purchased from Sonic Concepts Ltd. (Bothell, WA, USA). It consists of two 90°-crossed and confocally focused ultrasound transducers (Figure 4-1 (b)). The two transducers were tightly mounted on a base with a 45° angle relative to the horizontal plane of the base (separated 50 mm on the base). Also, their foci were overlapped at their focal planes at a 90° angle (achieved by the manufacturer). The diameter and the focal lengths of each transducer are 23 and 35 mm, respectively. The central frequency is 9-MHz. At the center of the base (between the two transducers) there is a central hollow hole for positioning the B-mode ultrasound imaging transducer that will be introduced in the next section.

To be able to control the driving power of each transducer, the two transducers were driven separately. To do this, a driving signal was generated via two channels of function generator (FG-2) and its power was amplified via two radio-frequency power amplifiers (RFPA1 and RFPA2). First, the channel-2 (CH2) of the FG-1 (AFG 3252, Tektronix, TX, USA) generates a gate signal (i.e., a square pulse). This gate signal is input into FG-2 (Agilent 33500B, Chicago, IL, USA). Thus, two gated 9-MHz sinusoidal waves are respectively generated from the two channels of the FG-2. Their peak-to-peak voltages (V_{pp}) can be controlled individually. These two signals are amplified by the RFPA-1 and RFPA-2 and then they drive the two transducers, respectively. Note that the gate width of

the two gated sinusoidal waves is controlled by FG-1, which determines the exposure time of the two transducers. The peak-to-peak voltages of the two sinusoidal waves are controlled by the two channels of FG-2, which determines the ultrasound exposure power. In this work, the exposure times of the two transducers are kept the same. The driving V_{pp} of each transducer is adjusted so that the two transducers roughly have the same exposure power at their foci. Note that the two transducers were found to have different electrical-to-acoustic transfer efficiency, which requires that the transducer with the lower transfer efficiency be driven with higher electrical power (i.e., higher V_{pp}). To estimate the HIFU-induced temperature rise in its focal volume within the tissue sample, MRI-based thermometry may be needed for an accurate result. However, it is complicated and expensive. Therefore, we adopted a relatively rough but simple method in which the HIFU was focused on the tissue surface and an infrared camera (A325sc, FLIR, Boston, MA, USA) was used to image the temperature. The measured temperature is ~5 degrees Celsius.

4.2.3.2 The excitation light source.

A continuous wave laser was used as the excitation light source: an 808-nm laser (MGL-II-808-2W, Dragon lasers, ChangChun, JiLin, China) for an indocyanine green (ICG)-based USF contrast agent or a 671-nm laser (MLL-FN-671-500mW, Optoengine LLC, Midvale, UT, USA) for another USF contrast agent based on a new fluorophore, aza-BODIPY conjugated with two hydroxyls at the bottom (denoted as ADP$(OH)_2$). The excitation light was coupled into a fiber bundle (OB-1, Model # 39366, Edmund optics, Barrington, NJ, USA) and then delivered to the bottom of the tissue sample. The power at the output end of the fiber bundle of OB-1 used in this study are 7.6 and 0.139 mW for 808-nm and 671-nm laser, respectively. For 808-nm laser, the beam is large so that two plano-

convex NIR-lenses (AC254-035-B, Thorlabs, Newton, NJ, USA) were used to couple the beam into the fiber bundle. For a 671-nm laser, the beam is small and can be easily coupled into the fiber bundle without using the lenses. In both cases, an optical filter is placed in front of the laser head to attenuate any unknown laser lines from the laser: a band pass filter of 785/62 nm (FF01-785/62-25, Semrock, Rochester, NY, USA) for the 808-nm laser and a band pass filter of 671/11 nm (FF01-673/11-25, Semrock, Rochester, NY, USA) for the 671-nm laser. The other end of the fiber bundle is submerged into water and arranged such that the excitation light illuminates the bottom of the tissue sample but without blocking the ultrasound waves. The intensity of the laser is modulated at 1 kHz via the third function generator (FG-3, 33220A, Agilent, Chicago, IL, USA). The synchronized output (i.e., a 1-kHz square wave) from another channel of the FG-3 is input into the lock-in amplifier (LIA) as the reference.

4.2.3.3 The sample configuration.

Three silicone tubes (ST, marketed as 1–3 from right to left; 60-011-01, Hellix Medical, Carpinteria, CA, USA) were inserted into a piece of porcine muscle tissue (see Figure 4-1 (b)). The tissue thickness is around 14 mm and the three tubes with an inner diameter (I.D) of 0.31 mm and an outer diameter (O.D) of 0.64 mm are located in the middle plane. The lateral distance between tube 1 and tube 2 is about 2 mm, and between tube 2 and tube 3 is about 3 mm. The tube 1 and 3 were respectively filled with pure $ADP(OH)_2$ and ICG-based USF contrast agent solutions. The tube 2 was filled with a mixed solution of the above two USF contrast agents and the volume ratio between ICG-based solution and $ADP(OH)_2$-based solution is 3:2.

4.2.3.4 The optical detection module.

A second fiber bundle (OB-2, Model # 39366, Edmund optics, Barrington, NJ, USA) was placed on the top of the tissue sample to collect fluorescence emission photons. The other end of this fiber bundle (OB-2) was fixed at the focal point of the NIR plano-convex lens (see L1 in Figure 4-1 c); AC254-030-B, Thorlabs, Newton, NJ, USA) so that the diverging photons from the fiber bundle could be collimated. Another NIR plano-convex lens (L2; AC254-030-B, Thorlabs, Newton, NJ, USA) was placed about 40 cm away from the lens L1 and faced the opposite direction so that the collimated optical beam was focused again on a cooled photomultiplier tube (PMT, H7422-20, Hamamatsu, Bridgewater, NJ, USA). To maximally block the excitation light and pass the emission light, two types of optical filters (interference and absorption filters) were positioned between the two lenses (L1 and L2). First, one interference long pass filter (LP1) was positioned right after the lens of L1 and the second interference long pass filter (LP2) was placed in the middle between the two lenses. Two absorption long pass filters (RG1 and RG2) were put before and after LP2 (Figure 4-1 (c)). Note that, in each measurement, four filters were used (LP1, LP2, RG1, and RG2), in which LP1 and LP2 are the same type filters and RG1 and RG2 are the same type filters. However, for different contrast agents, the four filters were accordingly changed to match the adopted fluorophore. For $ADP(OH)_2$-based USF contrast agents, LP1 and LP2 are 715-nm long pass interference filters (FF01-715/LP-25, Semrock, Rochester, NY, USA), and RG1 and RG2 are 695 nm long-wave pass cut-on filters (FSR-RG695, Newport, Irvine, CA, USA). For ICG-based USF contrast agents, LP1 and LP2 are 830-nm long pass interference filters (BLP01-830R-25, Semrock, Rochester, NY, USA), and RG1 and RG2 are 830 nm long-wave pass cut-on filters (FSR-RG830, Newport, Irvine, CA, USA). An iris (IR-1, SM1D12SZ, Thorlabs, Newton, NJ, USA) was

placed between RG2 and L2, and used as a shutter. This iris was adopted mainly for (1) protecting PMT by closing the shutter when adjusting the system; and (2) limiting the background photons by slightly reducing the aperture from its maximum size, as we found that more background photons were distributed around the edge than at the center. A second iris (IR-2; SM1D12SZ, Thorlabs, Newton, NJ, USA) was mounted behind the second lens L2 and in front of the PMT. The aperture was adjusted to ~2 mm (about ~20% of its fully opened aperture) and, functions as a pinhole to block background photons. To further block background photons from the environment, all these components in Figure 4-1 (c) were mounted into a closed stackable lens tube (SM1 lens tube, Thorlabs, NJ, USA). Finally, the PMT was also mounted on the tube system via a C-mount-to-SM1 convert (SM1A10, Thorlabs, Newton, NJ, USA).

The cooled PMT has an excellent spectral response in the range of 300–890 nm with minimized thermal noise. It was driven by a temperature controlled high-voltage power supply (C8137-02, Hamamatsu, Bridgewater, NJ, USA) and converted the fluorescence signal into an electronic current signal that also has the 1-kHz modulation frequency. A low-noise pre-amplifier (PreAmp; SR570, Stanford Research, Sunnyvale, CA, USA) converted the current signal into a voltage signal and also amplified the signal. The sensitivity of the pre-amplifier is set to 50 nA/V to pass 1-kHz fluorescence signal. Either a 10-kHz low pass filter (with 12 dB/oct rolloff) or a band pass filter (between 3 Hz and 10 kHz, with 6 dB/oct rolloff) could be set from the pre-amplifier to further reduce the noise.

After being processed by the pre-amplifier, the signal was input into a lock-in amplifier (LIA, SR830, Stanford Research, Sunnyvale, CA, USA) for detecting the amplitude of the 1-kHz signal. Note that the synchronized reference signal of the LIA was generated from the FG-3. The output of the LIA provided the dynamic variation of the amplitude of the 1-

kHz fluorescence signal and its phase delay relative to the reference. In this study, only the amplitude dynamic variation was needed and acquired. Generally, without ultrasound heating, LIA could also detect a 1-kHz background noise with nearly constant amplitude. This background noise was mainly generated from three sources: (1) laser leakage; (2) auto-fluorescence from the sample; and/or (3) fluorescence from those non-100%-off USF contrast agents. Fortunately, this background 1-kHz noise was independent of ultrasound. When ultrasound heating was applied, the fluorophores in the ultrasound focal region were switched on and then emitted a strong fluorescence signal. Note that the intensity was modulated at 1 kHz because the excitation light was always modulated at 1 kHz. On the other hand, the background noise remained the same as before. Thus, the amplitude of the 1-kHz signal output from the LIA was increased when ultrasound heating was applied. This amplitude change relative to the background was calculated as the USF signal strength. Note that the sensitivity of the LIA was controlled via two parameters, which could be adjusted, time constant and sensitivity. In this study, the time constant was set to 200 ms and sensitivity varied between 20 and 200 mV depending upon the signal strength or the contrast agents. Finally, the LIA signal was acquired by a national instrument data acquisition card (NI-DAQ; PCIE-6363, National Instruments, Dallas, TX, USA) at a sampling frequency of 8 KHz and eventually stored in a computer for offline processing.

4.2.3.5 The scanning module.

Three motorized linear translational stages (XN10-0040-E01 series, Motorized XSlide, Velmex, Bloomfield, NY, USA) were orthogonally stacked together to have a 3D scanning capability (3D-TS). The 3D-TS translation stages were controlled using three programmable stepping motor controllers (TS-CU; VXM-3, Velmex, Bloomfield, NY, USA).

These TS-CU controllers were connected to the computer via single serial port and were programmed accordingly to perform 1D, 2D, or 3D scanning. A MATLAB GUI was programmed to control these TS-CU controllers, such as step size, acceleration, scan speed, scan plane, number of scan locations within the plane, etc. The three transducers (including the two heating transducers and the one B-mode imaging transducer) were mounted on the base. The base was mounted on the 3D-TS for scanning. All other components remained stationary when scanning was performed.

4.2.4 US Sub-System

In general, ultrasound can provide the acoustic structure information while USF gives the optical information (which may be correlated with molecule events in future applications). If needed, ultrasound can be used to further optimize the localization of the targets in USF imaging. US sub-system was used to acquire A-lines and then form a B-mode ultrasound image (on the *x*-*z* plane). To achieve relatively high resolution, a single element focused ultrasound transducer (UST) with a central frequency of 10 MHz (V315, Olympus, Waltham, MA, USA) was adopted and inserted through the central hollow hole (Figure 4-1 (a)). The diameter and the focal length of this UST are 19 and 34 mm, respectively. The conventional pulse-echo principle was employed for ultrasound imaging. The UST was driven by a pulse transmitter-and-receiver (Pulse T/R, 5077RP, Olympus NDT, Waltham, MA, USA) that was triggered by the channel 1 of the FG-1. At each scan location, 300 triggers were generated from the FG-1 in 0.3 s to fire 300 narrow high-voltage pulses from the Pulse T/R. These high-voltage pulses were converted into 300 acoustic pulses via the UST. These ultrasound pulses propagated in the samples and were reflected by the samples. Eventually, 300 echoes were received by the UST and further amplified by the receiver with 20 dB gain. The signals were acquired by a digitizer with a sampling

frequency of 100 MS/s (NI-USB 5133, National Instruments, Dallas, TX, USA). These 300 A-lines were acquired at each scan location and their average was used to form the B-mode image. Note that the number of A-lines at each scan location can be controlled as any number between 1 and 300. In fact, in this study, we found that eight A-lines at each location were enough to acquire a US image with an acceptable signal-to-noise ratio. It is worth pointing out that the USF system requires a point-by-point scanning on the *x-z* plane while the US system requires a line-by-line scanning on the same plane. Thus, in this study many abundant A-lines were acquired during the USF point-by-point scanning. Only those A-lines when UST was focused on the tubes were selected to form the B-mode ultrasound image.

4.2.5 Synchronization of USF and US Sub-Systems

Figure 4-1 (d) shows the time sequences of different events of the entire system. A pulse delay generator with a frequency of 0.1 Hz (DG645, Stanford Research, Sunnyvale, CA, USA) was used as the master trigger (MT, Figure 4-1 (a)) to trigger both the function generator (FG-1) and the data acquisition card (NI-DAQ). The master trigger (the first row in Figure 4-1 (d)) initiated the two channels of the function generator FG-1 to send out the triggers (the second row in Figure 4-1 (d)) for US imaging and the gating pulse (the fourth row in Figure 4-1 (d)) for USF imaging. Because US imaging is faster than USF imaging, at each scan location multiple A-lines were acquired (the third row in Figure 4-1 (d)) before firing the heating ultrasound transducer (the fourth row in Figure 4-1 (d)) for USF imaging. Thus, the gating pulse was delayed 0.5 s relative to the master trigger to make sure enough A-lines were acquired. However, the NI-DAQ was triggered immediately by the master trigger and then acquired 6 s of the data from both the LIA and the pre-amplifier, which included 0.5-s before, 0.2-s during, and 5.3-s after the two heating ultrasound transducers

were fired. After both the US and USF data were acquired and stored into a matrix variable using MATLAB, the NI-DAQ was programmed to generate a trigger (see T-2 in Figure 4-1 (a)) 2 s after finishing acquiring the data, which means a total of 8 s was delayed from the previous master trigger (the sixth row in Figure 4-1 (d)). Thus, the transducers of USF and US were scanned to the next location (the seventh row in Figure 4-1 (d)) and then waited for the next master trigger coming for repeating the US and USF data acquisitions. In this study, the scanning is 2D raster scanning on the *x*-*z* plane.

4.3 Materials and Synthesis of USF Contrast Agents

The synthesis details of the ICG-based and the $ADP(OH)_2$-based USF contrast agents have been introduced in our previous publications [12, 21, 22]. In this study the switching thresholds for both agents are ~26–27 degrees Celsius and the background temperature is around 23–24 degrees Celsius. Basically, ICG molecules were encapsulated into thermo-sensitive nanoparticles that were made of poly-*N*-isopropylacrylamide (PNIPAM). The synthesis components include *N*-isopropylacrylamide (NIPAM), *N*-tert-butylacrylamide (TBAm), sodium dodecyl sulfate (SDS), *N*,*N*′-methylenebisacrylamide (BIS), *N*,*N*,*N*',*N*'-tetramethyl ethylene diamine (TEMED), ammonium persulfate (APS), Tetrabutylammonium iodide (TBAI), *N*-(3-Dimethylaminopropyl)-*N*′-ethylcarbodiimide hydrochloride (EDC), and ICG. All these materials were purchased from Sigma-Aldrich Corporate (St. Louis, MO, USA). All chemicals were used as received.

Similarly, $ADP(OH)_2$ molecules were encapsulated into thermo-sensitive nanocapsules that were made of Pluronic F98. $ADP(OH)_2$ was synthesized based on our earlier published method [62]. Pluronic F98 was obtained from BASF (Florham Park, NJ, USA). Pluronic F98 was dissolved in deionized water with the concentration of 50 mg/mL.

The dye/TBAI (molar ratio = 1:6) was dissolved in chloroform and kept in sonication for 30 min. The dye solution was then dropped into the pluronic aqueous solution with stirring and then was dispersed with a sonicator for 4 min. The chloroform was evaporated off to encapsulate the dye into the hydrophobic cores of Pluronic nano-capsules. Free dye was removed using Amicon Ultra centrifugal filters (10,000 molecular weight cut-off, Millipore, Billerica, MA, USA).

4.4 Processing of USF and US Data

In this study, to increase the system sensitivity the intensity of the excitation laser is modulated into a sinusoidal wave at 1 kHz [12]. Thus, both the background fluorescence emission and the USF signal are also sinusoidal waves at 1 kHz. Therefore, only the 1 kHz fluorescence signal is acquired, analyzed, and processed, while all other frequency components are rejected. The NI-DAQ acquired the dynamic change of the amplitude of the 1-kHz fluorescence signal before, during and after the heating pulse was applied. The background amplitude was estimated via the data acquired before applying the heating ultrasound pulse, which mainly included laser leakage through the emission filters, possible auto-fluorescence from the sample, and/or fluorescence emission from those non-100%-off USF contrast agents. After applying the heating ultrasound pulse, the amplitude of the 1-kHz fluorescence emission will increase. The difference between the maximum amplitude and the background amplitude was used as the USF signal strength at this location. After scanning, a 2D USF image can be acquired.

For US imaging, A-lines at each scan point were recorded and stored along with the coordinate information such as the location and the distance between the scan point along both the axial and lateral directions. In this study, a total of eight A-lines were averaged at

each location to achieve high enough signal-to-noise ratio (SNR) although many more A-lines were available. After all the averaged A-lines were acquired and calculated along the lateral direction (i.e., the *x* direction). A B-mode US image was generated by extracting the envelope of each averaged A-line. The gray scale of the B-mode US image represents the acoustic impedance mismatch between any interfaces in the tissue phantom. It should be noted that US B-mode imaging is a line scan technology so that only a lateral scanning along *x* direction is needed to form a 2D B-mode US image on the *x*-*z* plane. However, USF imaging is a point-by-point scanning technology, so that both lateral and axial scans are needed (i.e., along both *x* and *z* directions). Thus, the system acquired many more A-lines than what was needed to form a B-mode image because of the unnecessary *z*-direction scanning for US imaging. Therefore, some redundant A-lines were discarded.

4.5 Results and Discussions

4.5.1 Single Target USF Imaging

We started from the simplest case where a single micro-tube (ID = 0.31 and OD = 0.64 mm) was embedded in a piece of porcine muscle tissue. The tube was filled with the aqueous solution of the $ADP(OH)_2$ based USF contrast agent. To acquire a USF image, the overlapped region of the two crossed foci (OR-TCF) was scanned on the *x*-*z* plane. Figure 4-2 (a) shows the acquired USF image of the cross section of the micro-tube. The circle indicates the location and size of the micro-tube. The gray scale of each pixel on this image indicates the local USF signal strength when the OR-TCF was located at that pixel. Clearly, the USF image not only shows the tube but also shows four long tails. The OR-TCF region shows stronger USF signals than the tails do. This observation agrees to the idea that the OR-TCF region has a higher temperature increase (induced by two heating ultrasound transducers) than the tails (induced by one of the transducers). In fact, these tails are

artifacts, which do not represent regions where USF contrast agents are located, and should be shortened as much as possible.

Based on the classical acoustic diffraction theory, the ratio between the axial and lateral focal size is roughly equal to a product between a factor of 7 and the transducer's *f*-number that can be roughly calculated via the ratio of the focal length to the diameter of the adopted transducer. Currently, the two ultrasound-heating transducers have a relatively large *f*-number (~1.52). Therefore, the tails are relatively long in Figure 4-2 (a). To short these tails, using two transducers with *f*-number smaller than 1 will definitely be helpful. On the other hand, these tails can also be shortened (or even removed) via a few mathematical algorithms. The simplest method is to set a threshold for USF signal strength. Any signal below the threshold will be set as zero.

Figure 4-2 (b) shows the processed USF image by setting the threshold as 50% of the maximum USF signal. Accordingly, the tail artifacts are successfully shortened. The full width at half maximum (FWHM) of the crossed central region of this USF image is ~1.07 and ~1.5 mm along *x* and *z* directions, respectively. Although these sizes are still larger than the tube outer diameter (0.64 mm), which is mainly caused by the finite acoustic and thermal sizes of the OR-TCF, they are much more uniform along *x* and *z* directions compared with the non-uniform focal size of each individual heating transducer. Specifically, the lateral and axial acoustic OR-TCFs of the SU109 transducer are 0.2 and 0.4 mm respectively, which are specified by the manufacturer. In addition, their corresponding thermal sizes are 0.27 and 0.52 mm, respectively, measured via an infrared camera (the detailed method can be found in our previous publication [32]). However, the lateral and axial acoustic focal sizes are measured using pulse-echo method [63] to be around 0.56 mm and 0.62 mm along lateral and axial, respectively. The reason we selected

50% of the maximum USF signal as the threshold is because two ultrasound beams are used in this study. Ideally, the threshold should be selected close to the inverse of the number of the overlapped ultrasound beams. For example, if four beams are adopted, the threshold may be selected as 25% (i.e., one-quarter). Clearly, when the number of the beams increases, the threshold will be reduced. This is good to avoid artificial errors caused by using the threshold. However, it will become more difficult and complicated in practice. Therefore, the number of the crossed beams should be selected appropriately.

Based on the above results and discussions, the hypothesis that the axial resolution for USF imaging can be improved by using two (or more in future) ultrasound heating transducers with an overlapped focus is demonstrated. Certainly, this threshold-based method may be only good for samples with simple targets. Other methods, such as a morphological recognition method, a de-convolution method, or an ultrasound-guided localization method may be developed for more complicated samples.

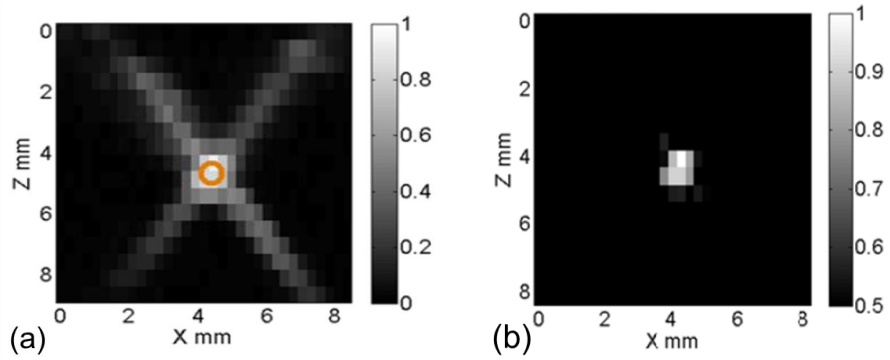

Figure 4-2 Ultrasound switchable fluorescence images obtained using dual-HIFU for a micro-silicone tube filled with ADP(OH)2 based contrast agent; (a) with no threshold applied; and (b) with 50% and above pass through applied.

4.5.2 Simultaneous Imaging of Multiple Targets Using Dual Modality Imaging

In this section, three tubes (see the configuration in Figure 4-1 (b)) were imaged using this dual-modality system. Tube 1 and 3 were filled with $ADP(OH)_2$ and ICG-based USF contrast agent, respectively. Tube 2 was filled with the two mixed solutions with a volume ratio of 3:2. Figure 4-3 (a) show their US B-mode image. The three tubes can be clearly localized as indicated by the three circles as depicted by yellow circles in Figure 4-3 (a) (no matter which solutions were filled). This is because US is sensitive to the difference in the acoustic impedance between the tube material and the surrounding porcine muscle tissue. However, US is insensitive to the fluorophore types so that it cannot differentiate which fluorophore is filled in each tube.

To differentiate the fluorophores, ICG-based USF contrast agents were first imaged using the USF system. An 808-nm laser was used as the excitation light source. The emission filters included two 830-nm long pass interference filters and two RG830 absorption filters. Figure 4-3 (b) shows the USF image (overlaid on the US image) without applying any thresholds. Figure 4-3 (c) show the similar images with a threshold of 50% of the maximum USF signal. It can be seen that the majority of the tail artifacts can be removed (although not all). After being processed with this threshold method, we realized that some remaining artifacts that were separated from the main central region (i.e., the tube region) could be further removed. The method was to convert the USF image in Figure 4-3 (c) into a binary image (see Figure 4-3 (d)). Any disconnected areas from the main central region were set as zero. Thus, a new binary image was generated and shown in Figure 4-3 (e). Then, multiplying this new binary image with the USF image shown in Figure 4-3 (c), most artifacts can be removed. The result is shown in Figure 4-3 (f). Besides finding the locations of the tube 2 and 3, more important result is that only tubes 2 and 3 that were

filled with ICG-based contrast agents are observed from the USF image. The tube 1 that was filled only with $ADP(OH)_2$-based contrast agents was not shown. This is because the 808-nm laser does not excite the $ADP(OH)_2$.

To image $ADP(OH)_2$-based USF contrast agents in tube 1 and 2, another USF scanning was conducted using a 671-nm excitation laser and a set of emission filters (two 715-nm long pass interference filters and two RG695 absorption filters). After processing the data using the similar method described above and the method described in our previous publication, the USF signals from the $ADP(OH)_2$-based USF contrast agents are overlaid on Figure 4-3 (f) and the final image is shown in Figure 4-3 (g). By comparing Figure 4-3 (a) and (g), the three tubes are clearly located by the US B-mode image and roughly located by the USF image. The fluorophores of ICG, $ADP(OH)_2$ and their mixture are clearly resolved via different colors (red and green), which cannot be achieved by the B-mode image. Accordingly, this dual-modality imaging system combines our color-sensitive USF imaging with a conventional B-mode US imaging to provide both the acoustical structural information (such as the location, shape, size, depth, etc., of the target) and the USF functional, biochemical, or molecular information.

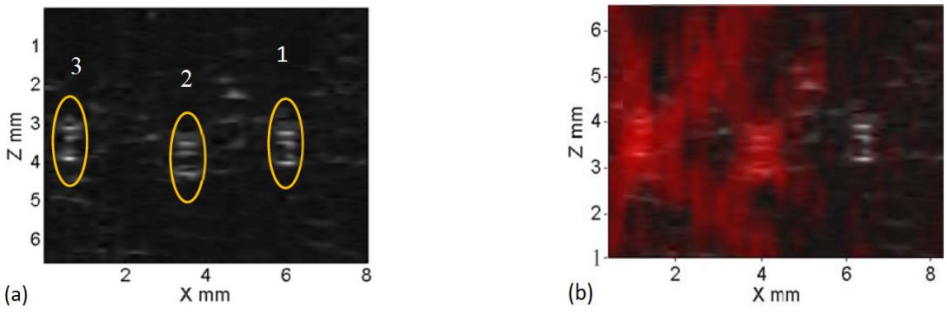

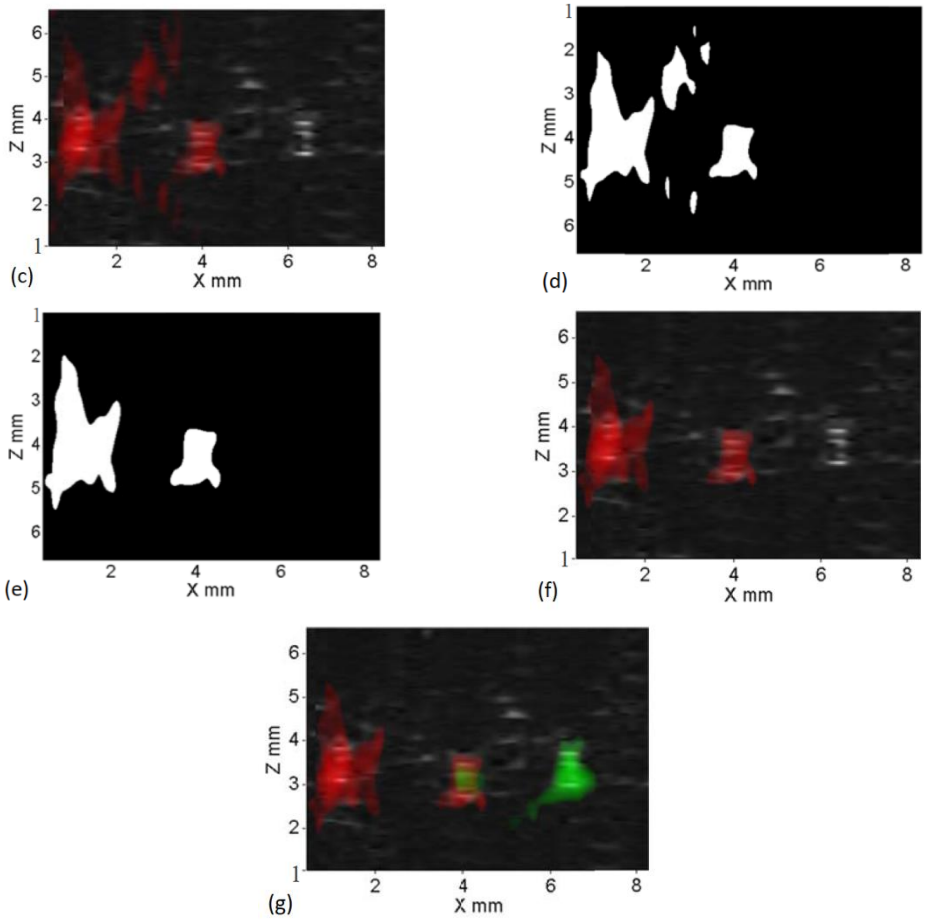

Figure 4-3 Results obtained using dual-modality imaging system; (a) US B-mode image depicting locations of three embedded silicone tubes within a porcine tissue sample, (b) USF-ICG image overlaid onto US B-mode image with no threshold applied; (c) USF-ICG image overlaid onto US B-mode image with 50% pass through threshold applied; (d) binary image obtained by morphological operations; (e) final binary image without tail artifacts; (f) processed USF-ICG image (using (e)) overlaid onto US B-mode image; and (g) multi-color (red-ICG and green-$ADP(OH)_2$ contrast agent) multi-modality processed image.

4.6 Conclusions

In conclusion, we developed a dual-modality imaging system by combining our recently developed USF imaging with the conventional ultrasound B-mode imaging. This dual-modality system has the several unique features. (1) By using two 90°-crossed ultrasound transducers with an overlapped focal region, the axial resolution (along the ultrasound wave propagation direction) of USF imaging has been significantly improved (close to its lateral resolution), which makes it possible to scan tissue on the *x*-*z* plane co-registered with a B-mode ultrasound image. In addition, it is helpful for developing 3D USF imaging in future; (2) By combining the two imaging modalities, the system can image multi-color fluorophores in tissues via the USF technology and image tissue acoustic structures via the B-mode ultrasound. Simultaneous imaging of multiple targets (SIMT) is an important goal for molecular imaging in the future. Therefore, this dual-modality imaging technology provides great potentials for achieving this goal.

Chapter 5

Ultrasound-Switchable Fluorescent Imaging Using a high-frequency (15 MHz) HIFU Transducer

5.1 Introduction:

As the previous chapters (3 and 4) reported, and as our previous work shows [12, 21], the ultrasound-switchable fluorescence (USF) imaging system has high spatial resolution and sensitivity for deep-tissue imaging. This high spatial resolution of the present USF system is achieved only along the lateral or x-y horizontal plane. Its spatial resolution greatly degrades along the axial direction due to large thermal focal size, which is directly influenced by the high-intensity focused-ultrasound (HIFU) transducer's focal volume. Hence, a major limitation of the present USF system is its axial resolution, which is severely compromised. Chapter 0 introduced a dual-HIFU USF system for improving the axial resolution of USF images [31]. Here, we introduce another approach which depends upon the concept that the focal volume is directly proportional to the frequency of the US transducer. This approach is also supported by a study discussed in Chapter 0. Since the resolution of the USF system depends entirely upon the focal volume of HIFU transducer used, we hypothesize that, by adopting a HIFU transducer with a high frequency, we can constrict the focal volume further along both lateral and axial directions, thereby improving the USF image resolution for deep-tissue, high-resolution imaging. For this study, we have adopted a 15 MHz HIFU transducer and performed a comprehensive study of single-target, multiple-target, multi-colour multiple-target and *in-vivo* USF imaging using the modified USF system. CT imaging was also performed for all the experiments to show the feasibility of the dual-modality CT-USF imaging technique with possible application for structural and molecular imaging.

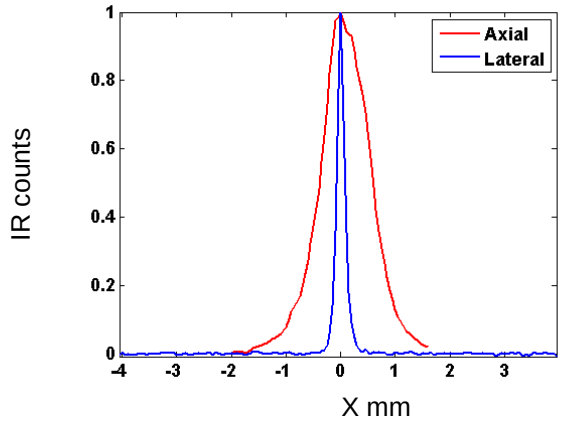

Figure 5-1 Lateral and Axial temperature profile of 15 MHz HIFU transducer recorded using IR camera setup.

Initial experiments were conducted to study the induced temperature distribution of a 15 MHz high-intensity, focused-ultrasound which could improve the ultrasound-switchable fluorescence imaging resolution along both axial and lateral planes. As in the experiment setup discussed in Chapter 1, an IR camera (A325sc, FLIR, Massachusetts, USA) was used to record the axial and lateral temperature profiles. Their full width at half maximum (FWHM) is calculated to be 0.98mm and 0.16mm, respectively, as shown in Figure 5-1. This is significantly less than the 2.5MHz HIFU's acoustic FWHM of ~2.9mm and ~0.6mm extrapolated from Figure 2-4 for an exposure duration of 20msec. The ratio of axial to lateral FWHM is calculated to be around ~6. This also agrees closely with the classical acoustic diffraction theory, according to which the ratio between the axial and lateral focal size is roughly equal to a factor of 7 and the transducer's *f*-number is equal to 1, which can be calculated via the ratio of the focal length (50.8mm) to the diameter (50.8mm) of the adopted transducer. From the previous chapters, it is inferred that the USF imaging resolution depends closely upon the temperature profiles of the adopted HIFU transducer. Therefore, using a 15 MHz HIFU transducer should significantly improve the USF imaging resolution.

5.2 Materials and methods:

5.2.1 Hardware of the system

A diagram of the USF imaging system is shown in Figure 5-2. The major components were introduced in our previous publication [12, 21]. For integrity, we very briefly introduce the entire system here. Like the previous ones [12], the current USF sub-system includes the following modules: (1) an ultrasound source, (2) an excitation light source, (3) a sample module, (4) an optical detection module, and (5) a scanning module.

5.2.1.1 The ultrasound source:

A single-element and water-immersible 15 MHz HIFU transducer (H-202, Sonic Concepts Ltd, Bothell, WA, USA) is used in the USF system, as shown in Figure 5-2. It has a geometric focal length of 50.8 mm and an active diameter of 50.8 mm. The *f*-number is calculated to be 1. Based on manufacturer-provided data, the lateral and axial acoustic focal sizes are 0.25 and 1.9 mm, respectively. The HIFU transducer is driven by a function generator (FG-1, Agilent 33522B, Chicago, IL, USA) via a radio-frequency power amplifier (RFPA; 325LA, Electronics & Innovation, NY, USA). The exposure power of the HIFU transducer can be controlled by varying the peak-to-peak voltage (Vpp) of the 15 MHz sinusoidal wave from the FG-1. The exposure duration of the HIFU transducer is controlled by driving the FG-1 in burst mode and by controlling the number of cycles in each burst. For this study, the exposure duration was kept at 400 msec. The time between each burst is also set in FG-1 and determines the time that passes from one scan location and the next scan location, thereby determining the overall scanning duration of USF imaging for a desired region of interest (ROI). Note that the FG-1 trigger/sync-out channel is used to

trigger the National Instruments data-acquisition card (NI-DAQ; PCIE-6363, National Instruments, Dallas, TX, USA) to record the data.

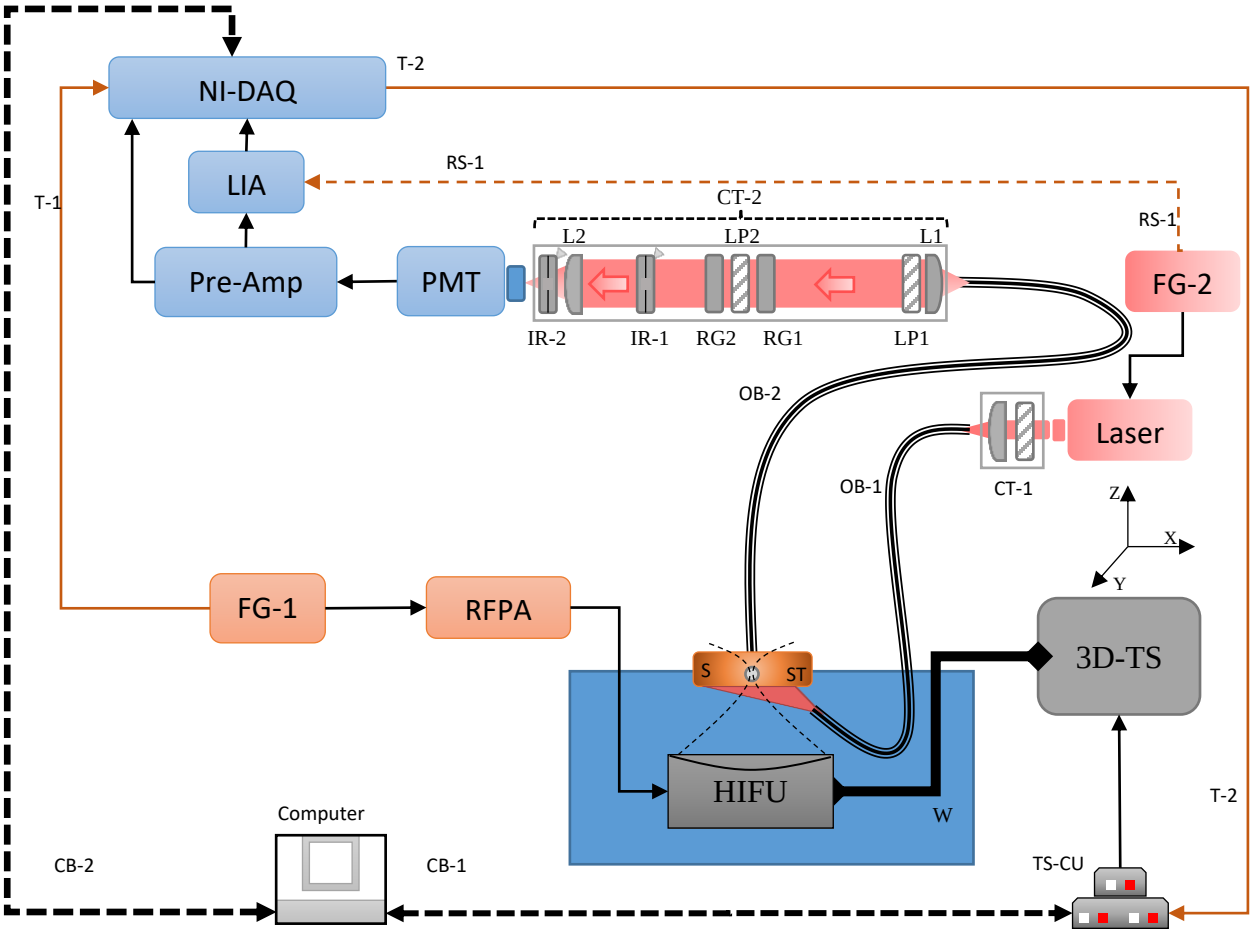

Figure 5-2 Schematic diagram of the USF system with 15 MHz HIFU transducer. FG-1: A function generator for driving the HIFU transducer by generating a 15 MHz sinusoidal signal amplified by a radio-frequency power amplifier (RFPA); FG-2: A function generator to modulate the excitation laser at a 1-KHz frequency and generate a reference signal (RS-1) for the lock-in amplifier; W: a water tank to immerse the HIFU transducer and partially immerse the sample (S); ST: A silicone tube with an inner diameter (ID) of 0.31mm and an

outer diameter (OD) of 0.64mm; 3D-TS: the three dimensional translational stages; TS-CU: 3D translational-stage, motorized control units; CT-1: a collimation tube to focus the excitation laser into an optical bundle (OB-1); CT-2: an optimized collimation tube to guide the collected fluorescence from the optical bundle (OB-2) to the photodetector (PMT) and best eliminate the excitation light and pass the emission light; PMT: A photo-multiplier tube to detect the optical fluorescence signal; Pre-amp: A preamplifier to amplify and filter the signal from the PMT; Laser: Excitation 671 nm or 808 nm laser source to irradiate the sample (S); LIA: A lock-in amplifier to detect the 1-KHz optical signal; Ni-DAQ: A National Instruments data-acquisition card; CB-1: serial communication bus to control TS-CU; CB-2: communication bus to transfer data; RS-1: a 1-KHz reference signal for LIA; T-1: a trigger signal for the NI-DAQ card; T-2: a single-cycle, digital-pulse signal to trigger the movement of the 3D-T.

5.2.1.2 The excitation light source.

Depending upon the type of USF contrast agent used, an either 671 nm or 808 nm laser source was selected. Similar to experimental setup described in chapters 3 and 4, a continuous-wave laser was used as the excitation light source: an 808 nm laser (MGL-II-808-2W, Dragon lasers, Changchun, Jilin, China) for an indocyanine green (ICG)-based USF contrast agent or a 671 nm laser (MLL-FN-671-500mW, Optoengine LLC, Midvale, UT, USA) for another USF contrast agent based on a new fluorophore, aza-BODIPY conjugated with two hydroxyls at the bottom (denoted as ADP$(OH)_2$). The excitation light was coupled into a fibre bundle (OB-1, Model # 39366, Edmund optics, Barrington, NJ, USA) and then delivered to the bottom of the tissue sample. For the 808 nm laser, the beam is large so that two plano-convex NIR-lenses (AC254-035-B, Thorlabs, Newton, NJ, USA) were used to couple the beam into the fibre bundle. For a 671 nm laser, the beam is

small and can be easily coupled into the fibre bundle without using the lenses. In both cases, an optical filter is placed in front of the laser head to attenuate any unknown laser lines from the laser: a band pass filter of 785/62 nm (FF01-785/62-25, Semrock, Rochester, NY, USA) is used for the 808 nm laser, and a band-pass filter of 671/11 nm (FF01-673/11-25, Semrock, Rochester, NY, USA) is used for the 671 nm laser. The other end of the fibre bundle is submerged in water and arranged such that the excitation light illuminates the bottom of the tissue sample but without blocking the ultrasound waves. The intensity of the laser is modulated at 1 kHz via the second function generator (FG-2, 33220A, Agilent, Chicago, IL, USA). The synchronized output (i.e., a 1-kHz square wave) from another channel of the FG-2 is input into the lock-in amplifier (LIA) as the reference.

5.2.1.3 The sample configuration.

The 15 MHz HIFU transducer-based USF imaging study involved four types of sample preparations depending upon number of targets and type of study:

a) Single-target USF imaging: A silicone tube (ST; 60-011-01, Hellix Medical, Carpinteria, CA, USA) was filled with the solution of a USF contrast agent and embedded into a piece of porcine muscle tissue (Figure 5-2 and Figure 5-3 (a)). The thickness of the muscle tissue was ~10 mm. The tube with an inner diameter (ID) of 0.31 mm and an outer diameter (OD) of 0.64 mm was located around the middle along the depth direction. The contrast solution used for this study is ADP-based USF contrast agent encapsulated in pluronic F98 nano-capsules [12, 41] mixed with CT contrast agent (Exitron nano 12000, Miltenyi Biotec, Auburn, CA, USA) with a volume ratio of 1:1. Background temperature is maintained at ~21 degrees Celsius. The USF contrast agent switching temperature (LCST) is ~27 degrees Celsius.

b) Multiple ('V'-shaped) target USF imaging: Two silicone tubes (60-011-01, Hellix Medical, Carpinteria, CA, USA) are embedded into a piece of porcine muscle tissue such that they cross each other forming a 'V' shape around middle of the sample, as shown in Figure 5-3 (b). This setup is useful for testing the USF system's ability, using a 15 MHz HIFU transducer, to perform a 3-dimentional imaging of two targets with a variable distance between them. The thickness of the muscle tissue was ~8 mm. The USF-CT contrast-agent solution used was same as above, where a volume ratio of 1:1 of $ADP(OH)_2$ was encapsulated in pluronic F98 nano-capsules [12, 41] and Exitron nano 12000 CT contrast agent. The background temperature is maintained at ~21 degrees Celsius. The USF contrast agent switching temperature is ~27 degrees Celsius.

c) Multiple-target, multi-colour USF imaging: Like the sample prepared for the dual-HIFU based USF imaging study described in Chapter 4, three silicone tubes (ST, marketed as 1–3 from right to left; 60-011-01, Hellix Medical, Carpinteria, CA, USA) were inserted into a piece of porcine muscle tissue, as shown in Figure 5-3 (c). The tissue thickness is around ~8 mm and the three tubes with an inner diameter (I.D) of 0.31 mm and an outer diameter (O.D) of 0.64 mm are in the middle plane. The lateral distance between tubes 1 and 2 is about 1.9 mm, and the distance between tubes 2 and 3 is about 1.7 mm. Tubes 1 and 3 were filled with $ADP(OH)_2$ [12, 41] and ICG-based USF contrast-agent solutions [22], respectively, mixed with CT contrast agent (Exitron nano 12000) in a volume ratio of 1:1 each. Tube 2 was filled with a mixed solution of the above two USF contrast agents and CT contrast agent (Exitron nano 12000) in a 1:1:1volume ratio of ICG-based solution, $ADP(OH)_2$-based solution, and CT contrast solution. The background temperature was maintained at ~21 degrees Celsius. ADP-based USF contrast agent is encapsulated in pluronic F127 with a switching temperature threshold of ~23 degrees Celsius. The ICG-based USF contrast agent had a switching threshold at ~ 26 degrees Celsius.

d) *In-vivo* USF imaging: BALB/cJ mice (female, 20 – 25 gram) were purchased from Taconic Farms Inc. (Germantown, NY, USA). The animal protocols were approved by the University of Texas at Arlington's Animal Care and Use Committee. All animals were anesthetized with 1.8% isoflurane. Hair was removed from the right leg and abdomen, and 20-30 μL of final solution (mixture of the ICG-based USF contrast agents and CT contrast agent at a 1:1 volume ratio) was injected locally. The ICG-based USF contrast agent is comprised of ICG-encapsulated, ACA-initiated, SDS-surfactant and poly(N-isopropylacrylamide) nanoparticles, and, in particular, with P(NIPAM-AAm 86:14) nanoparticles with a threshold switching at 40 degrees Celsius [22]. This is used because the typical mouse body temperature is ~36 degrees Celsius. An intra-muscular localized injection was administered near the right leg of the mouse 10 minutes prior to fluorescence imaging and was followed immediately by USF imaging.

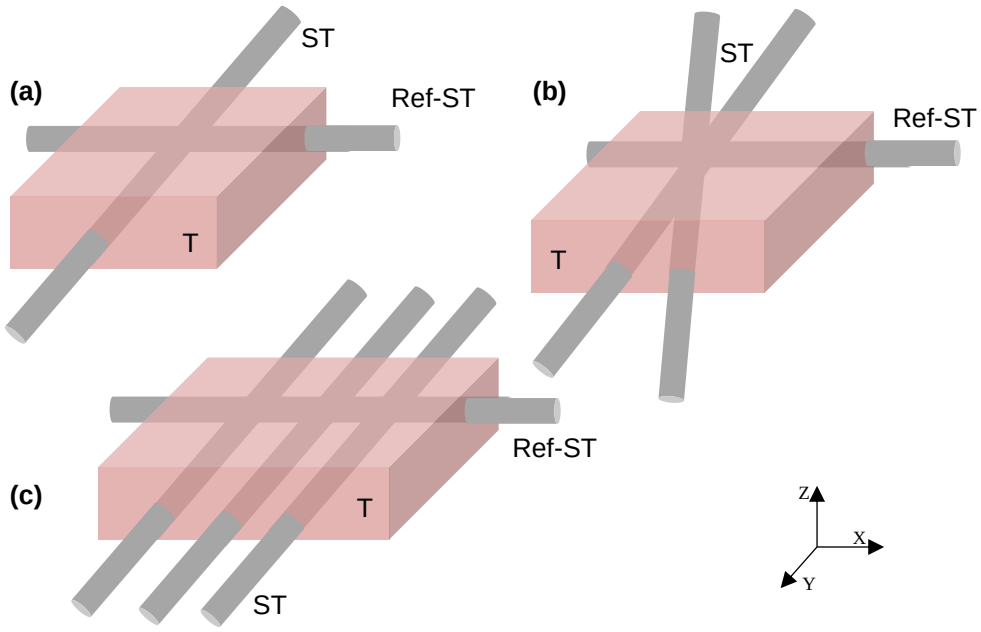

Figure 5-3 Tissue samples used for different experiment studies. ST: Silicone tube (1D: 0.31 mm and OD: 0.64 mm), Ref-ST: reference silicone tube and T: porcine tissue sample.

5.2.1.4 The optical detection module.

Depending upon the USF contrast agent used, either of the following optical detection setup was chosen.

(a) For ADP-based USF imaging setup: A collimation and filtering system consisted of the following components: (1) two NIR plano-convex lenses for collimation (L1 and L2, AC254-030-B, Thorlabs, Newton, NJ, USA), and (2) two interference and two absorption filters for blocking exciting light (LP1 and LP2: 715 nm long pass interference filters, FF01-715/LP-25, Semrock, Rochester, NY, USA; RG1 and RG2: 695 nm long-wave pass cut-on filters, FSR-RG695, Newport, Irvine, CA, USA).

(b) For ICG-based USF imaging setup: A collimation and filtering system consisted of the following components: (1) two NIR plano-convex lenses for collimation (L1 and L2, AC254-030-B, Thorlabs, Newton, NJ, USA) and (2) two interference and two absorption filters for blocking exciting light (LP1 and LP2: 830-nm long pass interference filters, BLP01-830R-25, Semrock, Rochester, NY, USA; RG1 and RG2: 830 nm long-wave pass cut-on filters, FSR-RG830, Newport, Irvine, CA, USA).

The rest of the system components are the same as the USF system introduced in previous chapters (chapters 3 and 4): The emission photons were collected via another fibre bundle (OB-2) positioned on the top of the tissue sample. The collected photons were delivered to a collimation and filtering system for collimating the scattered photons and blocking the excitation light. Two irises (IR1 and IR2, SM1D12SZ, Thorlabs, Newton, NJ, USA) were used to protect the photo-detector by closing the optical path when needed and to control the aperture size for further blocking of the background photons. The photons were eventually converted into an electronic signal by a cooled photomultiplier tube (PMT, H7422-20, Hamamatsu, Bridgewater, NJ, USA) and further amplified by a low-noise pre-amplifier (PreAmp; SR570, Stanford Research, Sunnyvale, CA, USA). The electronic signal was input into the first lock-in amplifier (LIA; SR830, Stanford Research, Sunnyvale, CA, USA) for detecting the amplitude variation of the 1-kHz signal using a synchronized reference signal from the FG-2 (RS-1, at the same frequency of $f_{M\text{-}OPT}$=1kHz).

In general, the 1-kHz optical signal consisted of both USF signal and background noise. As discussed in previous chapters, the background noise originated mainly from the following: (1) laser leakage, (2) auto-fluorescence from the sample, and/or (3) fluorescence from non-100%-off USF contrast agents. Fortunately, all three of these

components of the noise were independent of ultrasound. The time constant of LIA was set to 100 ms, and the sensitivity varied between 200 or 500 mV nA depending on signal strength. A National Instruments data-acquisition card (NI-DAQ; PCIE-6363, National Instruments, Dallas, TX, USA) was used to acquire the signals from LIA and Pre-amplifier (fluorescence signal via PMT).

5.2.1.5 The scanning module:

The scanning module was the same as used in previous systems [12, 63]. Briefly, three motorized linear translational stages (3D-TS) were orthogonally arranged together to yield 3D scanning capability (although this study uses only 2D scanning) controlled by the 3-axis programmable stepping motor controller (TS-CU). The controller was connected to a computer. A MATLAB GUI was programed to control the controller and further scan the HIFU transducer for acquiring USF images (in this study, only 2D images were scanned). Note that, since the sample stage is mounted to the 3D-TS, only 2-dimensional *x-y* scanning is possible. This ensures that the sample will not hit the stationary optical collection fibre bundle (OB-2). For the purpose of 3-dimensional scanning, a 2-dimensional *x-y* plane scan is first performed; then the HIFU transducer's focus is moved to the next desired depth within the sample along *z*-direction and the process is repeated. The 2-dimensional (*x-y*) USF images thus generated are stacked with respect to ultrasound transducer depth to generate 3-dimensional USF images using MATLAB.

5.2.2 System event and operational flow diagram:

The time sequence of events and the system-operational flow diagram is shown in Figure 5-4. A master trigger starts the entire system by triggering both the FG1 and the

NI-DAQ, as shown in panels 1 and 8 of Figure 5-4, respectively. Channel 1 of the FG-2 function generator modulates the laser with 1-kHz sinusoidal signal, as shown in Panel 4, and sends out a reference signal to LIA using FG-2 trigger channel, as shown in Panel 6. The HIFU exposure time is 400 ms (Panel 2) to induce a temperature rise around the focal volume (Panel 3), which leads to a change in the 1-kHz fluorescence signal (Panel 5). The typical duration of optical signal acquisition was 4-15 seconds (Panel 8). Once all the data are acquired and stored, the MATLAB GUI generates a voltage pulse via the output port of the NI-DAQ (Panel 9) and triggers the Velmex 3D-translational stages to move to the next location (Panel 10). Care must be taken to ensure that the summation of the DAQ acquisition duration (4-15 seconds) and the movement duration of translational stages (less than 2 seconds) do not exceed the duration between the two adjacent master triggers. Hence, for this study, the master trigger was set to have a trigger-to-trigger duration of 10 - 35 seconds. The duration between the two master triggers determines the duration between the two scanning locations and thereby the overall duration of the system scan.

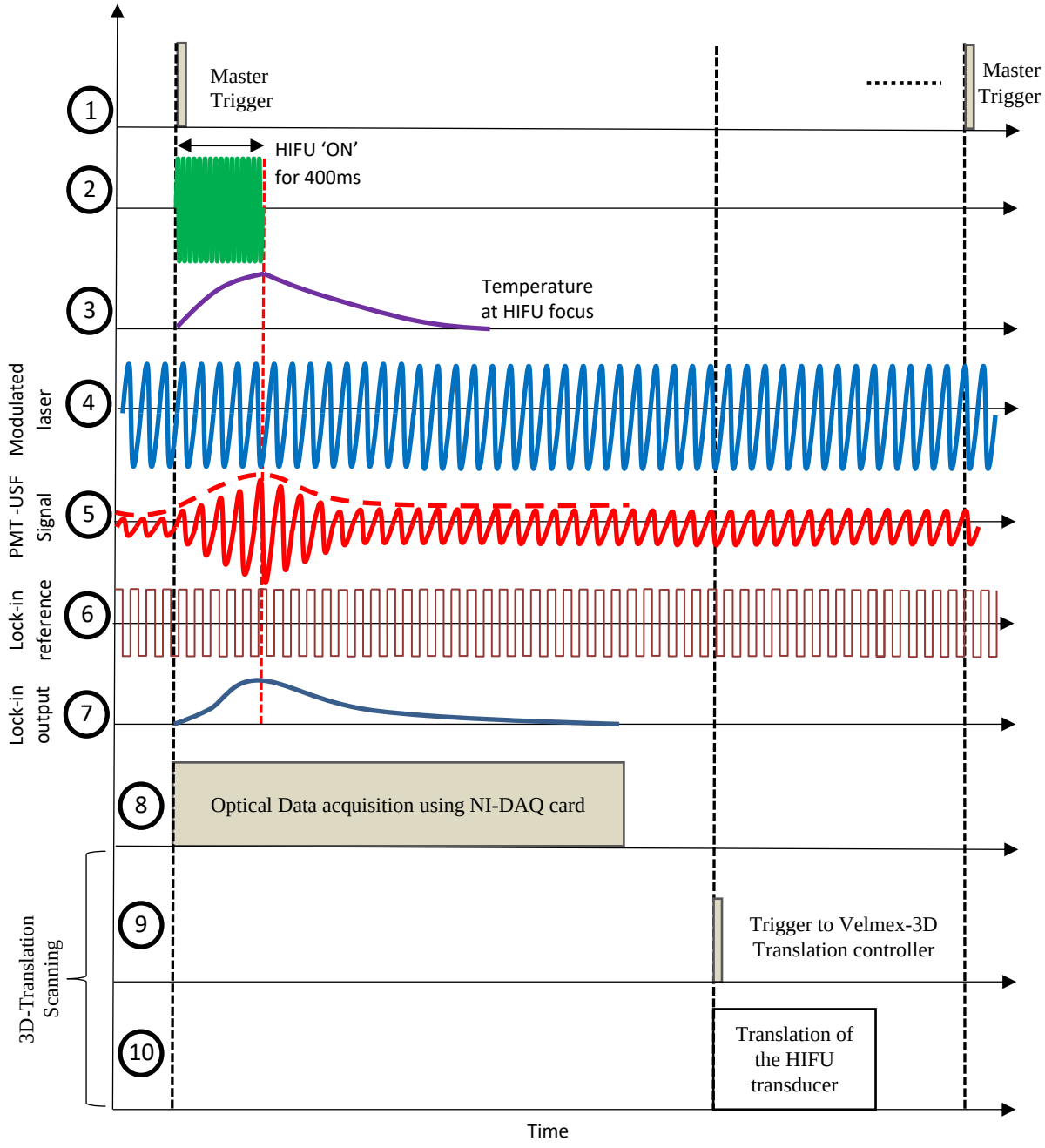

Figure 5-4 Time sequence of events and operations in USF imaging.

5.2.3 Processing of USF and CT Data and method for co-registration:

USF signal is processed as described in the previous chapter. Just to reiterate for this study, to increase the system sensitivity, the intensity of the excitation laser is modulated into a sinusoidal wave at 1 kHz. Thus, both the background fluorescence emission and the USF signal are also sinusoidal waves at 1 kHz. Therefore, only the 1 kHz fluorescence signal is acquired, analysed, and processed, while all other frequency components are rejected. The NI-DAQ acquired the dynamic change of the amplitude of the 1-kHz fluorescence signal before, during and after the heating pulse was applied. The background amplitude was estimated via the data acquired before the application of the heating ultrasound pulse, which mainly included laser leakage through the emission filters, possible auto-fluorescence from the sample, and/or fluorescence emission from those non-100%-off USF contrast agents. After the heating ultrasound pulse is applied, the amplitude of the 1-kHz fluorescence emission increases. The difference between the maximum amplitude and the background amplitude was used as the USF signal strength at this location. After scanning, a 2D USF image can be acquired.

Skyscan 1178 (Bruker, Kontich, Belgium) is used for CT imaging, which is a high-performance, ultra-fast, micro-CT system for high-throughput *in-vivo* and *in-vitro* scanning of small laboratory animals (typically used for preclinical research). The CT scanner was set to have 640 ms exposure with a rotation step of one degree. The projection is averaged twice at each degree increment in rotation to improve signal quality. Using the manufacture's reconstruction software (CTRecon), 16-bit TIFF images are created with a voxel size of 0.085x0.085x0.085 mm^3. These CT-reconstructed images can be read by MATLAB, and 2D or 3D images are created to co-register with the USF images, which are discussed later in this chapter.

To co-register two modalities, a reference silicone tube (Ref-ST, ID: 0.31 mm) is embedded perpendicular to the target silicon tubes in each of the three-tissue samples, as shown in Figure 5-3. Before USF scanning is performed, the reference silicone tube (Ref-ST) and target silicone tube (ST) are filled with air. Using the 15 MHz transducer as a conventional US imaging device (i.e., using pulse-echo technique), the coordinate information—such as the location and the distance of the reference silicone tube from the scan area (region-of-interest, ROI) containing the target silicone tube/s—is noted. While performing CT imaging, the reference silicone tube is filled with CT contrast agent (Exitron nano 12000). Using the distance information from the US imaging, USF reconstructed image is overlaid on to the appropriate CT reconstructed image (*x*-*z* plane), which is discussed later in the results section of this chapter.

5.2.4 Materials and Synthesis of USF Contrast Agents

Depending on the type of experiment performed, different types of USF contrast agent were used:

1) Single and two-target USF imaging: The USF contrast agent used in this study was $ADP(OH)_2$ encapsulated in Pluronic-F98-based thermos-sensitive nano-capsules [12, 41]. The initial concentration of Pluronic-F98 in deionized water is 50 mg/ml. The peak excitation and emission wavelengths were around 680 and 715 nm, respectively. The temperature-switching threshold is about ~27 degrees Celsius.

2) Multiple target and multi-colour USF imaging: The USF contrast agent used in this study was $ADP(OH)_2$ encapsulated in Pluronic-F127-based thermos-sensitive nano-capsules [12, 41]. Here, surfactant Pluronic F127 is dissolved in deionized water (pH 8.5, w/v:5%) and, then dissolved in the dye/TBAI (molar ratio = 1:6) in chloroform and

kept it in sonication for thirty minutes. We then dropped the dye/TBAI chloroform solution into the Pluronic aqueous solution with agitation, further dispersed the solution with a sonicator (Qsonica, LLC., Newtown, CT, USA) at 20 W for four minutes, and kept the resulting solution stirring until the chloroform was completely evaporated. We collected the USF contrast agents by solution filtration using a 1.2 μm membrane (Fisher Scientific, Pittsburgh, PA, USA) and an Amicon Ultra centrifugal filter (10000 molecular weight cut-off, Millipore, Billerica, MA, USA). The temperature-switching threshold is about ~23 degrees Celsius.

Another type of USF contrast agent used is ICG-based USF contrast agent. It is a third-generation ICG-nanoparticle that adopts 4-4'-azobis (4-cyanopentanoic acid) (ACA) as a reaction initiator with surfactant Pluronic F98 [22]. It is named ICG-encapsulated, ACA-initiated, Pluronic-surfactant poly(N-isopropylacrylamide) nanoparticles (in short, ICG-encapsulated ACA-PNIPAM-F98 NPs). It has a temperature-switching threshold of ~26 degrees Celsius.

3) *In-vivo* USF imaging: ICG-based USF contrast agent is used for this study. This USF contrast agent is a second-generation ICG-nanoparticle that adopts 4-4'-azobis (4-cyanopentanoic acid) (ACA) as a reaction initiator with surfactant sodium dodecyl sulfate (SDS). It is named ICG-encapsulated, ACA-initiated, SDS-surfactant poly(N-isopropylacrylamide) nanoparticles (in short, ICG-encapsulated ACA-PNIPAM-SDS NPs) [22]. Four such ICG-based USF contrast agents were synthesized with different temperature thresholds, among which P(NIPAM-AAm 86:14) nanoparticles exhibit the temperature switching at ~40 degree Celsius. Hence, it can be used for *in-vivo* USF imaging, as the typical background temperature of a mouse body is ~36 degrees Celsius.

Details regarding the above-mentioned ICG-based USF contrast agents can be found in our previous work [22].

5.3 Results and discussions:

5.3.1 Single target USF imaging using 15 MHz HIFU transducer:

Like the previous study, we started from the simplest case in which a single micro-tube (ID = 0.31 and OD = 0.64 mm) is embedded in a piece of porcine muscle tissue. The tube was filled with the aqueous solution of the $ADP(OH)_2$-based USF contrast agent. The USF image was obtained by scanning the *x-y* plane (lateral plane), which is perpendicular to the US propagation direction (axial or *z*-line). Figure 5-5 (a) shows the acquired USF image of the cross-section of the micro-tube using a 15 MHz HIFU transducer at 220 mVpp driving voltage with 400 ms exposure duration. The average lateral (*x*) size calculated for each of the lines across the tube (*y*-direction) is 0.63±0.06 mm, and SNR is calculated to be 18.34±1.66. In comparison, the lateral size calculated for the similar tube imaged using a 2.5 MHz HIFU transducer in our previous study [12, 13, 21] is about 0.91±0.04 mm, and SNR is ~88 in tissue mimicking (TMM) phantom. Clearly, the lateral resolution of a USF system using a 15 MHz HIFU transducer is better that that of a 2.5 MHz HIFU transducer. It should be noted that the signal-to-noise ratio (SNR) of USF images is dependent upon many factors such as the type of sample under imaging (i.e., tissue mimicking silicone sample, porcine tissue sample, etc.), exposure duration of HIFU transducer, conversion (electrical-to-acoustic transfer) efficiency of HIFU transducers, driving power, etc. To improve the SNR of the 15 MHz based USF images, the following approach is proposed. It is divided into a two-step process for USF image processing. Using a typical USF signal as a reference, a correlation matrix with each pixel representing correlation index is generated. Figure 5-5(b) shows the correlation matrix with a

correlation index of 0.7 and above. Later, a binary matrix is created from this correlation matrix such that the pixels with correlation index value of 0.7 and above are replaced by '1' and others with '0'. Then a morphological operation is applied to the binary image, thereby generating a binary mask, as shown in Figure 5-5 (c). A morphological operation is performed to remove scan locations that exhibit a high correlation index but are away from the tube and therefore could not have contributed to the USF signal recorded. The final step is to simply apply a binary mask to the original USF image, thereby not compromising lateral resolution but improving SNR exponentially, as shown in Figure 5-5 (d).

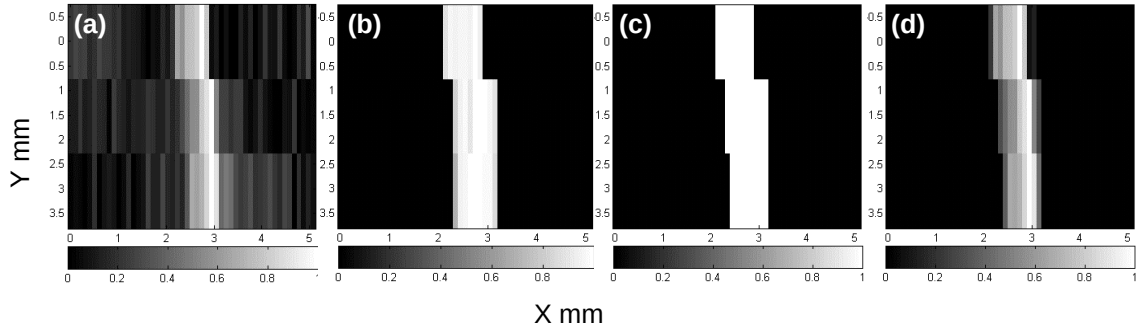

Figure 5-5 USF image of a single micro-tube filled with $ADP(OH)_2$ USF contrast agent using 15 MHz HIFU transducer in *x-y* plane (a) original USF image, (b) Correlation image with threshold cut-off at 0.7, (c) binary image of [b] and, (d) processed USF image.

The next part of single-target imaging is to obtain a USF image along the *x-z* plane (depth plane). Figure 5-6(a) shows the USF image obtained in the *x-z* plane using a 15 MHz HIFU transducer-based USF system. The size of the target, a single silicone micro-tube (ID = 0.31 and OD = 0.64 mm), in the USF image is obtained by calculating FWHM with respect to maximum USF signal Intensity of the USF image recorded. The

average of two target sizes of USF images (*x*-*z* plane) along the axial (*z*) is ~1.9 mm and the lateral (*x*) is ~0.62 mm. The large axial size is understandable, as the USF size of the target obtained is approximately a convolution of the thermal size at focus (~0.98 mm) and the target area (ID ~0.31 mm). In comparison, when USF imaging was done on the same silicone tube (ID ~0.31 mm) using a 2.5 MHz HIFU transducer with an axial-temperature focal size of ~2.9 mm driven at 140 mVpp and 400 ms, the USF sizes of the target were ~5.3 mm and ~1.3 mm along axial (*z*) and lateral (*x*) directions, respectively. This shows that both the axial and the lateral resolution of USF imaging can be significantly improved by using a high-frequency (15 MHz) HIFU transducer.

A customized processing algorithm was developed to isolate the high USF signal regions in the *x*-*z* plane, thereby further improving the resolution and SNR of USF imaging. This algorithm has a three-step process. The first step is identical to that of the previous processing algorithm in which the correlation matrix with a correlation index of 0.7 and above is calculated, as is shown in Figure 5-6 (b). It can be observed that the target area is large and that the binary image obtained from this correlation matrix would degrade the USF image along the axial direction after processing. Therefore, the second step applies the feature-extraction method uses the original raw USF image (Figure 5-6 (a)) and correlation matrix (Figure 5-6 (b)). This method uses a power formula, as follows:

$$B(i,j) = corr\big(A(i,j)\big).* P^{A(i,j)} ,$$

where, *A* is the original raw USF image, *corr* is the correlation matrix of *A*, and *P* is power/gain.

An USF image obtained using the power formula is shown in Figure 5-6 (c). The USF image target size along the axial direction is calculated to be ~1.6 mm (P = 2000),

thereby improving the axial size of the processed USF image. Note that the algorithm can be ended here and the processed image can be used. For this study, however, emphasis is placed on the original raw image; thus, further processing is performed. For the third step to the featured extracted USF image (Figure 5-6 (c)), a morphological operation is performed. Here, a threshold cut-off of 10% of maximum intensity is applied; then the processed image is converted to a binary image, as shown in Figure 5-6 (d). Applying a morphological operation to the feature-extracted USF image improved the algorithm slightly by generating the binary mask with smaller target region along with high correlation index. In contrast, target region of binary mask obtained using morphological operation applied to correlation matrix has larger area as shown in Figure 5-6 (b). Hence, the feature-extracted binary image improves the resolution of the USF image by selecting a smaller area of the target. Once the binary image is obtained, it is applied to the original raw image. The processed USF image obtained is shown in Figure 5-6 (e).

Dual-modality imaging is performed using the USF imaging system with a 15 MHz HIFU transducer and micro-CT imaging (Skyscan 1178, Bruker, Kontich, Belgium). CT imaging gives information about the dimensions of the target that is imaged in the USF imaging system. By setting the threshold at 50% of the maximum of the CT image in the region-of-interest (ROI), the FWHM obtained along the lateral-x is ~0.37 mm; along the axial-z, it is ~0.41 mm. This closely corresponds to the measurement of the inner diameter (ID) of the silicone tube embedded in the porcine tissue sample (~0.31 mm). To overlay the USF image on the CT image, the processed USF image in Figure 5-6 (e) is interpolated to the size of the CT image. The resultant image is shown in Figure 5-6 (f). Figure 5-6 (g) is the CT image obtained by applying threshold cut-off of 50% of its maximum to the normalized CT image. Figure 5-6 (h) shows the USF image overlaid onto

the CT image. Note that by using the feature-extracted USF image, the axial resolution can be improved to ~1.7 mm and will then be comparable to the axial resolution of the USF image (about ~1.5 mm), which was obtained using the dual-HIFU USF system discussed in Chapter 4 of this dissertation.

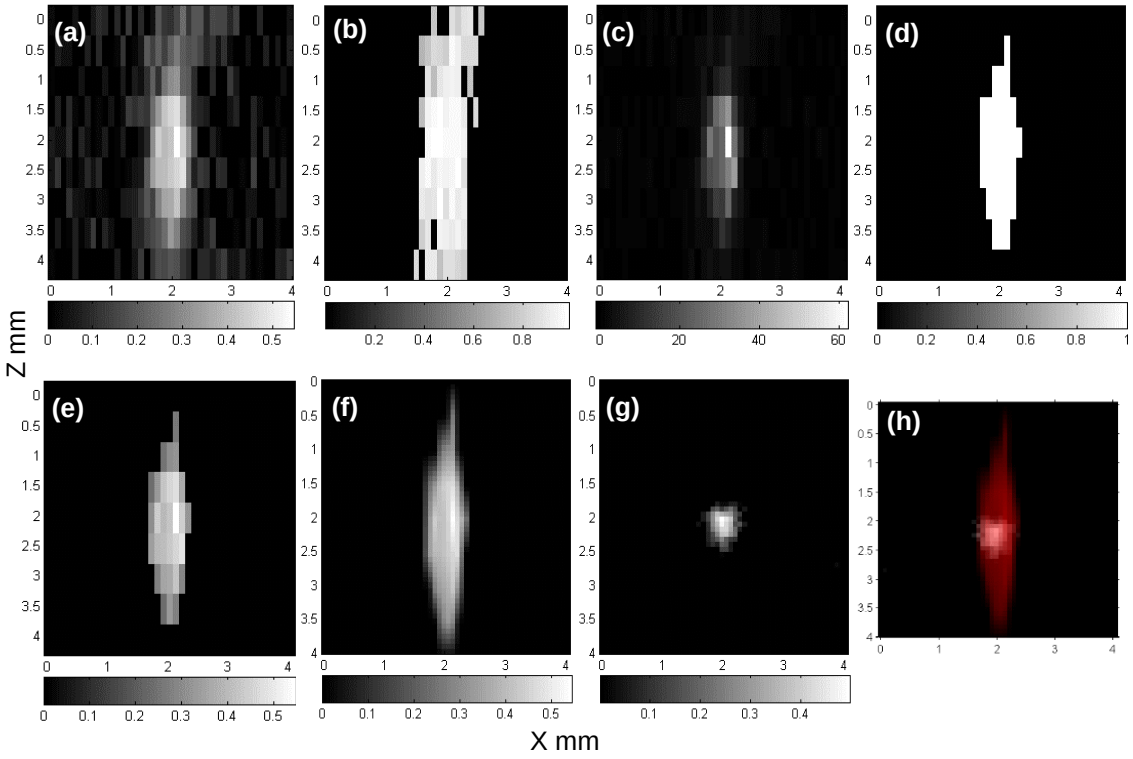

Figure 5-6 USF image of a single micro-tube filled with $ADP(OH)_2$-USF contrast and CT contrast agents (1:1) using 15 MHz HIFU transducer in x-z plane (a) original USF image, (b) Correlation image with threshold cut-off at 0.7, (c) Feature-extracted image using [a] and [b], (d) binary image of [c], (e) processed USF image, (f) smoothed USF image of [e], (g) CT image with 50% threshold cut-off and, (h) USF image (red) [f] overlaid onto CT image (white) [g].

5.3.2 Multiple target USF imaging:

The next step in the 15 MHz based USF imaging experiment involved a study to resolve two targets at variable separation distances. Also, the study was conducted with the variable driving power of the HIFU transducer to observe its influence on the ability of the USF system to detect and resolve multiple targets with good precision and SNR. Two micro-tubes (ID = 0.31 and OD = 0.64 mm) were embedded in a piece of porcine muscle tissue such that they crossed each other to form a 'V' shape, as shown in Figure 5-7. Scanning was performed in the *x-y* plane with an increment of 0.5 mm, and a total of nine such *x-y* planes are recorded. Scanning was performed such that the fifth *x-y* plane approximately coincides with the plane of the two tubes. Five lines along the *y* direction are recorded such that the distance from the centre of each tube to another tube varies with a distance of 0, 0.5, 0.81, 1.27 and 1.7 mm, respectively. This is recorded by using the 15 MHz HIFU transducer as a conventional (pulse-echo method) ultrasound (US) device when the two micro-tubes were filled with air as shown in Table 5-2.

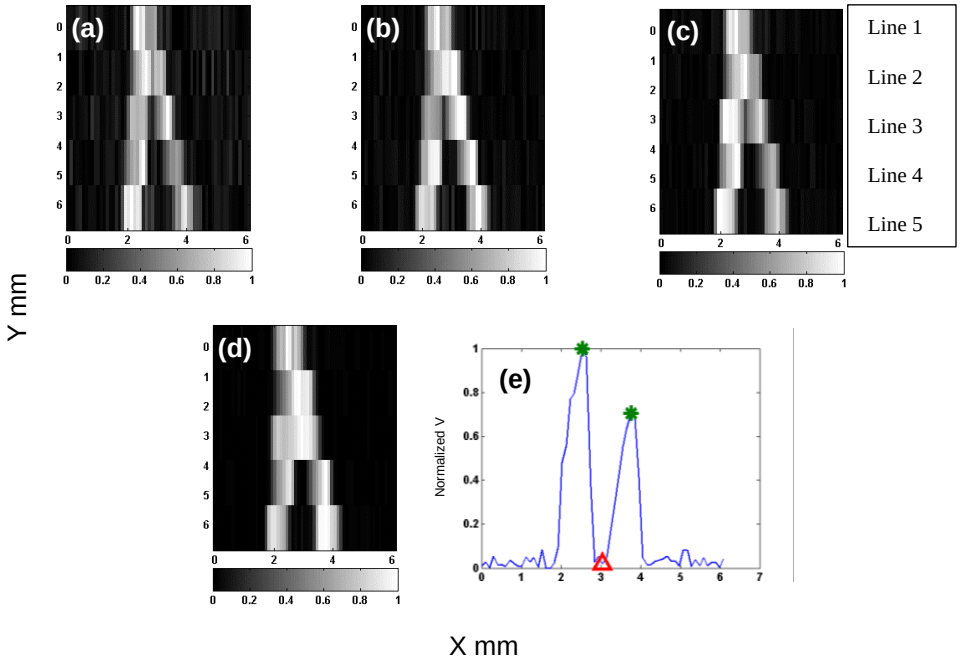

Figure 5-7 USF image of two micro-tubes ('V' arrangement) filled with $ADP(OH)_2$ USF contrast agent using 15 MHz HIFU transducer in x-y plane at (a) 160 mV_{pp}, (b) 180 mV_{pp}, (c) 200 mV_{pp}, (d) 220 mV_{pp} and, (e) Line profile of 'Line 4' of image [c].

Figure 5-7 (a), (b), (c) and (d) depicts the *x-y* USF image recorded for varying driving voltages of 160, 180, 200 and 220 mV_{pp} for driving the 15 MHz HIFU transducer via a 50 dB RF power amplifier. Corresponding to each of the five lines across the tubes in the *x*-direction, the average FWHM and SNR of two tubes were calculated and are shown in Table 5-1. The *X* in Table 5-1 represents the two micro-tubes (targets) that were not resolved. Targets are resolvable if the FWHM calculated is around ~0.65±0.07 mm for each respective target. Figure 5-7 (e) shows Line 4 of Figure 5-7 (c) where the peaks (green asterisk) and minimum in the valley (red triangle) are calculated, followed by FWHM and SNR for each of the targets. It was observed that the targets were not

resolvable in Line 3 when HIFU transducer was driven at 220 mV_{pp}. But Line 4 and Line 5 have SNRs of 102 and 119, respectively. Targets in Line 3 are not resolvable because the higher driving power of the ultrasound transducer yields higher temperatures, leading to a larger temperature spread in its focal depth, which evidently yields a larger spread of the USF signal. It is also observed that the SNR steadily increased with increasing driving voltage without compromising its lateral (*x*-*y*) resolution. Table 5-2 shows the distance calculated between two targets using conventional US imaging techniques and the USF imaging technique along with the FWHM calculated for individual targets. Clearly, the US imaging has a higher resolving capability than the USF imaging, as it can resolve two tubes in Line 2. On the other hand, USF imaging with a 15 MHz HIFU transducer could not resolve two targets with a separation distance of less than ~0.8. In conclusion, then, the higher driving voltage of the 15 MHz HIFU transducer yields a higher SNR and can resolve two or more targets greater than 0.8 mm apart without compromising the lateral resolution (~0.68 mm) of the USF system.

Table 5-1 Average of FWHM and SNR along each y-line for varying driving power of 15 MHz HIFU transducer.

FWHM mm				**SNR**			
160	**180**	**200**	**220**	**160**	**180**	**200**	**220**
X	X	X	X	X	X	X	X
X	X	X	X	X	X	X	X
0.5712	0.6605	0.6958	X	22.9670	37.9304	58.0849	X
0.6221	0.6104	0.6218	0.5945	20.1664	36.4943	43.9900	119.3541
0.6154	0.6674	0.6853	0.7108	20.9125	20.7766	56.1131	102.0377

Table 5-2 Comparison of US imaging and USF imaging to resolve two targets

US Imaging	USF Imaging	Lateral FWHM in mm	
		Target 1 (Tube 1)	Target 2 (Tube 2)
X	X	X	X

0.5	X	X	X
0.81	1.12	0.76	0.62
1.27	1.22	0.66	0.57
1.7	2.03	0.67	0.69

Figure 5-8 depicts the 2D and 3D visualization of the USF image obtained for the above sample when the 15 MHz HIFU transducer was driven at 200 mV_{pp}. Figure 5-8 (a) and (b) shows a processed 2D USF and 2 CT image along the *x*-*z* plane for Line 5 of Figure 5-7 (c). The lateral (*x*) FWHM for individual targets, from left to right as shown in Figure 5-8 (a), are 0.66 and 0.69 mmm respectively, and the corresponding axial (*z)* FWHM are 1.54 and 1.88 mm, respectively. Therefore, the axial size is about 1.71±0.24 mm, which is comparable to ~1.5 mm for the USF system with the dual-HIFU transducer discussed in the previous chapter, except that it has a better lateral size of 0.67±0.02 mm when compared to ~1.07 mm of same dual-HIFU-USF system. This implies that the USF system with the high HIFU transducer has a better lateral and axial resolution. The drawback, however, is that the higher the frequency of the transducer, the lower its power-conversion (electrical-to-acoustic transfer) efficiency with respect to penetration depth. This implies that it must be driven at higher powers to induce the desired temperature increase. But driving power is limited by the driving electrical capacity of the transducer itself, thereby limiting the maximum temperature that could be induced inside the sample under imaging.

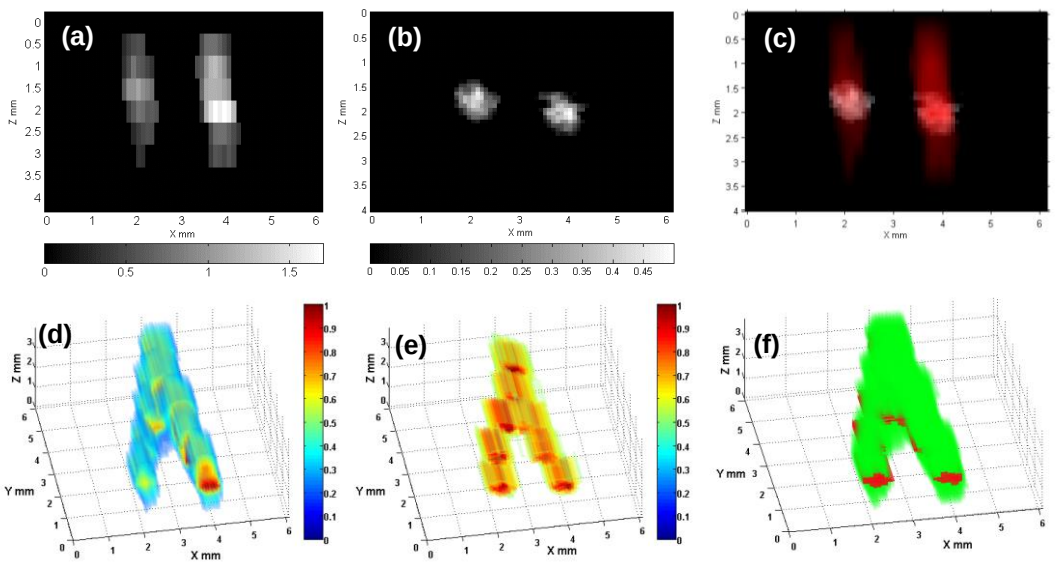

Figure 5-8 USF image of two micro-tubes ('V' arrangement) filled with $ADP(OH)_2$ USF contrast and CT contrast agents (1:1) using 15 MHz HIFU transducer in x-z plane of 'Line 5' obtained at 200 mVpp; (a) processed USF image, (b) processed CT image, (c) USF image (red) [a] overlaid onto CT image (white) [b], (d) 3D USF image, (e) 3D CT image and, (f) 3D USF image (green) [d] overlaid onto CT image (red) [e].

The processing algorithm discussed in Section 5.3.1 is applied to generate processed USF and CT images, as shown in Figure 5-8 (a) and (b), respectively. The same processing algorithm is applied to each of the *x-z* planes from Line 1 to 5 along with corresponding CT data. Figure 5-8 (c) shows the *x-z* USF image of Line 5 (Figure 5-8 (a)) overlaid onto the corresponding CT image slice (Figure 5-8 (b)). The 3D-processed USF image is shown in Figure 5-8 (c) by setting the threshold to 40% of the maximum of the processed USF signal. Figure 5-8 (d) shows the CT-reconstructed image by setting 50% of the maximum of the normalized CT image. By assigning a value of 0.2 to USF data and 0.8 to CT data, a 3D co-registered USF-CT image is shown in Figure 5-8 (e). This

emphasizes the ability of the dual-modality USF-CT techniques to image multiple targets with varying distances of separation between each other.

5.3.3 Multiple target – multiple color USF imaging:

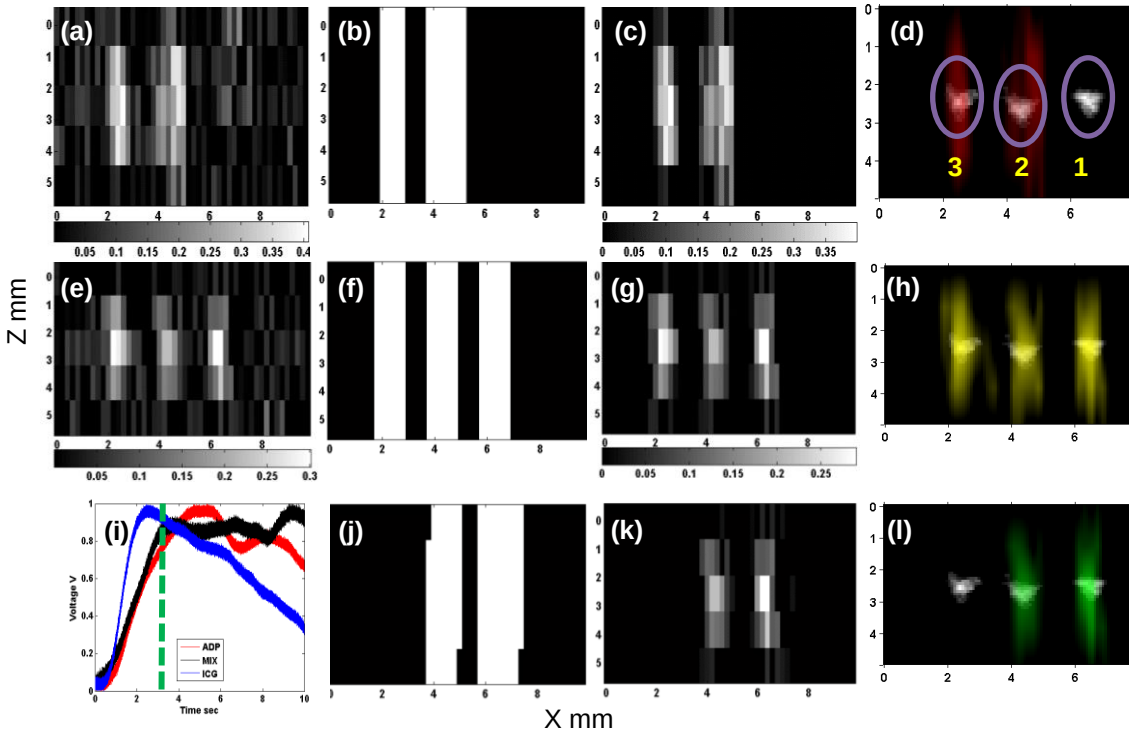

Figure 5-9 Dual modality USF-CT imaging of multiple (three) targets with two different USF contrast agents (tube 1 – $ADP(OH)_2$, tube 2 – Mix and tube 3 – ICG); (a) USF image with 808 nm excitation laser, (b) binary image of [a], (c) processed USF image [a], (d) USF image (red) [c] overlaid onto CT image, (e) USF image with 671 nm excitation laser, (f) binary image of [e], (g) processed USF image [e], (d) USF image (yellow) [g] overlaid onto CT image, (i) USF signal of ADP(red), Mix(black) and ICG(blue) with cut-off rise-time of 3.1 s (green dashed line), (j) new binary image of [e] obtained using rise-time (>3.1 s), (k) new processed USF image of [e] and, (l) USF image (green) [k] overlaid onto CT image.

In this section, three tubes (see the configuration Figure 5-3) were imaged by using a USF system with a 15 MHz HIFU transducer. Tubes 1 and 3 were filled with $ADP(OH)_2$ encapsulated in thermos-sensitive nano-capsules made of Pluronic-F127 (labelled 'ADP' in Figure 5-9 (i)) and an ICG-based USF contrast agent (labelled 'ICG' in Figure 5-9 (i)), respectively. They are mixed with CT contrast agent in a ratio of 1:1 each. They have a lower critical solution temperature (LCST) of about ~23-24 and ~26-27 degrees Celsius, respectively, with a background temperature of around 21-22 degrees Celsius. Tube 2 was filled with the three mixed solutions: $ADP(OH)_2$, ICG-based, and CT contrast with a volume ratio of 1:1:1 (labelled 'MIX' in Figure 5-9 (i)). The three tubes can be clearly localized as indicated by the three yellow circles in Figure 5-9 (d), where white colour indicates the CT image, set at threshold of 50% of maximum within the region of interest (ROI) of the tube filled with CT contrast agent (no matter which solutions were filled). Also, just like US imaging, CT imaging is insensitive to the fluorophore types and thus cannot differentiate which fluorophore is filled in each of the tubes.

To distinguish tubes based on the fluorophores, ICG-based USF contrast agents were first imaged using the USF system. An 808 nm laser was used as the excitation light source. The emission filters included two 830 nm long pass interference filters and two RG830 absorption filters. The USF image thus obtained is shown in Figure 5-9 (a). To remove noise, we used the algorithm described in Section 5.3.1 without the power function, as feature extraction is applied here as well. Therefore, a correlation image is generated. To this image, a threshold is set at 0.7 and above to obtain areas with the highest correlation coefficient. The next step is to generate a binary image by setting all the correlation coefficient values that are below 0.7 to zero and everything else to one. Any disconnected pixels are set to zero (using morphological operations). Only regions

with the highest correlation to the typical USF signal are to remain in the processed USF image, as shown in Figure 5-9 (b). A binary image is then applied to the original image in Figure 5-9 (a). The resultant processed USF image is shown in Figure 5-9 (c). The resultant USF image (from left to right) has an axial (z) FWHM of ~1.85 and ~1.82 mm, respectively. Figure 5-9 (d) shows the dual-modality of the USF image (red) overlaid on the CT image obtained by an 808 nm excitation laser. In Figure 5-9 (a-d), only tubes 2 and 3 are shown in the USF image, indicating that the both the tubes are filled with ICG-based USF contrast agent. Tube 1 is not visible, as the ADP-based USF contrast agent is not excited by the 808 nm laser source.

On the other hand, Figure 5-9 (e-l) shows the USF image obtained using a 671 nm excitation laser and a set of emission filters (two 715 nm long pass interference filters and two RG695 absorption filters). Figure 5-9 (e-h) shows the USF images obtained using steps similar to those used to process the USF image excited with the 808 nm laser source. In this case, all three tubes are visible in the USF image (yellow in Figure 5-9 (h)), thereby indicating that both $ADP(OH)_2$ and ICG-based USF contrast agents are excited with a 671 nm laser source. To distinguish tubes filled with $ADP(OH)_2$ contrast agent, a direct approach based on the dynamic trend of their respective USF signal is exploited. It can be observed from Figure 5-9 (i) that the $ADP(OH)_2$-based USF signal has a longer rise time (> 4 seconds) compared to that of the ICG-based USF signal (around 2.2 seconds). Therefore, a new algorithm is needed to process the USF images excited using the 671 nm laser source. Instead of a correlation method, a different approach is opted for in which an image is generated with the rise-time (time taken to reach maximum) at each of the pixel locations. A cut-off of ~3 seconds is applied to get the regions with longer rise-time (time to peak), as shown by the green dashed line in Figure 5-9 (i). This image

is then converted to a binary image, as shown in Figure 5-9 (f), by using morphological operations. Figure 5-9 (g) shows the resultant USF image when the binary image in Figure 5-9 (f) is multiplied by the original USF image in Figure 5-9 (e). Therefore, Figure 5-9 (l) shows the true-positive USF image (green) with tubes filled with $ADP(OH)_2$ contrast agent successfully distinguished from tubes filled with ICG-based contrast agent. The USF image (green) is overlaid onto the processed CT image to show the locations of the three tubes that are imaged using the USF technique.

More accurate results of the targets in the USF images could be recorded if the step size in the *x*-direction and *z*-direction is decreased, but this would increase the overall scan time. For this study, the emphasis is on showing the ability of the USF system to image multiple target with multiple colours by using different USF contrast agents and a simple algorithm to distinguish targets filled with two different USF contrast agents based on the dynamic trend of the respective contrast agents, as shown in Figure 5-9 (i). The overall scan time of the USF imaging is reduced by the following steps. First, the step size taken between each scan location along *x*-direction is increased from 0.1 mm to 0.2 mm; second, the number of *x*-*y* scan planes recorded is decreased from nine planes to five planes. This is because the $ADP(OH)_2$-F127 has threshold switching at ~23 degrees Celsius, which is very close to the background temperature of ~21 degree Celsius. For this reason, it has a long decay duration of USF signal, which requires a longer duration of about 35 seconds between each scan location compared to 15 seconds for $ADP(OH)_2$-F98, which has threshold switching at ~26 degrees Celsius. Note that the $ADP(OH)_2$ encapsulated in the Pluronic-F98 nano-capsule is not used in this study, since its threshold switching of ~26-27 degrees Celsius is close to that of the ICG-based USF contrast agent and the USF signal is dependent on the lower critical solution temperature

(threshold switching temperature) and not on type of fluorophore used. This makes it impossible to distinguish the USF signal of $ADP(OH)_2$-F98 contrast agent from that of the ICG-based contrast agent, as both have a similar trend of USF signal. On the other hand, $ADP(OH)_2$-F127 contrast agent has a threshold switching of ~23 degrees Celsius, which is far from that of the ICG-based contrast agent (~26 degrees Celsius). Thus, the trends are different, as shown in Figure 5-9 (i).

5.3.4 In-vivo *USF Imaging:*

The next step is to undertake *in-vivo* study and observe the ability of the USF system with a 15 MHz HIFU transducer to image a small target via the intra-muscular localized injection of mixture of ICG-based USF contrast agent and CT contrast agent at a 1:1 ratio. Figure 5-10 (a) and (b) shows the fluorescence image obtained via a spectroscopy camera system (ProEM-HS, Princeton Instruments, NJ, USA) before and after injection of 20 micro-litres of the mixture solution near the right leg of the mouse under imaging. Figure 5-10 (c) shows the injection site obtained using CT imaging, highlighting the mouse's skeletal system and the injection region in red and blue colour, respectively.

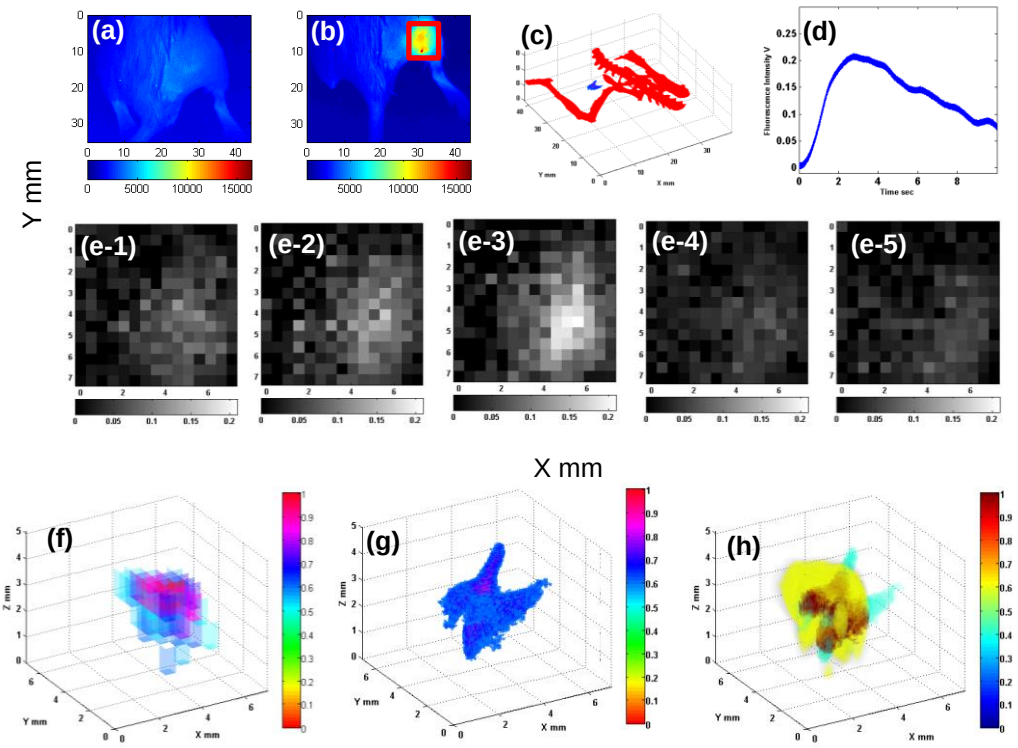

Figure 5-10 In-vivo mouse USF imaging using 15 MHz HIFU transducer; fluorescence image of mouse (a) before and (b) after intra-muscular injection of ICG-based and CT contrast agent (1:1), (c) 3D CT image of skeletal and injection areas of mouse, (d) USF signal of ICG-based USF contrast agent (LCST ~ 40 ^{O}C), (e) Five (x-y) USF images at 1.27 mm apart in depth (z) direction, (f) 3D processed USF image, (g) 3D processed CT image and, (h) USF image (yellow) overlaid onto CT image (blue) with common regions (red).

Figure 5-10 (d) shows a typical USF signal obtained at the pixel location with maximum intensity from the USF image shown in Figure 5-10 (e-3). This signal is used as a reference signal to obtain the respective correlation matrix for all five USF images at each layer. Figure 5-10 (e-1 to -5) shows the 7x7 mm^2 region of interest (scan area indicated by red box in Figure 5-10 (b)) of five USF images along the *x-y* plane. The plane

(Figure 5-10 (e-3)) that exhibits the most intense USF signal recorded is in middle, along the *z* direction. From the left to the right, Figure 5-10 (e) shows the USF images in the *x*-*y* plane obtained from bottom to top with a step size of 1.27 mm along the *z*-direction. It is evident that USF signal intensity is significantly reduced when the depth of the HIFU transducer focus moves away from the middle layer (Figure 5-10 (e-3)) to successive layers along the *z*-direction. Using the USF signal in Figure 5-10 (d), a correlation matrix is generated. A binary matrix is then obtained by setting the threshold cut-off at 0.7. This implies that the binary matrix has zero value for all the pixels with correlation coefficients less than 0.7; everything else set to value one. Similar operations are performed on all the five *x*-*y* USF images, as shown in Figure 5-10 (e-1 to -5). Figure 5-10 (f) is the 3-dimentional USF image obtained from all five processed USF images stacked one on top of another (bottom to top). Figure 5-10 (g) shows the intra-muscular injection location of mixture solution in 3-dimensions. It was processed using the MATLAB and obtained using CT imaging. It shows the isolated region-of-interest of the localized injection solution, setting the threshold to 50% of the maximum CT signal. Figure 5-10 (h) shows the overlaid regions of the processed USF and CT 3D images. Once again, it is clearly observed that the USF image volume size of the injection solution (=10.28 cubic mm) closely matches the CT image volume size (=7.06 cubic mm), thereby showing the high-resolution capabilities of USF imaging obtained using a 15 MHz HIFU transducer.

5.4 Conclusion

In conclusion, a comprehensive study was performed which can be categorized in three steps: 1) characterization of the USF imaging system based on a 15 MHz, high-intensity focused-ultrasound transducer, 2) feasibility of a dual-modality imaging system for imaging single and multiple targets by combining USF imaging with the popular CT

imaging, and 3) application of the developed USF system for *in-vivo* mouse imaging. The initial study showed that by using the high-frequency (15 MHz) HIFU transducer, the USF image sizes obtained for a small target (ID 0.31 mm) was ~0.65±0.07 mm and ~1.7±0.2 mm along the lateral and axial directions, respectively. This is a significant improvement in the resolution of the USF system. It also been demonstrated that USF imaging can be combined efficiently with other modalities such as CT imaging (gives information on dimension and distribution of target) while performing multi-colour (multi-colour fluorophores) USF imaging for multiple targets with good resolution and SNR. A simple but effective algorithm was proven not only to distinguish the target filled with two different USF contrast agents (ADP-based and ICG-based with threshold switching at ~23 and ~26 degrees Celsius, respectively) based on the dynamic behaviour of their respective fluorescence outputs, but also to improve the SNR without compromising the resolution of the USF system. A preclinical experiment was also performed with promising results. Here, the volume of the mixture solution (1:1 volume ratio of ICG-based USF contrast agent and CT contrast agent) injected intra-muscularly near the right leg of a mouse is efficiently (good SNR) imaged using both a USF system and a CT system. The volumes calculated were 10.28 cubic mm and 7.06 cubic mm, respectively. This demonstrates the high resolution of the USF system using a 15 MHz, high-intensity, focused-ultrasound transducer.

Chapter 6

Conclusion and future work

6.1 Conclusions

This dissertation aims to develop solutions with system-design and/or imaging techniques to improve the axial resolution and sensitivity of USF imaging technique. The specific objectives of this work are the following: (1) to study and characterize the high-intensity focused-ultrasound transducer's performance so as to induce the desired temperature and improve resolution; (2) to develop a USF imaging system to improve the sensitivity of the USF imaging; (3) to develop a USF imaging system to improve the axial resolution of the USF imaging by using a dual HIFU design; and (4) to develop a USF imaging system to improve the resolution using a high-frequency HIFU transducer. These newly developed USF systems can be combined with conventional imaging modalities (such as, Ultrasound and CT imaging) to show their versatility for dual-modality imaging and *in-vivo* application. The specific objectives have been accomplished in the studies presented in Chapters 2-5.

The study reported in Chapter 2 was conducted to achieve spatial resolution beyond the acoustic diffraction limit for deep-tissue high-resolution imaging. Generally, in centimetre-deep tissues, the spatial resolution of pure optical imaging techniques is limited to ~millimetres by tissue light scattering [33]. To break this limit, ultrasonic techniques have been incorporated into optical methods. One such imaging modality is ultrasound-switchable fluorescence (USF) imaging techniques that has been developed recently [15, 17-19]. A high-intensity focused-ultrasound (HIFU) transducer was used to heat temperature-sensitive fluorescent probes only in the HIFU focal volume. This enabled a HIFU-enhanced or HIFU-generated fluorescence signal to be detected for optical imaging

with acoustic spatial resolution in deep tissues. USF has shown a potential to break the acoustic diffraction limit based on a temperature threshold of switching on or off [15]. While the temperature-threshold based method is promising, the improvement in spatial resolution is relatively limited if it is used alone. Therefore, we experimentally demonstrated that ultrasound-induced temperature focal size can be significantly influenced by the driving power and exposure time of a HIFU transducer. It has shown to be reduced beyond the acoustic diffraction limit if nonlinear acoustic effects occur and if the ultrasound-induced thermal energy is confined within the focal volume. For USF- or UTF-based imaging techniques, the ultrasound-induced peak temperature increases only a few degrees. The nonlinear acoustic effect can occur by appropriately controlling the ultrasound exposure power, and the thermal confinement can be satisfied by appropriately controlling the ultrasound exposure time. Also, it was shown that thermal focal size and temperature rise remained consistent for a small area of 5 x 7 mm for fixed parameters of HIFU transducer such as exposure time, driving voltage and the depth of focus of the transducer. Therefore, the proposed method in this study may be an alternative way to break the acoustic limit and can potentially be used for deep-tissue high-resolution imaging via USF or UTF techniques. High-resolution USF imaging beyond the acoustic diffraction limit in deep tissues will be the focus of future studies.

Chapter 3 reported on a unique approach to improve sensitivity without compromising the spatial resolution of USF imaging in deep tissue for highly desired biomedical applications [3, 11, 34, 40]. The recently developed ultrasound-switchable fluorescence (USF) imaging has demonstrated its ability to achieve high SNR (or sensitivity) and high spatial resolution in tissue at a depth of centimetres [12, 13, 15, 21, 22, 31, 41]. In this study, we hypothesize that the SNR (or sensitivity) of the USF imaging

can be improved by modulating ultrasound exposure by gating the high-intensity focused-ultrasound (HIFU) transducer. The gating signal applied to the transducer switches the ultrasound exposure on and off at a certain frequency, which leads to the modulation of the temperature and the USF signal within the focal volume of the transducer. By detecting the modulated USF signal at this specific modulation frequency, the SNR (or sensitivity) can be increased. In summary, an innovative USF imaging method is developed by modulating HIFU exposure at a specific frequency ($f_{M\text{-}HIFU}$=1-2 Hz) with a small duty cycle (10-20%). Thereby, the temperature at the HIFU focal volume is modulated, which leads to the modulation of the USF signal at the modulation frequency of the HIFU transducer. Modulation of the USF signal has been clearly demonstrated, and by specifically detecting this USF signal, the SNR of USF images (or equivalently, the detection sensitivity) has significantly improved compared with our previous methods [12] (without modulation and without processing by the correlation method). A total of four HIFU modulation methods and four signal processing methods have been investigated. The highest SNR level is achieved by modulating the HIFU at $f_{M\text{-}HIFU}$=1 Hz at 20% of the duty cycle and processing it by using the FFT of the signal from the first lock-in amplifier (LIA-1).

Chapter 4 investigated a new system design to improve the axial resolution of USF imaging toward a possible application of the simultaneous imaging of multiple targets (SIMT) with high spatial resolution. Compared with single-target therapy, combination therapy, which involves the simultaneous use of multiple targeting drugs, has great potential to increase treatment efficiency by simultaneously blocking multiple signalling pathways [42, 43]. Accordingly, SIMT can visualize multiple signalling pathways and their interactions [5, 44], which can significantly benefit the investigation of drug resistance mechanisms and the monitoring or evaluation of targeted therapies [42, 45-50]. As stated

earlier, a relatively new technique, “ultrasound-switchable fluorescence” (USF), based on our recent finding that a focused-ultrasound wave can switch fluorescence emission on and off [17]. Thus, USF can provide fluorescence images of deep tissue with ultrasonic resolution [17, 37, 59-61]. Compared with pure fluorescence techniques, USF overcomes the limitation of the spatial resolution caused by tissue light scattering. Compared with pure ultrasound techniques (US), USF can conduct SIMT based on fluorescence spectroscopy. Current USF imaging can provide in-plane fluorescence images with excellent resolution on the x-y horizontal plane. This is because its axial resolution along the z direction, which is the ultrasound wave-propagation direction, is ~4–7 times lower than its in-plane lateral resolution (i.e., along x or y directions). Thus, it degrades the image quality along the z direction, which is also true for optical microscopy. On the other hand, the ultrasound B-mode image shows tissue information on a vertical plane (i.e., an x-z or y-z plane, the so-called tissue cross-section plane). Therefore, we developed a dual-modality imaging system by combining our recently developed USF imaging with the conventional ultrasound B-mode imaging. This dual-modality system has several unique features. (1) By using two 90°-crossed ultrasound transducers with an overlapped focal region, the axial resolution (in the direction of ultrasound wave propagation) of USF imaging has been significantly improved (close to its lateral resolution), which makes it possible to scan tissue on the *x-z* plane co-registered with a B-mode ultrasound image. In addition, it is helpful for developing 3D USF imaging in the future. (2) By combining the two imaging modalities, the system can image multi-colour fluorophores in tissues via USF technology, and it can image tissue acoustic structures via the B-mode ultrasound. Therefore, this dual-modality imaging technology shows great potential for simultaneously imaging multiple targets (SIMT), which can be implemented for molecular imaging in the future.

Chapter 5 investigated the relatively simple approach of using a high-frequency (15 MHz) high-intensity focused-ultrasound (HIFU) transducer in a USF system to improve its resolution. In this study, a comprehensive set of experiments was performed which can be categorized into three steps: 1) characterization of the USF imaging system based on a 15 MHz high-intensity focused-ultrasound transducer; 2) feasibility of a dual-modality imaging system for imaging single and multiple targets by combining USF imaging with a micro-CT imaging, and 3) application of the developed USF system for *in-vivo* mouse imaging. A preliminary investigation revealed that, by using a 15 MHz HIFU transducer in a USF system, the USF image sizes obtained for a small target (ID 0.31 mm) were ~0.65±0.07 mm and ~1.7±0.2 mm in the lateral and axial directions, respectively. This is a significant improvement in the resolution of the USF system compared to the conventional design [12, 15, 21]. It has also been demonstrated that USF imaging can be combined efficiently with other modalities, such as CT imaging (gives information on dimension and distribution of target), while performing multi-colour (fluorophores with different spectrum) USF imaging for multiple targets at good resolution and SNR. A simple but effective algorithm has distinguished targets filled with two different USF contrast agents (ADP-based and ICG-based with threshold switching (lower critical solution temperature, LCST) at ~23 and ~26 degrees Celsius, respectively) based on the dynamic behaviour of their respective fluorescence output. It has also improved the SNR and resolution of the modified USF system. A preclinical experiment was also performed with promising results. Here, the volume of the mixture solution (1:1 volume ratio of ICG-based USF contrast agent (LCST, 40 degree Celsius) and CT contrast agent) injected intra-muscularly near the right leg of a mouse is efficiently (good SNR) imaged using both the USF system and the CT system. The volume sizes calculated were 10.28 cubic mm and 7.06 cubic mm, respectively. This close approximation of volume sizes from two different modalities of the

same target demonstrates the high-resolution capability of the modified USF system. Here, a 15 MHz, high-intensity, focused-ultrasound transducer was able to induce desired heat and improve the axial and lateral resolution of USF imaging.

6.2 Limitation and future directions

Preliminary investigation was successfully conducted to characterize the performance of a high-intensity focused transducer (HIFU) with respect to induced temperature rise and its focal volume. This investigation demonstrated its potential to improve ultrasound-switchable fluorescence (USF) imaging. In addition, imaging techniques to improve the SNR and resolution of the USF imaging have been developed successfully. The experimental results will provide useful reference for continuing work in developing more efficient contrast agents and imaging systems for USF tomography in biological tissue and clinical applications. Limitations and potential future directions are discussed in what follows.

6.2.1 Modulation of ultrasound-switchable:

In the conventional USF system design, the SNR (~sensitivity) is based upon the modulation frequency ($f_{M\text{-}OPT}$) of the excitation laser source [15, 21]. In the modified USF system design, the temperature is modulated by switching the HIFU transducer, the heat source, on and off at a fixed modulation frequency ($f_{M\text{-}HIFU}$). This encodes the USF signal with the frequency of the HIFU modulation ($f_{M\text{-}HIFU}$). The major limitation of the proposed USF imaging technique is the low modulation frequency of HIFU transducer ($f_{M\text{-}HIFU}$) and its corresponding small duty cycle (which determines the duration of HIFU exposure per cycle). As the duty cycle increases the duration for which the HIFU exposure per cycle also increases, it thereby increases the duration and intensity of the temperature within the

HIFU focal region. On other hand, the increase in the duty cycle decreases the duration of successive gating pulses to switch HIFU 'OFF'. This in turn influences the USF signal to have less duration to decay (output of LIA) between the pulses, thereby reducing the SNR. Therefore, to achieve good SNR, either the duration between the successive gating pulses that drive the HIFU transducer should be large or the duty cycle should be small. (Note that a very short duty cycle may not induce sufficient temperature for the USF contrast agents (fluorophores) to undergo fluorescence intensity switching.) For example, for the proposed USF imaging technique, the highest SNR (175, from FFT of LIA-1) was calculated for the HIFU modulation sequence of 1 Hz at 20% of duty for three cycle pulse trains; but when the duty cycle was increased to 30% and/or the HIFU modulation frequency ($f_{M\text{-}HIFU}$) was increased to 2 and 4 Hz, the SNR drastically reduced. In addition, by using low modulation frequency ($f_{M\text{-}HIFU}$) to drive the HIFU transducer to achieve high SNR, the duration of acquisition of the USF signal at each location (within the scan area) increases, thereby increasing the overall duration of scanning. Therefore a trade-off needs to be established between the acceptable duration of data acquisition and that of the desired SNR for the proposed USF imaging.

In the future, investigations can be conducted on the HIFU transducer and USF system design such that it can induce a desired temperature within a much shorter duty cycle but without thermal ablation and can have fast acquisition for dynamic switching of USF contrast agents. Thereby, the modulation frequency ($f_{M\text{-}HIFU}$) can be increased, while achieving high SNR without compromising resolution but with short scanning duration.

6.2.2 Dual-HIFU USF imaging technique:

Two major attributes of the proposed dual-HIFU transducer-based USF imaging system are the following: (1) By using two 90°-crossed ultrasound transducers with an overlapped focal region, the axial resolution (along the ultrasound wave-propagation direction) of USF imaging has been significantly improved (close to its lateral resolution), which makes it possible to scan tissue on the *x*-*z* plane co-registered with a B-mode ultrasound image. In addition, it is helpful for developing 3D USF imaging in the future. (2) By combining the two imaging modalities, the system can image multi-colour fluorophores in tissues via USF technology and image tissue acoustic structures via B-mode ultrasound. Due to the unique system design, four major limitations have been observed. First, the temperature increase at the overlapped region of the two crossed foci (OR-TCF) is not high enough compared to the temperature in the focal regions of the individual HIFU transducers (*f*-number is ~1.52). For this reason, considerable fluorescence switching is observed along the major axes (fluorescence tails) of the individual focal regions (considering a focal region to be an ellipse with a major axis along the axial direction of the HIFU focus). For a second limitation, multiple targets acquired using the proposed USF imaging cannot be efficiently separated if they are very close to each other. This is especially true if the targets are located close to each other and if their locations are approximately 45 degrees with respect to each other, since the fluorescence tails of USF images obtained for one target will overshadow the other target. The third limitation is that the two HIFU transducers' focal regions should be accurately overlapped so that they have confocal arrangement. Any misalignment of the OR-TCF would yield a temperature rise which sparsely distributes and degrades the USF image. The fourth limitation is characteristic of ultrasound wave propagation where the attenuation increases with

penetration depth as the frequency of ultrasound increases. It is usually characterized in terms of the half-value depth (i.e., the distance at which 50% of the ultrasound energy has been dissipated) for the specific ultrasound frequency [64, 65]. The ultrasound attenuation coefficient for muscle tissue is about 0.5-1.5 $dB.cm^{-1}.MHz^{-1}$ [66]. Therefore, using a 9 MHz HIFU transducer for a dual-HIFU system design will significantly limit the depth of penetration of ultrasound in comparison to our previous USF system design, which uses a 2.5 MHz HIFU transducer [12, 15, 21]. It should also be noted that the ultrasound is focused on the sample at an angle of 45 degrees, which also degrades the penetration depth to some extent.

Possible approaches that can be undertaken to minimize or rectify these limitations are, 1) to use a dual-HIFU transducer with a smaller *f*-number, 2) to have more than two HIFU transducers (with their focal regions in confocal arrangement), and 3) to use a unique design in which a single HIFU with a small *f*-number has rotational freedom of moment. By opting for the latter of the above approaches, a USF image obtained at different angles with respect to HIFU transducer will have a higher SNR. As the number of HIFU transducers or number of angles of USF acquisition using a rotationally mounted, single HIFU transducer increases, the system gets more complicated and requires robust-level post-processing algorithms.

6.2.3 USF imaging technique using 15 MHz HIFU transducer

The proposed USF design with a 15 MHz HIFU transducer is a simple way to improve the resolution of the USF imaging technique. It has been demonstrated to have excellent lateral and axial resolution and good SNR after post-processing. As indicated in the previous section, the major limitation of the proposed design lies in the basic

characteristics of ultrasound wave propagation. Here, by using a HIFU transducer with a 15 MHz frequency, the effective ultrasound attenuation is increased with penetration depth [66]. This also decreases the conversion efficiency of the applied power, to drive the HIFU transducer, to a temperature rise within its focal region to be reduced significantly. So depending upon the desired resolution, SNR and depth of imaging, either the conventional USF design (with a 2.5 MHz HIFU transducer [12]) or this proposed USF design with a 15 MHz can be opted. Future studies can focus on USF system designs with different frequencies of HIFU transducers and develop a USF system to have variable frequencies of HIFU transducers in one module. This might yield USF images with different resolutions that, in combination with other modalities can become a powerful tool for molecular imaging.

References:

1. Fass, L., *Imaging and cancer: a review.* Mol Oncol, 2008. **2**(2): p. 115-52.
2. *Breast Cancer: Statistics | Cancer.Net*. 2012 2012-06-25; Available from: http://www.cancer.net/cancer-types/breast-cancer/statistics.
3. Wang, L.V., *Ultrasound-mediated biophotonic imaging: a review of acousto-optical tomography and photo-acoustic tomography.* Dis Markers, 2003. **19**(2-3): p. 123-38.
4. Luker, G.D. and K.E. Luker, *Optical imaging: current applications and future directions.* J Nucl Med, 2008. **49**(1): p. 1-4.
5. Cai, W. and X. Chen, *Multimodality molecular imaging of tumor angiogenesis.* J Nucl Med, 2008. **49 Suppl 2**: p. 113S-28S.
6. Lakowicz, J.R., *Principles of frequency-domain fluorescence spectroscopy and applications to cell membranes.* Subcell Biochem, 1988. **13**: p. 89-126.
7. Wang, L.V., *Multiscale photoacoustic microscopy and computed tomography.* Nat Photonics, 2009. **3**(9): p. 503-509.
8. Stephen, R.M. and R.J. Gillies, *Promise and progress for functional and molecular imaging of response to targeted therapies.* Pharm Res, 2007. **24**(6): p. 1172-85.
9. Seddon, B.M. and P. Workman, *The role of functional and molecular imaging in cancer drug discovery and development.* Br J Radiol, 2003. **76 Spec No 2**: p. S128-38.
10. Rudin, M. and R. Weissleder, *Molecular imaging in drug discovery and development.* Nat Rev Drug Discov, 2003. **2**(2): p. 123-31.
11. Wang, L.V. and L. Gao, *Photoacoustic microscopy and computed tomography: from bench to bedside.* Annu Rev Biomed Eng, 2014. **16**: p. 155-85.
12. Cheng, B., et al., *High-Resolution Ultrasound-Switchable Fluorescence Imaging in Centimeter-Deep Tissue Phantoms with High Signal-To-Noise Ratio and High Sensitivity via Novel Contrast Agents.* PLoS One, 2016. **11**(11): p. e0165963.
13. Cheng, B., et al., *Development of Ultrasound-switchable Fluorescence Imaging Contrast Agents based on Thermosensitive Polymers and Nanoparticles.* IEEE J Sel Top Quantum Electron, 2014. **20**(3).
14. Liu, Y., et al., *Ultrasound-modulated fluorescence based on fluorescent microbubbles.* J Biomed Opt, 2014. **19**(8): p. 085005.

15. Yuan, B., et al., *High-resolution imaging in a deep turbid medium based on an ultrasound-switchable fluorescence technique.* Appl Phys Lett, 2012. **101**(3): p. 33703.
16. Razansky, D., et al., *Multispectral opto-acoustic tomography of deep-seated fluorescent proteins in vivo.* Nature Photonics, 2009. **10.1038/Nphoton.2009.98**(3): p. 412 - 417.
17. Yuan, B., *Ultrasound-modulated fluorescence based on a fluorophore-quencher-labeled microbubble system.* J Biomed Opt, 2009. **14**(2): p. 024043.
18. Lin, Y., et al., *Temperature-modulated fluorescence tomography in a turbid media.* Appl Phys Lett, 2012. **100**(7): p. 73702-737024.
19. Lin, Y., et al., *Temperature-modulated fluorescence tomography based on both concentration and lifetime contrast.* J Biomed Opt, 2012. **17**(5): p. 056007.
20. Wei, M.Y., et al., *Synthesis and characterization of NIR fluorophore-encapsulated thermo-sensitive nanoparticles as contrast agents for ultrasound-switchable fluorescence imaging.* Journal of Biomedical Optics, 2013.
21. Pei, Y., et al., *High resolution imaging beyond the acoustic diffraction limit in deep tissue via ultrasound-switchable NIR fluorescence.* Sci Rep, 2014. **4**: p. 4690.
22. Yu, S., et al., *New generation ICG-based contrast agents for ultrasound-switchable fluorescence imaging.* Sci Rep, 2016. **6**: p. 35942.
23. Chen, Y. and X. Li, *Near-infrared fluorescent nanocapsules with reversible response to thermal/pH modulation for optical imaging.* Biomacromolecules, 2011. **12**(12): p. 4367-72.
24. Chen, D., et al., *A feasibility study of temperature rise measurement in a tissue phantom as an alternative way for characterization of the therapeutic high intensity focused ultrasonic field.* Ultrasonics, 2009. **49**(8): p. 733-42.
25. Lee, K.l. and M.J. Choi, *Prediction and Measurement of the Size of Thermal Lesion Induced by High Intensity Focused Ultrasound in a Tissue-Mimicking Phantom.* Japanese Journal of Applied Physics, 2009. **48**(2): p. 027003.
26. Haar, G.T. and C. Coussios, *High intensity focused ultrasound: physical principles and devices.* Int J Hyperthermia, 2007. **23**(2): p. 89-104.
27. Harris, G.R., *FDA regulation of clinical high intensity focused ultrasound (HIFU) devices.* Conf Proc IEEE Eng Med Biol Soc, 2009. **2009**: p. 145-8.

28. Morris, H., et al., *Investigation of the viscous heating artefact arising from the use of thermocouples in a focused ultrasound field.* Phys Med Biol, 2008. **53**(17): p. 4759-76.
29. Faqi, L., et al. *Measuring Temperature Rise in Phantom to Determine High Power High-Intensity Focused Ultrasound Sound Field*. in *Bioinformatics and Biomedical Engineering (iCBBE), 2010 4th International Conference on*. 2010.
30. Olympus, *Panametrics transducers*. Envirocoustics.
31. Kandukuri, J., et al., *A Dual-Modality System for Both Multi-Color Ultrasound-Switchable Fluorescence and Ultrasound Imaging.* Int J Mol Sci, 2017. **18**(2).
32. Yuan, B., Y. Pei, and J. Kandukuri, *Breaking the acoustic diffraction limit via nonlinear effect and thermal confinement for potential deep-tissue high-resolution imaging.* Appl Phys Lett, 2013. **102**(6): p. 63703.
33. Corlu, A., et al., *Three-dimensional in vivo fluorescence diffuse optical tomography of breast cancer in humans.* Opt Express, 2007. **15**(11): p. 6696-716.
34. Wang, L.V. and S. Hu, *Photoacoustic tomography: in vivo imaging from organelles to organs.* Science, 2012. **335**(6075): p. 1458-62.
35. Resink, S.G., A.C. Boccara, and W. Steenbergen, *State-of-the art of acousto-optic sensing and imaging of turbid media.* J Biomed Opt, 2012. **17**(4): p. 040901.
36. Filonenko, E.A. and V.A. Khokhlova, *Effect of acoustic nonlinearity on heating of biological tissue by high-intensity focused ultrasound.* Acoustical Physics, 2001. **47**(4): p. 468-475.
37. Yuan, B., et al., *Microbubble-enhanced ultrasound-modulated fluorescence in a turbid medium.* Applied Physics Letters, 2009. **95**(18): p. 1113.
38. Foster, F.S., et al., *Advances in ultrasound biomicroscopy.* Ultrasound Med Biol, 2000. **26**(1): p. 1-27.
39. Hunt, J.W., M. Arditi, and F.S. Foster, *Ultrasound transducers for pulse-echo medical imaging.* Bio-Med. Eng., 1983. **30**(8): p. 453.
40. McDonald, D.M. and P.L. Choyke, *Imaging of angiogenesis: from microscope to clinic.* Nat Med, 2003. **9**(6): p. 713-25.
41. Cheng, B., et al., *The Mechanisms and Biomedical Applications of an NIR BODIPY-Based Switchable Fluorescent Probe.* Int J Mol Sci, 2017. **18**(2).

42. Dorrell, M.I., et al., *Combination angiostatic therapy completely inhibits ocular and tumor angiogenesis.* Proc Natl Acad Sci U S A, 2007. **104**(3): p. 967-72.
43. Abdollahi, A. and J. Folkman, *Evading tumor evasion: current concepts and perspectives of anti-angiogenic cancer therapy.* Drug Resist Updat, 2010. **13**(1-2): p. 16-28.
44. Niu, G. and X. Chen, *Has molecular and cellular imaging enhanced drug discovery and drug development?* Drugs R D, 2008. **9**(6): p. 351-68.
45. Huang, C.W., et al., *Porous Hollow Gold Nanoparticles for Cancer SERS Imaging.* J. Nano Res., 2010. **10**: p. 137-148.
46. Faivre, S., S. Djelloul, and E. Raymond, *New paradigms in anticancer therapy: targeting multiple signaling pathways with kinase inhibitors.* Semin Oncol, 2006. **33**(4): p. 407-20.
47. Hecht, J.R., et al., *A randomized phase IIIB trial of chemotherapy, bevacizumab, and panitumumab compared with chemotherapy and bevacizumab alone for metastatic colorectal cancer.* J Clin Oncol, 2009. **27**(5): p. 672-80.
48. Quesada, A.R., M.A. Medina, and E. Alba, *Playing only one instrument may be not enough: limitations and future of the antiangiogenic treatment of cancer.* Bioessays, 2007. **29**(11): p. 1159-68.
49. Shariat, S.F., et al., *Multiple biomarkers improve prediction of bladder cancer recurrence and mortality in patients undergoing cystectomy.* Cancer, 2008. **112**(2): p. 315-25.
50. Zavaleta, C.L., et al., *Multiplexed imaging of surface enhanced Raman scattering nanotags in living mice using noninvasive Raman spectroscopy.* Proc Natl Acad Sci U S A, 2009. **106**(32): p. 13511-6.
51. Gambhir, S.S., *Molecular imaging of cancer with positron emission tomography.* Nat Rev Cancer, 2002. **2**(9): p. 683-93.
52. Ntziachristos, V., et al., *Looking and listening to light: the evolution of whole-body photonic imaging.* Nat Biotechnol, 2005. **23**(3): p. 313-20.
53. Culver, J., W. Akers, and S. Achilefu, *Multimodality molecular imaging with combined optical and SPECT/PET modalities.* J Nucl Med, 2008. **49**(2): p. 169-72.
54. Wang, L.V., *Photoacoustic imaging and spectroscopy*. Optical science and engineering. 2009, Boca Raton: CRC. xx, 499 p.

55. Wang, L.H.V., *Ultrasound-mediated biophotonic imaging: A review of acousto-optical tomography and photo-acoustic tomography.* Disease Markers, 2003. **19**(2-3): p. 123-138.
56. Yuan, B. and Q. Zhu, *Separately reconstructing the structural and functional parameters of a fluorescent inclusion embedded in a turbid medium.* Opt Express, 2006. **14**(16): p. 7172-87.
57. James, J., V.M. Murukeshan, and L.S. Woh, *Integrated photoacoustic, ultrasound and fluorescence platform for diagnostic medical imaging-proof of concept study with a tissue mimicking phantom.* Biomed Opt Express, 2014. **5**(7): p. 2135-44.
58. Kang, J., et al., *A prototype hand-held tri-modal instrument for in vivo ultrasound, photoacoustic, and fluorescence imaging.* Rev Sci Instrum, 2015. **86**(3): p. 034901.
59. Liu, Y., B. Yuan, and J. Vignola, *Effect of fluorescent particle size on the modulation efficiency of ultrasound-modulated fluorescence.* Int J Opt, 2012. **2012**.
60. Yuan, B., J. Gamelin, and Q. Zhu, *Mechanisms of the ultrasonic modulation of fluorescence in turbid media.* J Appl Phys, 2008. **104**(10): p. 103102.
61. Yuan, B. and Y. Liu, *Ultrasound-modulated fluorescence from rhodamine B aqueous solution.* J Biomed Opt, 2010. **15**(2): p. 021321.
62. Bandi, V., et al., *Excitation-wavelength-dependent, ultrafast photoinduced electron transfer in bisferrocene/BF2-chelated-azadipyrromethene/fullerene tetrads.* Chemistry, 2013. **19**(22): p. 7221-30.
63. Kandukuri, J., Y. Liu, and B. Yuan, *Cost-efficient and multi-functional systems for ultrasound measurement and imaging.* Austin J Biomed Eng, 2014. **1**(1).
64. ter Haar, G., *Basic physics of therapeutic ultrasound.* Physiotherapy, 1978. **64**(4): p. 100-3.
65. Hayes, B.T., et al., *Three-MHz Ultrasound Heats Deeper Into the Tissues Than Originally Theorized.* J Athl Train, 2004. **39**(3): p. 230-234.
66. Haiat, G., et al., *Velocity dispersion in trabecular bone: influence of multiple scattering and of absorption.* J Acoust Soc Am, 2008. **124**(6): p. 4047-58.

Biographical Information

Jayanth Kandukuri received his Bachelor of Technology degree in Biomedical Engineering from Jawaharlal Nehru Technological University, Hyderabad, Telangana, India, in 2005. He then continued his graduate studies in Australia. Jayanth received his Master of Engineering in Electronic Engineering from University of Queensland, Queensland, Australia, in 2007. From 2008 to 2010, he worked as Jr. Biomedical engineering at CARE Hospital Ltd. Jayanth received another Master of Science degree in Biomedical Engineering from University of Texas at Arlington, Texas, USA, in 2012. From 2012 to 2017, he was involved in the research of developing ultrasound-switchable fluorescence optical tomography techniques for cancer detection. In 2012 fall, Jayanth started his Ph.D. in Biomedical Engineering at the Joint Program of University of Texas at Arlington and University of Texas Southwestern Medical Center at Dallas, Texas, completing it by summer 2017. During this time, he worked as a research assistant in the ultrasound and optical imaging lab. His research expertise is in medical instrumentation, ultrasound and optical imaging, and signal processing. His projects focused on developing novel method of characterizing high-intensity focused ultrasound and later in improving ultrasound-switchable fluorescence-imaging techniques for applications in medical diagnostics and therapy. During his graduate studies, he has three first-authored journal papers and two co-authored journal paper, and presented about four talks in prestigious conferences. Jayanth has received Franklyn Alexander Scholarship at the University of Texas at Arlington in 2016, and Graduate Studies Dissertation Fellowship from the University of Texas at Arlington in 2017. In the near future, he hopes to contribute in the medical device industry for developing innovative medical technologies that can support healthcare professionals and individuals to advancing human health.